THE INSTITUTION'S 1963 CONVENTION

NEARLY two hundred engineers, representative of a broad cross-section of British Industry, took part in the Convention on "Electronics and Productivity" at the University of Southampton last month. Organized as the Institution's principal contribution to National Productivity Year, the main theme of the Convention was to show some of the ways in which electronics can be applied throughout industry to increase productivity. In his opening address (printed in the May issue of the *Proceedings*) the Chairman of the Convention Committee, Mr. J. L. Thompson (Senior Vice President), stressed the collaboration which must exist between the electronics industry and users when he said "Industry—management, union and employees—must accept these contributions and put them to use. Furthermore, Industry must demand solutions to the problems as yet unsolved and the new problems that will arise as productivity continues to expand".

The thirty-two papers presented during the Convention were described in the synopses which were published in the February and March issues of *The Radio and Electronic Engineer*, where they will appear in final form, with reports of discussions, during the next six months. Many useful points were brought out during the discussions, notably on reliability considerations and on means of ensuring that equipment is designed with its eventual environment clearly in mind.

In spite of the inescapable fact that much electronic equipment intended for industrial applications is relatively large and immovable, several authors brought equipment described in their papers to the Convention for demonstration. Other practical aspects of the theme of the Convention were looked after by the courtesy of the heads of several Departments of the University's Faculty of Engineering who arranged tours of their laboratories; in addition a party of delegates were guests of the Esso Petroleum Company at their Fawley Refinery.

The Convention was concluded by a Banquet in the Guildhall, Southampton, at which the principal guests were The Worshipful The Mayor of Southampton, Councillor E. K. Lyons, J.P., and the Deputy Vice Chancellor of the University, Professor A. Phillips, O.B.E., M.A., Ph.D. Proposing the Toast of "The Town and the University of Southampton", Mr. J. L. Thompson recalled previous Institution Conventions in Southampton and spoke of the growth of the University, in particular its establishment of a chair in Electronics. He reminded those present of the importance of reliability in electronic equipment developed for industrial applications and stressed the importance of expanding and co-ordinating research.

Professor Phillips welcomed the Institution's collaboration with the University of Southampton and praised its work in encouraging research in the Universities. His comments on the Institution's Research Report aptly pointed a moral which was drawn several times during the Convention but which is perhaps not sufficiently widely realized—that adequate research effort must support the introduction of electronic aids to increased productivity.

C

INSTITUTION NOTICES

Symposium on "Berkeley and Bradwell Nuclear Power Stations"

The Nuclear Energy Group of the Institution of Mechanical Engineers, in collaboration with The British Nuclear Energy Society, is holding a Symposium on "Berkeley and Bradwell Nuclear Power Stations" at 1 Birdcage Walk, London, S.W.1, on 27th June 1963. In addition to the two general papers on the Power Stations there will be three others covering "Commissioning Programmes and Procedures", "Nuclear Fuel Management" and "Operational Performance".

The British Institution of Radio Engineers is a constituent society of the British Nuclear Energy Society. Preliminary programmes and registration forms can be obtained from 9 Bedford Square, London, W.C.1.

British Conference on Automation and Computation

The Second International Congress on Automatic Control, organized by the International Federation of Automatic Control, will be held in Basle, Switzerland from 27th August to 4th September 1963. This Congress takes place on the invitation of the Swiss Association for Automatic Control.

At the second I.F.A.C. Congress (the first was held in Moscow in 1960) current theories of higher automatics will be discussed in 25 sessions. In addition 26 sessions will be devoted to control devices and their applications. These sessions will be divided into four groups run simultaneously and altogether 156 papers will be presented.

An International Exhibition of Industrial Electronics will be held in Basle from 2nd September to 7th September. In connection with this exhibition there will be a presentation of papers on electronics.

The complete programme and registration forms may be obtained from the British Conference on Automation and Computation, c/o The Institution of Electrical Engineers, Savoy Place, London, W.C.2.

Quality and Reliability Principles and Practices

As a contribution to National Productivity Year the National Council for Quality and Reliability has organized a residential course at the College of Aeronautics, Cranfield, Bedfordshire on 14th–26th July 1963.

The National Council, on which the major engineering and managerial institutions are represented consider that previous courses of this kind have often emphasized only the statistical aspects of quality control. This course has been prepared in such a manner that all branches and grades, from planning to engineering inspection and senior management, may achieve maximum practical benefit.

Accommodation for the course, which is limited to thirty, is included in the fee of £65. Full details and application forms may be obtained from the Honorary Secretary, National Council for Quality and Reliability, Vintry House, Queen Street Place, London, E.C.4.

European Organization for Civil Aviation Electronics

At an international meeting held in Lucerne, Switzerland, on 24th April, 1963, some thirty European manufacturers of civil aviation electronic equipment decided to form an association to be known as the European Organization for Civil Aviation Electronics (EUROCAE). Representatives of European airlines and aviation administrations also attended the meeting and indicated their intention of participating in the technical work of EUROCAE.

The aims of EUROCAE stated in the Memorandum of Understanding accepted by the representatives of the Companies concerned are:

To advance the application of electronics to civil aviation.

To study in Europe on an international level technical problems facing users and manufacturers of electronic equipment for civil aviation and all related questions.

To contribute at national and international levels to the solution of technical problems confronting European manufacturers and users of electronic equipment for civil aviation.

To advise and assist international bodies in the establishment of international standards.

To study other appropriate technical or operational subjects as decided from time to time.

The work of EUROCAE will be controlled by a Steering Committee which will develop the policy and guide the technical work. Initially, Working Groups on All-Weather Operations, Engineering Design of Equipment and Installations, Airborne Weather Radar, and Airborne Search and Rescue Equipment are to be formed. Monsieur P. Lizon, managing director of Le Matériel Téléphonique in France, was elected as the first President of EUROCAE and Dr. B. J. O'Kane, manager of the Aeronautical Division of Marconi's Wireless Telegraph Company in England, was elected Chairman of the Steering Committee.

Correction

The following correction should be made to the paper "An Instructional Aid for Digital Computer Logic", published in the April issue of *The Radio and Electronic Engineer*:

Pages 338–9: Fig. 4 and Fig. 5. The circuits of these two illustrations should be interchanged.

Cryotrons and Cryotron Circuits—A Review

By

P. A. WALKER, Ph.D. †

Summary: The characteristics of crossed-film and in-line cryotrons are described and their dependence upon film thickness, operating temperature is discussed. Factors affecting current gain and time-constant are considered. General aspects of cryotron circuits are described, particular attention being paid to cycle time considerations. It is shown how cryotrons may be used in simple logic circuits. Three cryotron storage loops are discussed and it is shown how they may be used in word-organized memories. The advantages of associative memories are pointed out and it is shown how they may be realized by the use of cryotrons, i.e. by combining the logic and memory circuits previously described. The technical feasibility of the use of cryotrons is considered and an attempt is made to assess the outstanding technical problems.

1. Introduction

Since the original description of the wire-wound cryotron by Buck[1] in 1956, much has been said and written about their potential usefulness as computer components. The modern concept of the cryotron as a multi-layer thin-film sandwich has many advantages over its predecessor. In addition to having a much lower inductance and hence faster switching speed it also has a small physical size and is compatible with batch fabrication techniques. These last considerations become important when one considers the cycle time and manufacturing cost of a very large, high-speed cryotron memory.

Buck showed how the two stable states of a superconductor, i.e. the superconducting and resistive, could be controlled by current flowing through a second, independent conductor, and used to represent the 0 and 1 of binary logic. Although the cryotrons he made were very slow by present standards, he was, nevertheless, able to show their great potential as circuit elements. The purpose of the present review is to show the great versatility of the cryotron as a circuit element, and in particular to consider its usefulness as a computer component. No mention will be made of ring oscillator circuits[2], inverter circuits[3] or the use of cryotrons as linear amplifiers[4].

A good review of the early work on cryotrons has been given by Young[5] and this serves as a useful introduction to the subject. A short introduction has also been given by Rhoderick[6]. More detailed aspects of cryotrons and simple cryotron circuits are contained in the proceedings of the 1960 Washington Symposium on Superconducting Computer Techniques which have been published in the September 1960 issue of *Solid State Electronics*. Recently Lock[7] has discussed thin film cryotrons in a review of superconducting switching devices.

† International Computers & Tabulators (Engineering) Ltd., Stevenage, Hertfordshire.

2. Cryotrons

In its original form, the wire-wound cryotron used a niobium control wire wound round a tantalum gate wire. Due to the great difficulty of preparing thin films of these materials with good superconducting properties, it has been necessary to replace them in the thin film cryotron by lead and tin respectively.

A typical crossed-film cryotron configuration is shown diagrammatically in Fig. 1. The tin gate film is crossed orthogonally by a lead control film and insulated from it by a suitable dielectric film such as silicon
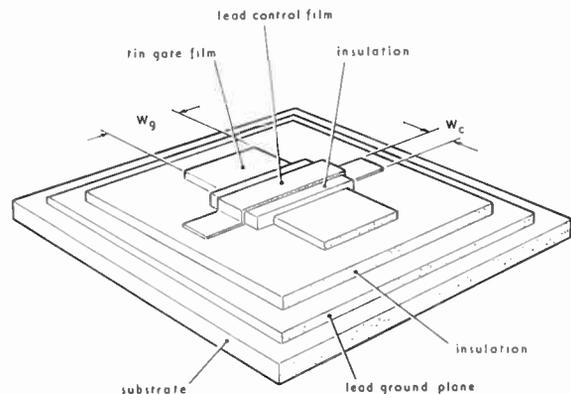
(a) Crossed film cryotron.
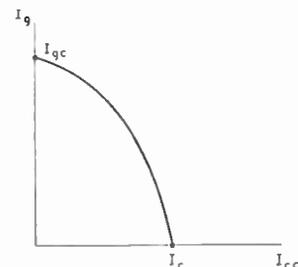
(b) Ideal cryotron characteristic.

Fig. 1.

monoxide. At the operating temperature of the device, say $3 \cdot 6^\circ$ K, both the tin and lead films are below their superconducting transition temperatures ($3 \cdot 74^\circ$ K and $7 \cdot 2^\circ$ K respectively). Current through the control film generates a magnetic field that may be used to switch the tin gate film from the superconducting to the normal resistive state.

The magnetic field acting on the tin gate film is actually the vector sum of the fields due to the current I_c in the control and a current I_g in the gate film. The superconducting ground plane below the cryotron localizes the magnetic field due to the control current. Taking into account the doubling effect between the film and ground plane, the magnetic field due to a current I in a film of width W is given by

$$H = 0 \cdot 4 \, \pi I / W$$

If the subscripts g and c refer to the gate and control films, then the total field acting on the gate film is given by

$$H_t = 0 \cdot 4\pi \sqrt{\left(\frac{I_g}{W_g}\right)^2 + \left(\frac{I_c}{W_c}\right)^2}$$

and the film will switch when $H_t > H_{cf}$, the critical field of the gate film. If I_{gc} and I_{cc} represent the currents required to switch the gate film when the control and gate currents respectively are zero, c.f. Fig. 1(b), then the current gain G of the cryotron may be defined as

$$G = I_{gc}/I_{cc} = A \, W_g/W_c$$

where A is the cryotron efficiency.

Assuming Silsbee's hypothesis that the critical current of a superconductor generates a magnetic field equal to the critical value one would expect the cryotron efficiency A to be unity. For thin films, however, this hypothesis breaks down and in general $I_{gc} < \dfrac{H_{cf} W.}{0 \cdot 4\pi}$. Solving London's equations for the critical field of a film and using an expression for the critical current suggested by Ittner[8], an equation may be obtained for the cryotron efficiency which is of the form

$$A = C \tanh \frac{t}{2\lambda} \left(1 - \frac{2\lambda}{t} \tanh \frac{t}{2\lambda}\right)^{\frac{1}{2}}$$

where t is the film thickness, λ is the magnetic field penetration depth and C is a quality parameter determined by film purity and homogeneity. The temperature variation of the penetration depth is given by

$$\lambda = \lambda_0 \left(1 - \left(\frac{T}{T_c}\right)^4\right)^{-\frac{1}{2}}$$

where λ_0 is the penetration depth at absolute zero. Assuming a value of $\lambda_0 = 540$ Å for the tin gate film, the cryotron efficiency varies with film thickness and temperature as shown in Fig. 2(a). Although the cryo-
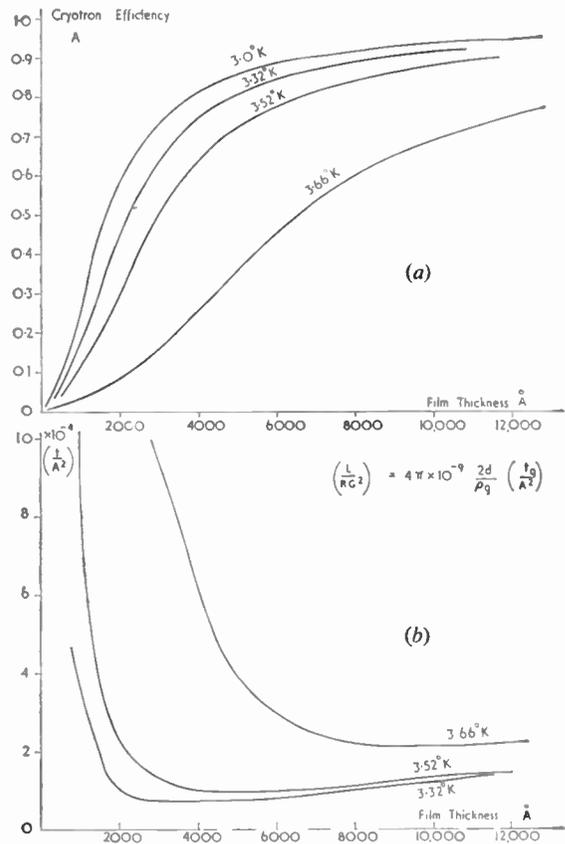
Fig. 2. (a) Cryotron efficiency vs film thickness and temperature
(b) Optimum film thickness for minimum L/RG^2.

tron efficiency is less than unity, current gain greater than one may be obtained by having a crossing ratio W_g/W_c greater than unity.

The time-constant of a cryotron circuit is determined by the L/R ratio, where the inductance L is that of the entire circuit being considered, and the resistance R is that introduced into the cryotron gate. For convenience we consider the inductance L to be the sum of the inductance L_1 of the cryotron and the inductance L_2 of the rest of the circuit. Since L_1 is the inductance between the control and gate films, the intrinsic cryotron time-constant becomes

$$\tau_1 = L_1/R = 8\pi d' t_g / \rho_g \, (W_g/W_c)^2 \times 10^{-9} \text{ seconds}$$

where ρ_g is the effective resistivity of the gate film and d' is the effective separation between the gate and control films. If d is the insulation thickness and λ_g and λ_c are the penetration depths in the gate and control films then

$$d' = d + \lambda_g + \lambda_c$$

In terms of current gain G, the time-constant becomes

$$\tau = 8\pi d' t_g / \rho_g \, (G/A)^2 \times 10^{-9} \text{ seconds}$$

and we see that for a given film thickness and resistivity,

current gain must be sacrificed for switching speed in cryotron design. As shown in Fig. 2(b), there is an optimum film thickness which gives the minimum time-constant for a given gain.

The second contribution to the time-constant arises from the inductance of the interconnecting films. The resistance involved is still that of the cryotron gate and the time-constant is given by

$$\tau_2 = L_2/R = 4\pi d' t_g l/\rho_g W_c \times 10^{-9} \text{ seconds}$$

assuming the interconnecting films are of width W_g and length l. To minimize the time-constant it is thus necessary to use short, wide interconnecting films having a small separation d from the ground plane.

To estimate the magnitudes of these time-constants consider a cryotron having the following dimensions

$$W_c = 0.1 \text{ mm} \quad W_g = 0.5 \text{ mm} \quad t = 4000 \text{ Å}$$
$$d = 4{,}000 \text{ Å} \quad \rho_g = 5 \times 10^{-7} \text{ ohm-cm}$$
$$T = 3.5° \text{ K}$$

From the equations given above, the cryotron time-constant for a current gain of 3 would be 2×10^{-9} seconds. Assuming the interconnecting lines are the same width as the gate film, the time-constant of the interconnections would be 4×10^{-9} s/cm. As an example of what may be achieved in practice, Cohen[2] has reported on a ring oscillator using cryotrons with a current gain $G = 3$ and a time-constant $\tau = 20 \times 10^{-9}$ seconds.

The minimum ground plane to film separation that can be used is determined by the technology of preparing pinhole-free dielectric films. Silicon monoxide is the dielectric material most frequently used for cryotron insulation and at present the thinnest film to be deposited pinhole-free is approximately 4000 Å thick. With the development of new and improved technologies and materials it seems reasonable to suppose that a factor of ten reduction in insulation thickness may be possible. This, of course, would lead to a decrease in the time-constant of cryotron circuits.

A further way of reducing the cryotron time-constant would be to use a gate film of higher resistivity ρ_g, i.e. to use alloys. To be useful as a cryotron gate, the alloy must be prepared in thin film form and must have good superconducting properties. In general, superconducting alloys have higher critical fields and broader magnetic field transitions than the pure metals. It is only possible, therefore, to use specially prepared dilute alloys and to obtain resistivity increases of a factor of five or so.

Power dissipation in the cryotron is a further factor which must be borne in mind particularly when considering the use of high resistivity films. The temperature rise resulting from this power dissipation is a complex function of the time-constant of the cryotron circuit and the thermal conductance between the gate film and the helium bath. It may be kept to a minimum by using low resistivity films, high conductivity substrates and an operating temperature near the critical temperature T_c so that the currents involved are small. From the systems point of view, this power dissipation limits the maximum allowable cryotron packing density for a given pulse repetition frequency and duty cycle. Sobol[9] has recently considered this problem and concludes that cryotron packing density may be increased by using small area gate films, a low duty-factor and by designing circuits having wide temperature tolerances. For a cryotron having a 0.010 in wide gate and 0.001 in wide control film, and allowing for a temperature rise of 0.06° K, Sobol shows that a packing density of 720 per square inch is possible when the pulse repetition frequency is 100 Mc/s and the duty cycle is 0.1. Any increase in gate resistivity and hence of power dissipation will reduce the allowable packing density or duty cycle.

The discussion so far has referred to the crossed-film cryotron in which the control and gate films are orthogonal. In the "in-line" cryotron, the control and gate films are parallel as shown diagramatically in Fig. 3. Young[10] has discussed the characteristics of the in-line cryotron which in the idealized case have the form shown in Fig. 3(b). Since the crossing ratio $W_g/W_c = 1$, the current gain of the in-line cryotron equals the cryotron efficiency which is less than unity. The usefulness of the in-line cryotron arises from the fact that its resistance is directly proportional to its length, so it can be used for matching to output lines
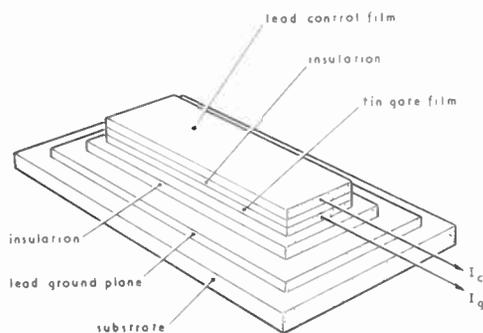

(a) In-line cryotron.
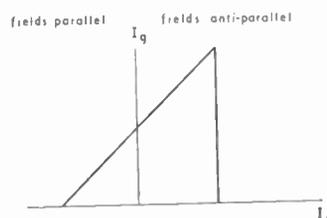

(b) Ideal characteristic.

Fig. 3.

etc. The time-constant of this form of cryotron is independent of current gain and is given by

$$\tau = L/R = 8\pi d' t_g/\rho_g \times 10^{-9} \text{ seconds}$$

For $d = 4000$ Å, $t = 4000$ Å and $\rho_g = 5 \times 10^{-7}$ ohm cm, $\tau = 10^{-10}$ seconds. Provided the reduced gain is acceptable, the use of the in-line cryotron would be expected to reduce considerably the switching time of a cryotron circuit. By suitable biasing, it has been suggested that the in-line cryotron may be operated at a point on its characteristics such that the incremental current gain $\Delta I_g/\Delta I_c$ is greater than unity. Under these conditions it may be possible to realize simultaneously the advantages of high speed and current gain.
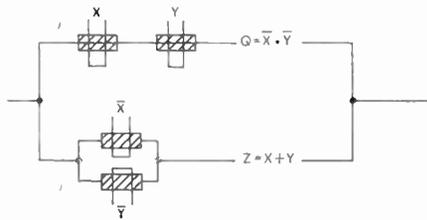
(a) Cryotron AND/OR combination.
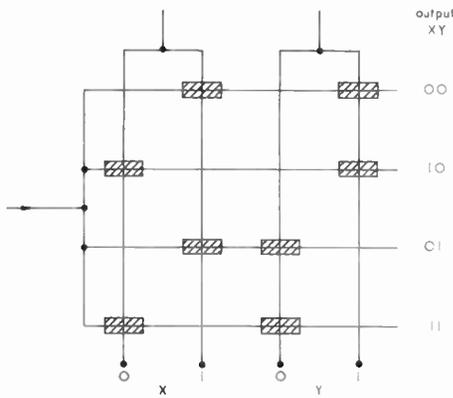
(b) Cryotron 4-position switch.

Fig. 4.

Most of the equations derived above refer to the behaviour of ideal superconducting films. In actual fact, the films as prepared in a vacuum coating plant are far from ideal in that they contain a large amount of impurity absorbed during the deposition. The films also have a large built-in stress which originates (a) from the difference in the thermal expansion of the film and substrate, and (b) from the presence of impurities in the film. These effects all tend to change slightly the superconducting parameters of the film.

The most significant departure from ideal behaviour, however, is a consequence of the sloping edges of the film which are caused by penumbra effects through the fabrication mask used to define the geometry of the film. Since the critical field of a superconducting film increases as the film thickness decreases, there is a change of critical field across the film edges. This results in a broad magnetic field transition and a cryotron with low efficiency A. Removal of the film edges by mechanical or chemical means sharpens the magnetic field transition[11] and a similar effect may be obtained by depositing the film in a vacuum of 10^{-8} mm Hg.

3. Logic Applications

At first sight the cryotron appears to be very similar to a high-speed relay in so far that the control and gate circuits are independent and change in resistance is used to control the current flowing through the gate. There is one very significant difference however. In a relay the resistance introduced is infinite whereas in the cryotron only a low resistance is introduced into the gate. This means that current will flow through a cryotron when it is in the resistive state unless an alternative superconducting path is provided.

From a logical point of view, the cryotron should be regarded as an inversion, i.e. a "Boolean" NOT gate. Thus in Fig. 4(a), an output at Q represents the AND combination while output at Z represents the inclusive OR.

An example of the use of cryotrons in simple logical circuits is the four-position switch shown in Fig. 4(b). More complex logic circuits have been designed. For instance, Haynes[12] describes the binary adder shown in Fig. 5 which employs only 14 cryotrons compared to the 42 required in an earlier design of Buck[1].
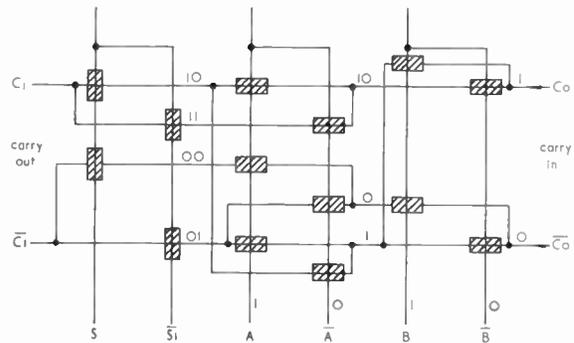
Fig. 5. Binary full adder.

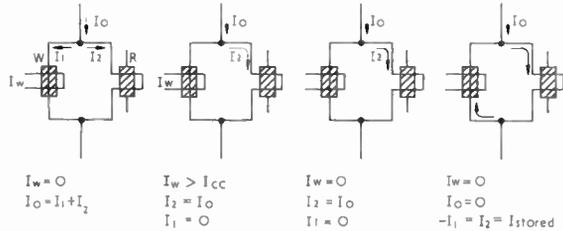## 4. Storage Circuits

These may be of two types, either flip-flop loops or storage loops. In the flip-flop loop (Fig. 6(a)) current I is directed to flow in the left- or right-hand branches of the loop according to the instructions given to the

(a) Flip-flop loop.

| $I_w = 0$
 $I_0 = I_1 + I_2$ | $I_w > I_{cc}$
 $I_2 = I_0$
 $I_1 = 0$ | $I_w = 0$
 $I_2 = I_0$
 $I_1 = 0$ | $I_w = 0$
 $I_0 = 0$
 $-I_1 = I_2 = I_{stored}$ |

(b) Cryotron storage loop.

Fig. 6.

Fig. 7. Cryotron shift register.

Fig. 8. Three cryotron-per-bit shift register.

write cryotrons. Once the current has been directed into one of the branches, it will continue to flow down the branch although the write pulse is removed. As long as the branch remains superconducting there will be no energy dissipation in the branch so no redistribution of currents. Read cryotrons in the branches will detect whether a "0" or "1" is stored. This form of loop is extensively used in the associative storage circuits described later. It is also used in the shift register shown in Fig. 7.

The mode of operation of the shift register is as follows: Information is stored in loops I, II, III etc., a 0 or 1 being represented by current flowing along the left- or right-hand branches of the loop. A second series of loops IA, IIA, IIIA etc. are used as dummy stores during the shifting operation. To move information along the register, the "shift to A" lines are pulsed and the information is transferred into the A loops. On pulsing "shift from A" the information moves on into the next storage loop. Although this register requires 8 cryotrons per bit, it has the advantage of simplicity of operation in so far that it requires only alternate pulsing of the "shift to A" and "shift from A" lines.

Storage loops (Fig. 6(b)) differ from flip-flop loops in so far that there is only one write cryotron and one read cryotron. With no write pulse, current into the loop divides between the branches according to the ratio of inductances. On energizing the write cryotron W the current I_0 is forced to flow down the opposite branch. On removing the write pulse, I_0 will continue to flow through this branch as explained previously.
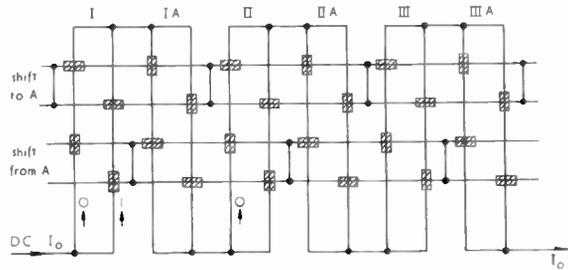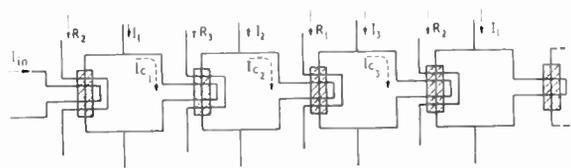
On removing the drive current I_0, a circulating current I_{stored} is induced into the superconducting loop so as to maintain constant the magnetic flux through the loop. This persistent current will continue to flow as long as the loop remains superconducting, and is used to represent a "stored" 1. The presence of the circulating current is detected by the output cryotron R, the control of which forms part of the storage loop.

Newhouse et al.[13] use this form of storage cell as the basis of a three-cryotron-per-bit shift register. As shown in Fig. 8 each cryotron has two independent controls—one of which forms part of the previous storage loop. To move the stored information along requires the application of current pulses to six inputs in the correct sequence. The operating cycle is as follows.

Sequence	Leaving
(i) I_1 on; I_{in} on—I_{in} off—I_1 off	Stored current I_{c1}
(ii) I_2 on—R_2 on, I_{c1} off—I_2 off	Stored current I_{c2}
(iii) I_3 on—R_3 on, I_{c2} off—I_3 off	Stored current I_{c3}
(iv) New information into 1st stage.	

By adding a third cryotron, Haynes[12] has obtained a three-cryotron-per-bit storage cell suitable for a word organized store (see Fig. 9). The storage loop abcd contains the write cryotron W, and the read cryotron R. In addition there is a read-select cryotron RS. To write into the cell the write-select and input lines are pulsed leaving a circulating current in the loop abcd. On pulsing the read-select and sense lines the sense current is forced to flow through the gate film of the appropriate read cryotron. If there is a circulating current in the loop being interrogated then the read cryotron will be resistive and no output
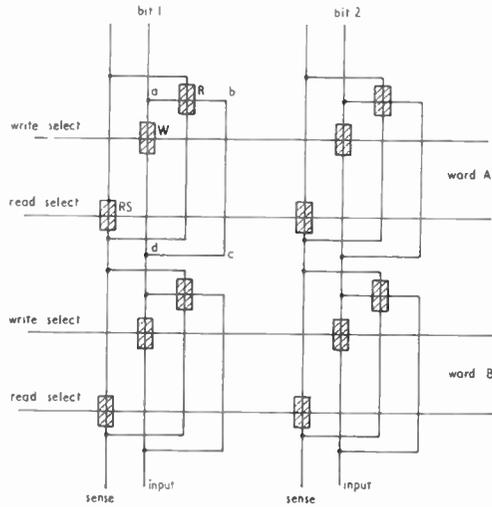
Fig. 9. Haynes' 3-cryotron-per-bit storage cell.

current will appear. The stored information is preserved so non-destructive read-out is obtained.

A considerable number of interesting systems are possible using this basic storage cell. These are described in full in the original paper and will only be listed here.

(i) By connecting the sense and input lines information may be transferred within store, i.e. from word N to word (N+1).

(ii) The addition of two more cryotrons per bit enables triple access to the store, i.e. simultaneous writing-in of one word and reading of two words.

(iii) By suitable interconnection, right or left shifting along a word or to other location in store is possible.

(iv) Counting within store is possible.

(v) The provision of additional reset cryotrons (1 per bit) enables shift register operation to be obtained.

The design principle used in the build-up of systems from the basic storage cell is to provide an alternative current path for the sense current for the case when a stored current, i.e. a 1 is sensed in the storage loop and the read cryotron R is resistive. This alternative path may form the input to a following storage cell and so transfer of information is obtained.

The memory cell described above has been fabricated in large planar arrays by I.B.M.[14]. The reported size of the cell was $0 \cdot 12$ in $\times 0 \cdot 13$ in and the packing density obtained was 40 cells on a 1 in $\times 2\frac{3}{8}$ in substrate. Good reproducibility was claimed and the cycle time was 4 μs.

Slade of the A. D. Little Co. has recently proposed[15] an alternative triple access storage cell using 3 cryo-

trons per bit (Fig. 10). The storage loop abcd contains the enable cryotron E and controls for the read cryotrons R1 and R2. The interrogate lines 1 and 2 form a second pair of controls for R1 and R2. To write into the cell, the enable and write lines are pulsed and a persistent current is stored in the loop abcd of magnitude equal to $I_{cc}/2$ of cryotrons R1 and R2. To read-out, the appropriate interrogate and read lines are pulsed, the current in the interrogate line I_{cc} causing an induced current $I_{cc}/2$ in the loop abcd. The response of the cell upon interrogation depends upon the sum of the cryotron control current as shown in Table 1. When incorporated into a store this cell enables simultaneous reading of two words and writing in of a third. The physical size of the cell is $0 \cdot 025$ in $\times 0 \cdot 05$ in, enabling a packing density of 600 per in^2 to be obtained. Although no cycle time has been given, it will be quite small $\leqslant 1$ μs or so, due to the small physical size and consequently inductance of the device.
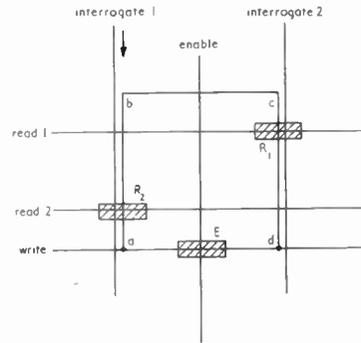
Fig. 10. Triple access storage cell.

Table 1

Response of triple access storage cell

	Interrogate 1			
	R1	R2	R1	R2
I_{stored}	$\dfrac{I_{cc}}{2}$	$\dfrac{I_{cc}}{2}$	0	0
$I_{induced}$	$\dfrac{I_{cc}}{2}$	$\dfrac{I_{cc}}{2}$	$\dfrac{I_{cc}}{2}$	$\dfrac{I_{cc}}{2}$
$I_{interrogate}$	0	$-I_{cc}$	0	$-I_c$
I_{total}	I_{cc}	0	$\dfrac{I_{cc}}{2}$	$\dfrac{-I_{cc}}{2}$
State of cryotron	resistive	superconducting	superconducting	superconducting

5. Associative Stores

Considerable economies are possible in computer programming by the use of associative stores. In conventional random access stores, each word has a

fixed address and the computer program must include these addresses. For large capacity stores, the address itself will be of considerable length, and the rapid extraction of words from within the store will require careful programming.

In the associative store the words are inserted into the first vacant cell within the store, i.e. in a random order. The words are identified by a key which may be formed from a combination of bits within a word. To extract a word from the store, the appropriate key is presented to all the cells simultaneously and an indication of match is obtained. The matching word or words may then be read out as required. This recognition of the key by the cells within the store requires a logical "yes" or "no" decision. In other words, the storage cells must be capable of performing logic as well as storage.
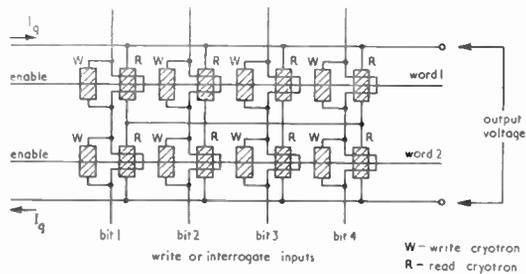

Fig. 11. A cryotron catalogue store.

If the identification key can be varied, the associative store becomes extremely attractive. Suppose, for instance, each word contained information $A+B+C+D+E$, then by changing the key it would be possible to extract all words with identical A, all those with identical B and so on. Alternatively, by changing the key systematically, it would be possible to extract words in a sorted sequence.

Using existing techniques, the associative store is too costly to be seriously considered for present day computers. However, this is not the case with cryotrons. As has been previously shown, cryotrons may perform logic and storage functions, and are consequently ideally suited to the associative store. The question of cost is dominated by the cost of the necessary helium refrigeration and this of course should be no higher than that required for any other form of superconducting store. It is reasonable to suppose therefore that we shall be able to choose between random access or associative superconducting stores purely on performance considerations.

Although an associative store using 1800 wire-wound cryotrons was built by A. D. Little Co. in 1957, the first proposal for a thin film version was not made until 1960[16]. Based on the cryotron storage loop previously described (see Fig. 6(b)), the catalogue

store (Fig. 11) was capable of recognizing words held in storage. Information is written into the cell by pulsing the input and enable lines, bipolar pulses being used to represent 1 and 0. To interrogate, the input lines are activated according to the word it is required to identify within the store. An output voltage is only observed when all the read gates of a particular word are resistive, i.e. when a positive interrogate pulse corresponds to a positive stored current etc.
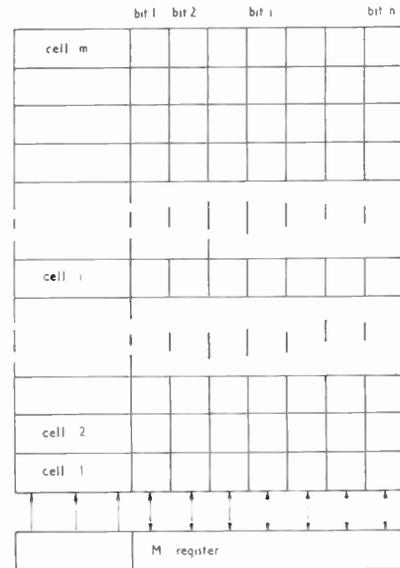

Fig. 12. Block diagram of associative store.

A more advanced associative store has been developed by A. J. Learn of the Space Technology Laboratory and has been described in papers by Davies[17] and Maquire[18]. A block diagram of the store is given in Fig. 12. Each cell consists of a control module and N data bits. The control module controls the writing, comparing and reading between the M register and the cell. A word to be stored is placed in the M register and simultaneously transmitted to all cells along vertical data lines. The first empty cell is selected by signals from the control module which then sends a signal along this cell causing the transmitted data to be stored. To select a word the appropriate key is placed in the M register and transmitted to all cells together with enabling signals which constitute the key. Comparisons are performed in each cell, and when a match is obtained, a signal is sent from the appropriate control module to the M register. A returning signal from this register to the appropriate cell causes the word to be transferred out of the cell to the register. The read-out may be non-destructive or destructive as required.

The cryotron store bit element is shown in Fig. 13(a). A 1 is represented by a stored current in the loop pqrs, a 0 by no stored current. To write into the loop, lines Vi Wj are pulsed, a circulating current being established in the manner shown in Fig. 6(b). The comparison current consists of line Ci and Ej. Current on Ej and Wj lines corresponds to the key in the M register. If a 1 is stored, the nett current on the line pq will be zero when $I_w = 1$, i.e. cryotron 2 is superconducting. When there is mismatch 2 will be resistive. Thus line Ci will only be superconducting when there is match between words in the cell and M register. The function of the enable lines Ej is to select what part of word to use as key. Read-out of identified word is now obtained by pulsing Ri and Oj. If a 1 is stored then cryotron 5 will be resistive as well as cryotron 4 and so there will be a voltage across the cell indicating a 1 stored.
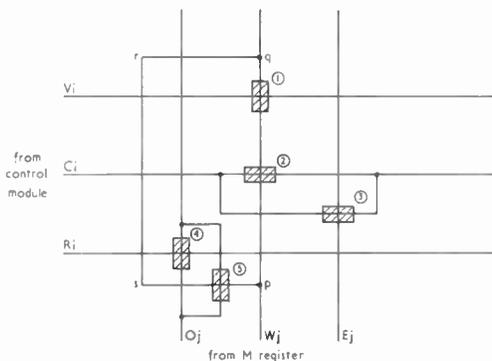
(a) Cryotron storage bit.
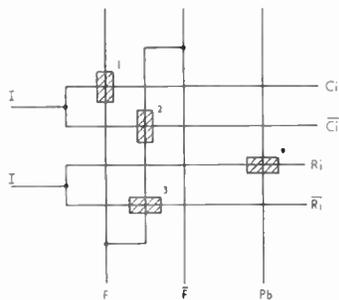
(b) One stage of F(Ci) control module.

Fig. 13.

The control module interprets the signals on the Ci line and produces the appropriate Vi and Ri signals. Although full details of the control modules are given in the original paper only a small part, namely the F(Ci) network for turning on Ri corresponding to the first Ci that is on, is shown in Fig. 13(b). The vertical lines F, $\bar{F}$ and Pb pass through all the control modules, the horizontal lines Ci, $\bar{Ci}$, Ri and $\bar{Ri}$ pass along the words through the memory bit elements. The sequence of operations is as follows—line Pb is pulsed to reset

the Ri's then F is pulsed. If Ci is off, cryotron 2 is resistive, cryotron 1 is superconducting and no current flows from F to $\bar{F}$. When Ci is on cryotron 1 is resistive, 2 is superconducting and current flows from F to $\bar{F}$ making cryotrons 3 resistive and directing current from $\bar{Ri}$ to Ri.

The complete control module uses 9 cryotrons and there are 5 cryotrons per storage bit element. It has been estimated, on the basis of the cryotron time-constants, that the access time to the store would be approximately 300 ns.

Descriptions have recently been given of two types of associative stores developed by I.B.M. Seeber[19] reported on an associative self-sorting store and more recently Seeber and Linquist[20] have reported on an associative store with ordered retrieval. In the self-sorting store words enter in random order and are then placed in proper relationship to previously sorted words. The functions that such a store must be capable of performing are

(i) comparison between word in entry register and words already in store to decide high-equal-low status,

(ii) insertion of entry word between high and low words already in store,

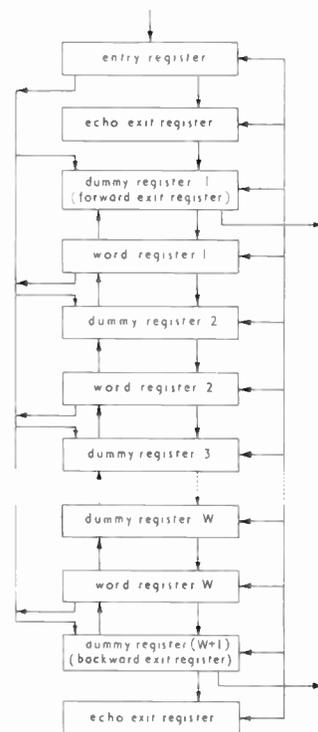(iii) moving up of all high words to accommodate the new word.

Fig. 14. Self-sorting associative store—block diagram.

To enable the insertion of a new word into the store between words already there it is necessary to provide dummy registers between the main registers.

A block diagram of the store is shown in Fig. 14. The comparison circuits from the entry register extend through all the word registers and indicate the status of word with respect to word in entry register. On first half of cycle the entry word is moved into dummy register appropriate to its position in memory and all words above selected dummy registers move up into higher dummy registers. On next half cycle a new word enters entry register and the words in the dummy registers move up into main registers. When the store fills up, words are passed out through an exit register which remembers the word just ejected. An alternative mode of operation is possible which allows inverted sorting and the ejection of words from the bottom of the store.

The basic storage loop used is the flip-flop type described in Section 4. Comparison and shifting circuits are provided and the complete bit register with dummy register is shown in Fig. 15. A stored 1 is represented by a current down the left-hand branch of the storage loop and 0 by the right-hand branch. Information may be written into the dummy register using the select and entry lines. Transfer of information from the word register to the dummy register is achieved by activating the "dummy in" and the
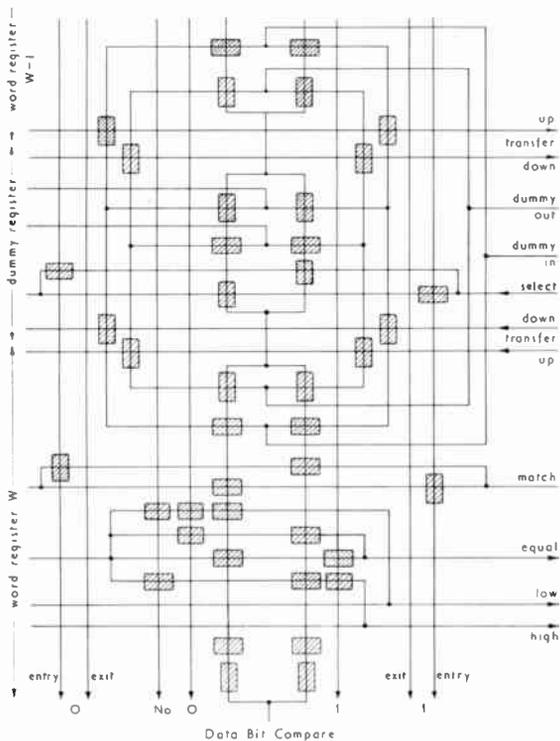

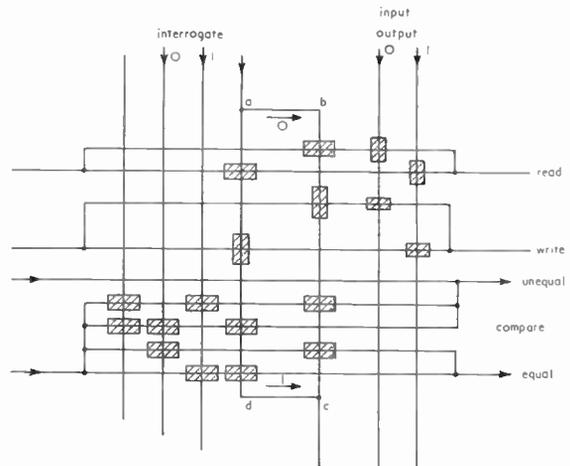Fig. 15. Self-sorting associative store—cryotron storage cell.

Fig. 16. Data tag storage cell for associative store.

appropriate transfer lines depending upon whether the information is moving up or down the store. In a similar manner the information may be read out of the dummy and transferred to the word register. The selection of the appropriate dummy register for the insertion of an entry word is determined by the equal/low/high matching circuits. Assuming an equal comparison has been made on the previous bits in the W word register so that a current flows along the equal line, then if we compare a 0 in the entry register with a 1 stored in the W register the current will come out along the high line. This indication of the status of the word is used to control the insertion of the entry word into the store. Details of the cryotron circuits used in the entry and transfer systems are also given in the original paper.

The associative store described by Seeber and Linquist[20] has facilities for the ordered retrieval of information held within the store. Starting with the left-hand bit of the word key, a systematic search is made to determine the lowest ranking word within the store. Successively higher words are then identified one by one. The word registers consist of a series of data tag cells—one per bit, together with a vacancy bit at the front of the word and a register select control at the end. The mask register selects that portion of the word in the interrogation register that forms the word key. This key is then compared with words held in storage, and if equality is established the comparing current will flow out on the appropriate equal line. The particular word will then be read out or read in as the case may be. The vacancy bit register indicates whether word register is occupied or vacant.

The basic data-tag cell of the store having write, read and comparison circuits is shown in Fig. 16. A flip-flop storage loop abcd is used, the current flow for a stored 1 and 0 being as indicated. The status

indication in this case is merely an equal/unequal decision.

Performance figures of an experimental associative store have recently been given by Newhouse and Fruin[21]. The store had a capacity of 3 words of 3 bits and facilities for comparison, and read-out of the matching word. Eighty one crossed film cryotrons having crossing ratios of $W_g/W_c = 30$, were used and switching tests indicated that the loop time-constants were ~ 5 µs. Considerable reduction in time-constant would be expected by the use of smaller cryotrons, and it was suggested that a 300 000 bit store might have a 50 µs comparison cycle time.

6. Technical Feasibility

The cryotron is unique among computer components in so far that with this one component, one can, in principle, perform all the necessary logic and storage functions. In addition, the device is intrinsically cheap, small and capable of high speed and reliability. Before it becomes commercially attractive, however, these advantages have to be sufficient to offset the great disadvantage of the low temperature environment required.

How great a burden in this requirement of a low temperature environment? At the present moment, a closed-cycle helium refrigerator capable of providing 1 watt of refrigeration at $4 \cdot 2°$ K costs in the region of £20,000. It seems likely that it would be necessary to have two such refrigerators associated with each cryoelectric computer. One would be used for cooling while the other would be used in an emergency and during servicing. In a year or two's time when the demand for such cooling units has increased, it is likely that the refrigerator costs will have dropped to about £10,000 per unit or £20,000 per computer. This high outlay could only be carried by a computer of large size. For instance, it is thought that a cryoelectric store only becomes economically attractive when its size is above 50 000 words or so. Of course economic considerations are not the only ones, since a user is generally prepared to pay for speed and size, both of which are offered by the cryoelectric devices.

The question still remains as to whether the cryoelectric computer is technically feasible. In an attempt to answer this question some of the outstanding problems will be considered, and indications given of their likely solution.

6.1. Fabrication

One of the major problems associated with the fabrication of these devices by vacuum-coating techniques is that of obtaining the required accuracy of pattern registration and line definition. On the materials side, trouble is being experienced with the dielectrics which must be thin, pinhole free and stable.

Most thin films prepared by vacuum-coating techniques possess large built-in stresses which may, in certain circumstances be sufficient to cause cracking or buckling of the films. Dielectric films have been found to be particularly susceptible to this stress relief which may be triggered off by atmospheric moisture or mechanical shock. Much effort is being devoted to understanding these effects which appear to be one of the major keys to successful device fabrication. New technologies and materials are constantly being developed, and there is no reason to doubt that large-scale automatic production of these planar arrays will be possible in the near future.

6.2. Heat Dissipation

As shown by Sobol[9], heat dissipation in the cryotron has a direct influence on the permitted packing density, pulse repetition frequency and duty cycle. It is not yet known how much of a restriction this will be, much work needs to be done both on the material, the device, and the systems side.

6.3. Circuit Problems

Due to the low impedance levels involved, the problem of terminating drive lines etc. becomes difficult and in complex circuits, unwanted reflections may prove troublesome. On the output side, for satisfactory signal transfer the output cryotrons must be matched to the transmission lines. In-line cryotrons, with their adjustable resistance are ideally suited to this purpose.

All interconnections within a circuit must be kept as short as possible to minimize the time-constant and this consideration will have to be borne in mind by a systems designer. The problem of interconnections between planes of cryotrons is particularly difficult since the inductance of a short length of screened cable is several orders of magnitude greater than the inductance in a cryotron circuit. Techniques using transmission lines along the edge of the planes may have to be used.

Few of these engineering and design problems have yet been tackled. They are obviously difficult ones—but we do not believe insoluble.

6.4. Reliability

From the reliability point of view one can reasonably expect a long life-time provided the cryoelectric assembly can withstand the initial thermal shock associated with cooling to low temperature. Subsequent warming to room temperature should be avoided if possible.

The possibility of plane failure must be considered. Repair of a faulty section is out of the question while the replacement of a faulty plane would be technically very difficult. A more acceptable solution would be to

provide a number of spare circuits within the assembly and to switch these in as required. In the event of a major failure involving many circuits, it is probable that the whole assembly would be thrown away and replaced by a new one.

7. Conclusions

The cryotron circuits discussed above illustrate most forcibly the great versatility of the cryotron as a computer component. It is difficult to comment on the switching speeds of these circuits since, as explained above, this is largely an L/R limitation and consequently will largely depend upon the precise geometrical configuration and dimensions of the circuit. Suffice it to say that the circuit speeds should be well into the submicrosecond region. With the possibility of an integrated logic and storage system, information path lengths, and consequently transit times will be considerably reduced, and this in turn will be reflected in a decrease in overall computing time.

Many technical difficulties remain to be overcome before the full potentialities of these devices may be exploited. Although many of these problems are being tackled, much remains to be done, and a considerable effort is required to bring the cryoelectric computer into fruition.

8. References

1. D. A. Buck, "The cryotron—a superconductive computer component", *Proc. Inst. Radio Engrs*, **44**, p. 482, 1956.

2. M. L. Cohen, "A 6 megacycle cryotron ring oscillator", *Proc. Inst. Radio Engrs*, **49**, p. 371, 1961.

3. P. M. Chirlian, "Phase inverters using controlled superconductors", *Proc. Inst. Radio Engrs*, **49**, p. 1574, 1961.

4. P. M. Chirlian, "On the linear circuit aspects of cryotrons", *Proc. Inst. Radio Engrs*, **49**, p. 1326, 1961.

5. D. R. Young, "Superconducting circuits", "Progress in Cryogenics", Vol. 1, p. 1. (Heywood, London, 1959).

6. E. H. Rhoderick, "Low temperature storage elements", *J. Brit.I.R.E.*, **20**, No. 1, p. 37, January 1960.

7. J. M. Lock, "Superconductive switching", *Reports on Progress in Physics*, **25**, p. 37, 1962.

8. W. B. Ittner, "Thin film cryotron time constants", 1960 Symposium on Superconductive Techniques for Computing Systems, p. 239, (Washington D.C.—Office of Naval Research).

9. H. Sobol, "Time average thermal properties of a computer utilizing thin-film superconducting elements", *Trans Inst. Radio Engrs (Electronic Computers)*, EC-11 p. 200, April 1962.

10. D. R. Young, "Recent developments in high speed superconducting devices", *Brit. J. Appl. Phys.*, **12**, p. 359, 1961.

11. R. B. De Lano, "Edge effects in superconducting films", *Solid State Electronics*, **1**, p. 381, 1960.

12. M. K. Haynes, "Cryotron storage, arithmetic and logical circuits", *Solid State Electronics*, **1**, p. 399, 1960.

13. V. L. Newhouse, J. W. Bremer and H. H. Edwards, "An improved film cryotron and its application to digital computers", *Proc. Inst. Radio Engrs*, **48**, p. 1395, 1960.

14. J. P. Beesley, "An evaporated film 135-cryotron memory plane", International Solid State Circuits Conf., 1961, p. 108.

15. A. E. Slade, "A cryotron memory cell", *Proc. Inst. Radio Engrs*, **50**, p. 81, 1962.

16. A. E. Slade and C. R. Smallman, "Thin film cryotron catalogue memory", *Solid State Electronics*, **1**, p. 357, 1960.

17. P. M. Davies, "A simplified superconductive associative memory", Private Communication, 1962.

18. T. Maquire, "Superconductive computers—common-place in ten years", *Electronics*, **34**, No. 47, p. 45, 24th November, 1961.

19. R. R. Seeber, "Associative self-sorting memory", *Proc. Eastern Joint Computer Conference*, **18**, p. 179, 1960.

20. R. R. Seeber and A. B. Linquist, "Associative memory with ordered retrieval", *I.B.M. J. Res. and Develop.*, **6**, p. 126, 1962.

21. V. L. Newhouse and R. E. Fruin, "Data addressed memory using thin cryotrons", *Electronics*, **35**, No. 18, p. 31, 4th May 1962.

Communications Developments

The Commonwealth Telecommunications Board

Mr. Dawson Donaldson, B.Sc., M.I.E.E., formerly Director General of the New Zealand Post Office, took up the post of Chairman of the Commonwealth Telecommunications Board on 1st December last. He succeeded Sir Ben Barnett, K.B.E., C.B., M.C., who had served in this capacity for over six years, having previously been Deputy Director General of the British Post Office.

The Commonwealth Telecommunications Board was set up in 1949, as a result of the Commonwealth Telegraphs Agreement, 1948, "for the purpose of promoting the efficiency and development of the external telecommunications of the British Commonwealth and Empire". The Board is composed of representatives of the Partner Governments with an independent Chairman. Its present members represent Britain, Canada, Australia, New Zealand, India, Ceylon, Malaya and Rhodesia and Nyasaland; there is also a member for Commonwealth territories not otherwise represented, and new members are due to be appointed by Cyprus, Nigeria and Ghana. Other independent Commonwealth territories have been invited to join the partnership and appoint members.

The Secretary-General of the Board is Mr. William Stubbs, C.B.E., M.C. (Member) whose appointment to this post in 1961 was announced in the June 1961 *Journal*.

London's New Radio Tower

The 580 ft high radio tower now under construction for the Post Office off Tottenham Court Road, has reached a height of 380 ft and is easily visible from the upper storey of the Institution's headquarters in Bedford Square which is about a quarter of a mile distant. The tower is being built by the Ministry of Public Building and Works and should go into service in January 1965.

The tower will add an impressive new feature to London's skyline. It will carry aerials and equipment for new trunk and television microwave links and should be high enough to ensure unhindered line-of-sight paths to avoid obstruction from the many tall buildings now going up or projected in the London area.

A revolving public restaurant near its top, at a point about 520 ft above ground level, will give customers a remarkable panoramic view of London. It will make a complete revolution in about half an hour. There will also be public observation galleries.

A constructional problem that had to be overcome is that the tower must be so rigid that even in the strongest winds the upper section, where the directional aerials for the television and telephone services

will be built, will not tilt more than one-third of a degree from the vertical. An internal hollow reinforced concrete shaft, tapering from 22 ft in diameter at the top to 35 ft at the bottom, provides the main stability of the tower. This shaft will contain the high speed lifts, the ventilation ducting and the service cables to the television and telephone equipment. The stability of the tower is assisted by a bridge deck, 80 ft above ground, connecting with the main building —the extension to the Museum Telephone Exchange.

From just above the main building sixteen floors providing accommodation for equipment will be built into the section between 115 ft and 355 ft above ground. The lower three floors provide accommodation for the high velocity ventilation plant. The remainder will house the microwave and associated apparatus. The floors are of reinforced concrete and are cantilevered out from the main shaft. The outside covering of the tower will be glass—50 000 square ft. From 355 ft to 477 ft above ground level there will be the section which provides the platforms for the main horn and dish-shaped aerials. The platforms are not enclosed so that there will be no interference with the transmission beams.

The restaurant and observation floors will be between the heights of 477 ft and 548 ft. The main shaft will rise a further 31 ft in order to provide lift over-run motor rooms and control gear. Crowning the structure will be a latticed tower approximately 40 ft high designed to carry additional aerials and meteorological instruments.

Construction work will start this summer on a similar tower—500 ft high but without restaurant and observation floors—in Birmingham, which is expected to come into operation towards the end of 1965. Its capacity will be 150 000 telephone channels and 40 television channels. A model is on show at the Royal Academy's Summer Exhibition.

Data Transmission in Technical Publications

The technical publications group of an American missile manufacturer, the Martin Company in Denver, uses high-speed data transmission techniques to transmit changes in technical manuals over telephone lines at 1000 words per minute. The changes are received on 8-channel paper tape in form for printing on lithographic matrixes. This permits rapid off-set reproduction and prompt distribution of the changes to all holders of the manuals. This new rapid communications system has made it possible to transmit changes in technical and operating data, from engineering through publications and into manuals, in a few hours. It is stated that similar terminals, developed by the Digitronics Corporation, are currently operating in over 100 installations in 40 cities in the United States, Canada and Great Britain.

An Investigation into the Acoustic Noise produced by the Ferrite Core used in Television Line Output Transformers

By

J. C. MacKELLAR,

(Associate Member)†

Summary: Details are given of the measurement of the acoustic noise produced by a line output transformer and polar diagrams are shown of the sound pressure around the core.

It is shown that in the region of the television line frequency, 10·125 kc/s, the core can resonate in a flexural mode giving extreme levels of noise. A detailed analysis is given of the radiation diagrams produced from a vibrating face of the core and from this information the relationship between flux density B and fundamental strain is found. Methods of clamping and glueing the core are suggested in order to reduce the noise from the core due to flexural resonance.

Finally, attention is drawn to new materials developed in conjunction with this work, which produce very little magnetostrictive strain over the flux density range in which the core is operated. Measured results of flux density against fundamental strain are given for these materials and existing materials.

List of Symbols

a width of piston source (cm)

b length of piston source (cm)

c velocity of sound (cm/s)

d separation of point sound sources (cm)

E modulus of elasticity in tension or compression

f frequency

I second moment of area about neutral axis

L effective length of beam (in)

M_B mass of beam (lb)

P sound pressure (dynes/cm²)

R distance from vibrating surface (cm)

ρ_0 density of air (g/cm²)

λ wavelength (cm)

v_0 maximum velocity of vibrating surface (cm/s)

ω angular frequency

x distance from centre of piston along major axis

1. Introduction

Over a long period there have been complaints of the high-pitched whistle produced by a television receiver operating on the 405 line standard. At one time or another practically all the parts of the receiver handling the high energy needed for the horizontal deflection at 10·125 kc/s were suspect as sources of the noise. Various investigations carried out in different industrial laboratories isolated the core of the horizontal (line) output transformer as the prime source. All agreed that the results obtained were

† Mullard Research Laboratories, Redhill, Surrey.

extremely confusing. Many people found ways of quietening the line transformer by cut-and-try methods but complaints continued sporadically. It was by no means clear whether the noise was generated by magnetostrictive movement of the core or by compression and relaxation of the gapping material due to the halves of the core acting as electromagnets. Certainly no correlation could be found between the noise produced by transformers and the currently available magnetostrictive coefficient figures for the core material.

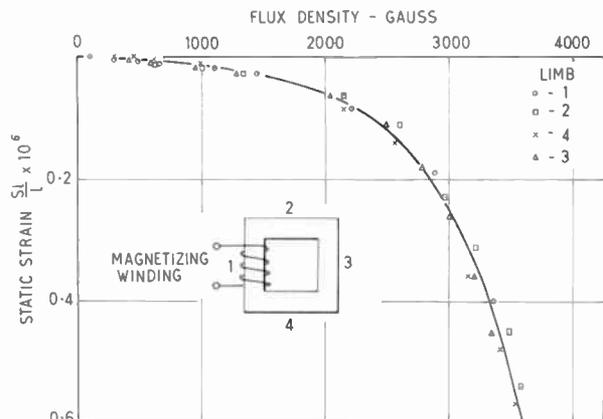Fig. 1. Static strain curve.

It was first established by static measurement that magnetostriction could be a contributing factor in determining the intensity of the noise produced by the core. A curve showing the strain produced by a given flux density for two FX 1412 U cores joined with synthetic resin glue is shown in Fig. 1. This curve was measured statically by means of a differential capacitor bridge.
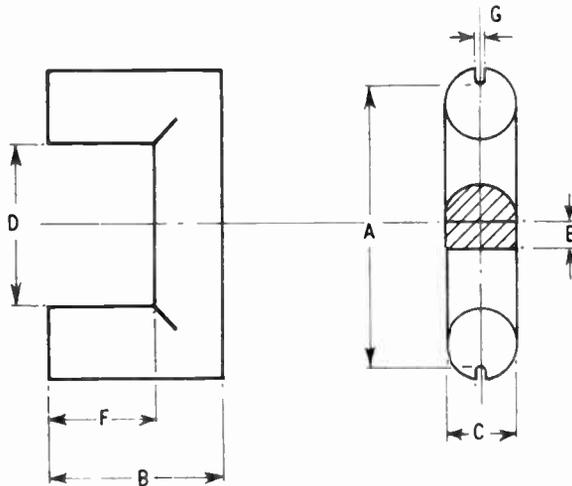
Fig. 2. Dimensions of U cores.

Table 1

Dimensions of U cores FX 1412, FX 1442, FX 1452 and experimental core.

Type	A	B	C	D	E	F	G
FX 1412	60·3	31·8	15·89	38·1	5·07	19·05	4·76
FX 1442	53·7	23·8	11·36	37·6	3·96	15·89	3·17
FX 1452	56·7	29·4	13·75	37·0	6·56	17·8	3·56
Exptl Core	49·5	28·4	15·9	27·5	6·5	16·0	4·7

Dimensions in millimetres

The next step was to measure the behaviour of the core operating as if in a line output transformer. Dynamic measurements of such small amplitudes are extremely difficult to make at frequencies in the order of 10 kc/s. For this reason it was decided to investigate the problem acoustically.

It was first definitely established by preliminary experiments that the majority of this noise was associated with the core of the line output transformer, and for this reason this paper will be primarily concerned with the ferrite core and the process by which excessive noise is generated.

The three most widely used cores are types FX 1442, FX 1452 and FX 1412. A drawing of these cores is shown in Fig. 2. Table 1 gives the dimensions of each.

The line output transformer is normally operated in the circuit shown in Fig. 3. Under these conditions the ferrite core is magnetically biased due to the mean current of V_1 flowing through N_{4-5} turns. The core is also taken through a magnetic cycle at line frequency.

Calculations show from a number of designs that the core is magnetically biased to a flux density of 1000 gauss, the alternating component has a peak to peak value of 2000 gauss.

3. Experimental Measurement of Acoustic Noise

The sound pressure at a certain distance from a television set when operated under normal conditions is made up of a large number of components due to multiple reflections. These reflections not only occur within the cabinet, but also within the room in which the set is being used. Since the frequency of the noise is relatively high the interference pattern set up will be very complex, making measurements under these conditions impossible.

In order to study the acoustic radiation from the transformer without interference from multiple reflections an anechoic enclosure was used.

3.1. *Anechoic Enclosure Design*

The design of the anechoic chamber can be relatively simple because of the frequency being considered. The object when designing an echo-free enclosure is to prevent reflections from the walls. This was achieved by the use of a wedge-form of construction. "Tentest" boarding of $\frac{1}{2}$ in. thickness provided the most convenient material to be used for the wedges.

If the enclosure is free from reflections the sound pressure from a simple point source, i.e. a source small compared with the wavelength at the frequency being considered, will drop by 6 dB each time the distance from the source is doubled. Any cyclic irregularities in this curve will indicate the presence of standing waves and thus give a direct indication of the performance of the enclosure. Figure 4 shows two such curves taken at 10 and 7 kc/s. From these curves it can be seen that, although the enclosure is not entirely free from reflections at 10 kc/s, these are small and the performance of the enclosure within the frequency range 7 to 10 kc/s and higher is adequate for
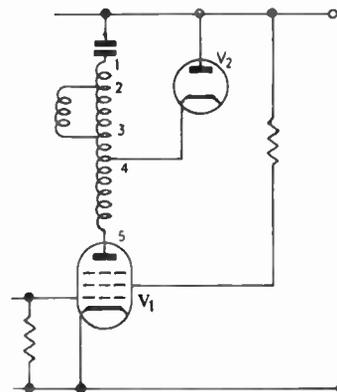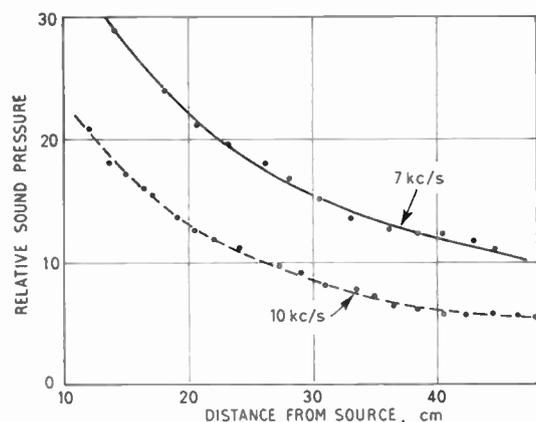

Fig. 3. Basic line output circuit.

Fig. 4. Relative sound pressure distribution in anechoic enclosure.

an investigation of this type. The overall size of the enclosure was $4\,ft \times 3\,ft \times 3\,ft$, thus enabling small assemblies to be measured.

3.2. *Auxiliary Equipment*

The threshold of hearing at 10 kc/s, according to measurements made at the National Physical Laboratory,[1] is 20 dB above 0.0002 dynes/cm^2 sound pressure. The apparatus should enable measurements to be made as near to this level as possible and should at the same time have a good frequency response at 10 kc/s and above. The microphone should also be of small size to prevent disturbances of the sound field under measuring conditions.

A block diagram showing the method of measurement is shown in Fig. 5. The transformer was mounted on a rotatable shaft so that the polar distribution of sound pressure around the core could be measured.

The magnetizing winding was fed from a sinusoidal voltage together with a d.c. polarizing current. This arrangement was adopted for the following reasons.
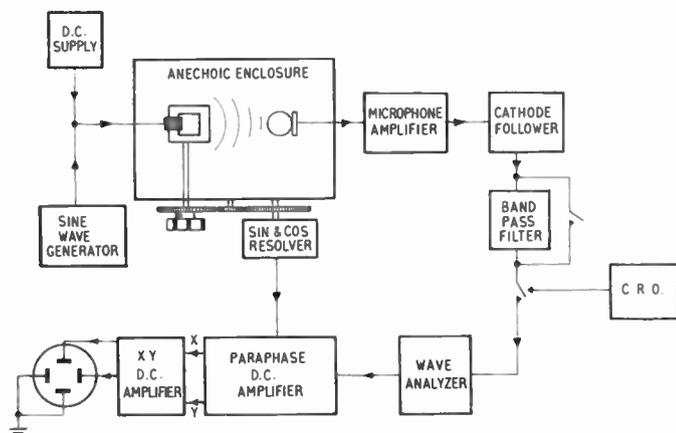
(a) The large voltage pulse produced during the flyback stroke in a normal time-base circuit can easily be detected directly by the measuring apparatus, thus giving false measurements.

(b) Additional noise not associated with the ferrite core might be produced by electrostatic forces during the flyback stroke; this could also lead to inaccuracy when measuring the noise from the core itself.

(c) It is necessary to investigate the frequency dependency of the noise. This would be difficult with an energy recovery time-base circuit at the same time keeping the flux swing constant.

It was felt early in the investigation that a quicker and more direct display of the polar distribution would be more revealing and save considerably in the time spent taking radiation diagrams manually. With this facility in view a polar plotter was built.

3.2.1. Polar plotter

The most direct approach to plotting automatically the radiation diagram around the transformer is to display the sound pressure polar diagram directly on a long persistance display tube. The circuit which achieves this is shown in Fig. 6. The output voltage from the wave analyser, V_{dc} which is directly proportional to sound pressure is applied to the first valve V1 which is a cathode-coupled paraphase amplifier. The potentiometers RV1 and RV2 are included to enable the initial balance of the system to be adjusted; RV3 is a sine and cosine resolver potentiometer which is geared by a 1 : 1 ratio to the shaft on which the transformer under test is mounted.

Under no-signal conditions, i.e. $V_{dc} = 0$ the points A, B and C are all at earth potential. When the shaft is rotated zero voltage is fed to the balanced d.c. amplifiers and only a spot is obtained on the display tube. This condition represents initial balance and is adjusted by RV1 and RV2.
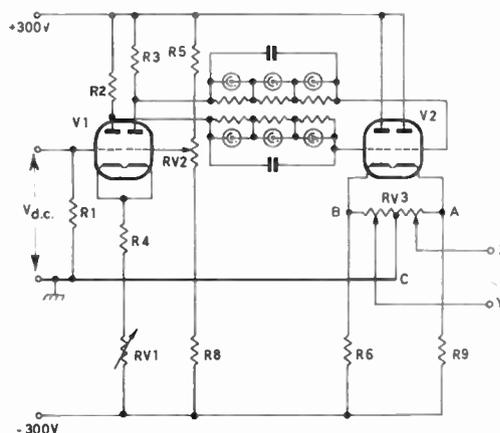

Fig. 5. Block diagram of measuring apparatus.

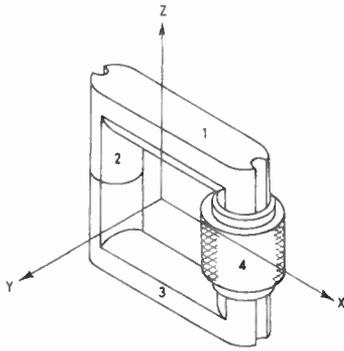Fig. 6. Circuit of d.c. paraphase amplifier.

Fig. 7. Typical line transformer core.

When a voltage is applied to the grid of V1 the points A and B go above and below earth respectively. The degree of unbalance is dependent on the amplitude of V_{dc}.

The voltage developed across the sine and cosine receiver potentiometer RV3, due to the input voltage V_{dc}, is resolved into two components $V \cos \theta$ and $V \sin \theta$, θ being determined by the angular position of the transformer. These two components are then fed to the balanced d.c. amplifiers and hence to the X and Y plates of the display tube. Rotation of the shaft on which the transformer is mounted results in the polar distribution of sound pressure around the transformer being displayed directly without any intermediate operations.

This facility considerably helped to eliminate the long and tedious process of plotting polar diagrams manually.

4. Analysis of Core Vibration

Before considering the fundamental factors on which the intensity of the sound depends, it was decided to investigate the way in which the noise varies with frequency. The reason for this becomes obvious when the shape of the core is considered. Because the core is a relatively complex structure, it is conceivable that different modes of mechanical resonance could exist within the audible range. Any resonant effects could make correlation between sound pressure and the magnetic conditions under which the core is operated extremely difficult.

The object of this part of the work was to determine the types of mechanical resonance which occur within the audible range, particularly at or near the television line frequency of 10·125 kc/s.

4.1. Radiation Diagram Analysis

Because the dimensions of the core are comparable with the wavelength in air at the frequencies concerned, the polar diagram of sound pressure around the transformer will change appreciably with frequency.

To show this effect a simple analysis can be carried out by considering the transformer core in Fig. 7. If the radiation in the YZ plane is considered, then the two limbs, 1 and 3 can be considered as being equivalent to two sound sources in antiphase.

If these sources are represented by A and B in Fig. 8, then the far field polar diagram can be found as follows.
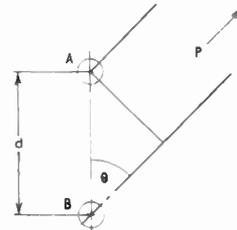

Fig. 8. Simplified representation of a line transformer as a sound source.

Consider a point p at a distance large compared with d so that rays from A and B can be considered as being parallel.

From Fig. 9, path difference $= d \cos \theta$.

therefore phase difference $= \dfrac{2\pi d \cos \theta}{\lambda}$

total phase difference $= \pi - \dfrac{2\pi d \cos \theta}{\lambda}$

If P_p is the sound pressure produced by A or B at point p considered separately, the resultant pressure $P_{p'}$ due to the vector sum of the radiations from A and B will be

$$P_{p'} = 2P_p \cos \left(\frac{\pi}{2} - \frac{\pi d \cos \theta}{\lambda} \right) \qquad \ldots\ldots(1)$$

The shape of the polar diagram will be given by

$$\cos \left(\frac{\pi}{2} - \frac{\pi d \cos \theta}{\lambda} \right)$$

This function is plotted in Fig. 9 for different frequencies. Photographs are also shown in Fig. 10 of the sound pressure polar diagram taken experimentally from the polar diagram display for an FX 1412 core in the Y Z plane.

When a bar of material is stressed longitudinally a tensile strain is produced in the same direction. Similarly a compressive strain is also produced in every direction perpendicular to the initial stress. The ratio of lateral strain/longitudinal strain, known as Poisson's ratio, could be the cause of the side-lobes present in the photographs which are not accounted for in the above analysis. The integrated sound pressure produced by lateral vibrations of this type would result in a radiation along the Y axis.

The above analysis, although over-simplified, does clearly show that in order to measure the relationship

between frequency and amplitude of vibration without very complicated measurements and calculations entering into the analysis, it is necessary to overcome the marked change in the polar distribution of sound pressure with frequency.

For the above reason it was decided to measure the radiation from one face of the transformer core without interference from other parts of the structure. This was achieved by acoustically screening all parts of the core except the face from which the radiation was being measured. This was done by covering the core with fibre glass and acoustic tiling, the whole assembly was then mounted in a small box. The

surface from which the radiation was being measured was not screened. With this technique not only is it possible to simplify considerably the analysis of the radiation diagram, but more important, it is possible to determine the way in which the core is moving from the shape of the radiation pattern produced.

4.2. *Analysis of Radiation from Piston Source*

With the above arrangement of mounting, the radiation can be considered as being the same as that produced by a piston moving in an infinite baffle.

The sound pressure P from a rectangular piston, all points of which are moving with the same amplitude
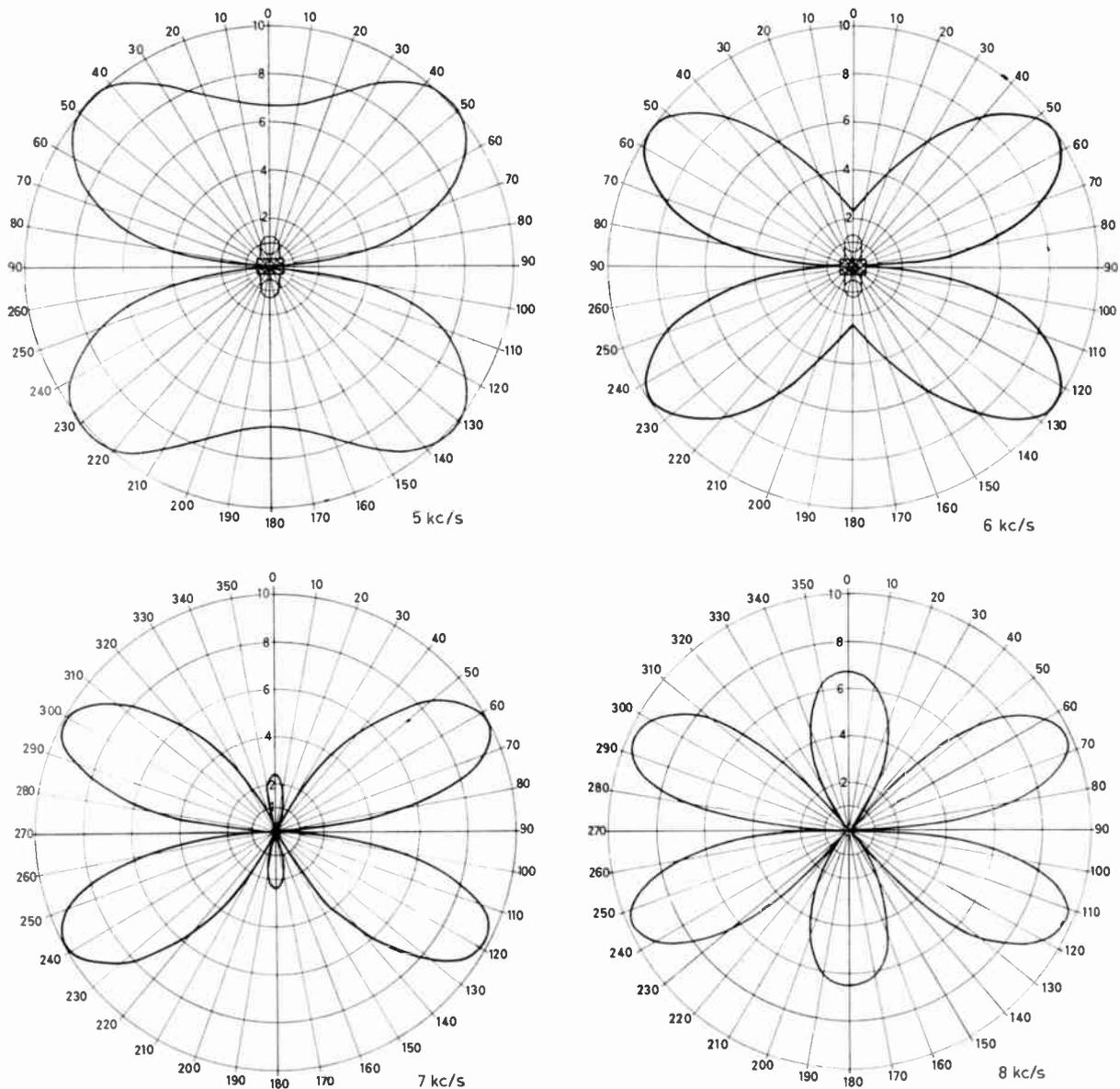

Fig. 9. Calculated radiation diagrams from simplified sound source.
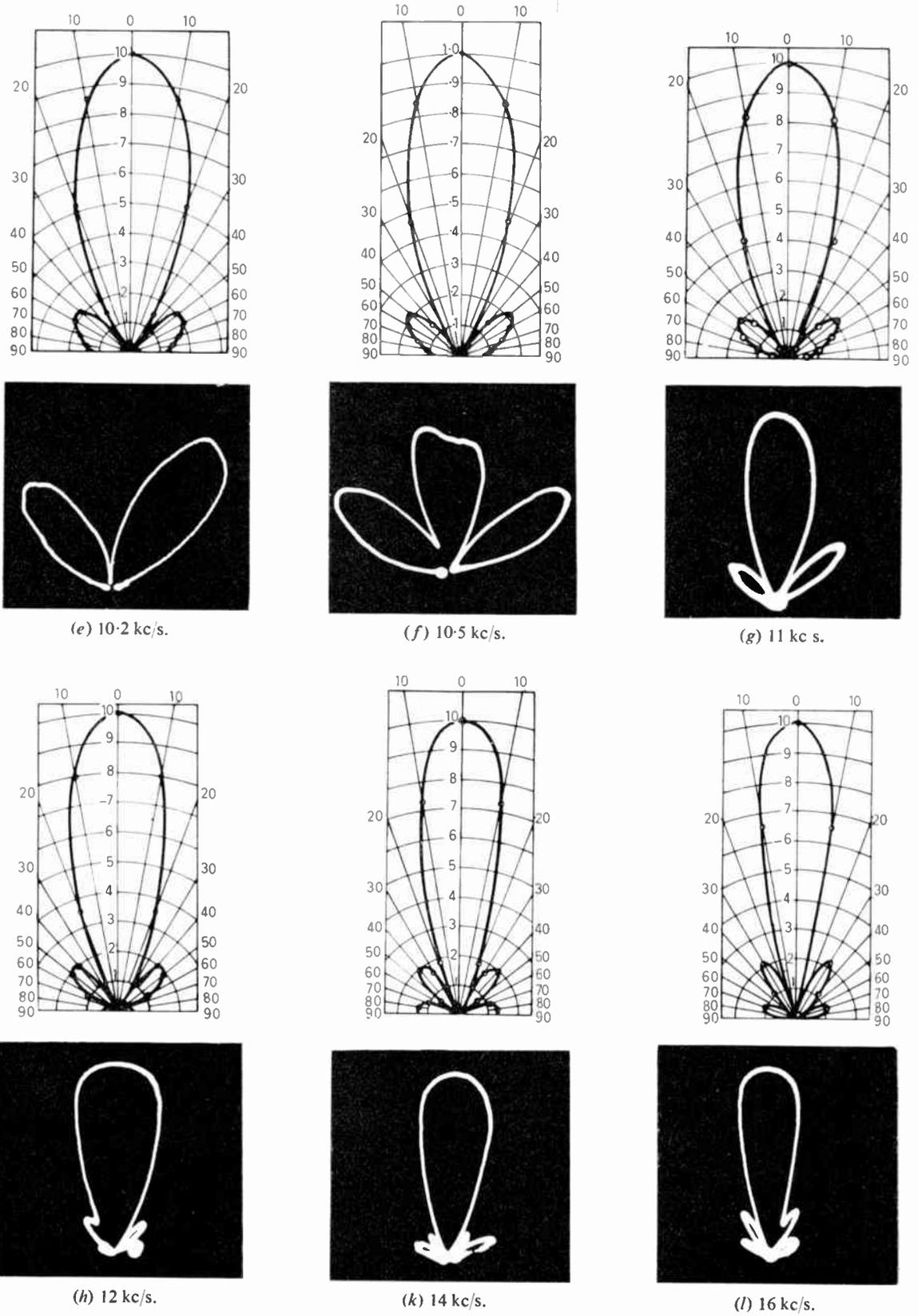
(e) 10·2 kc/s.

(f) 10·5 kc/s.

(g) 11 kc s.

(h) 12 kc/s.

(k) 14 kc/s.

(l) 16 kc/s.
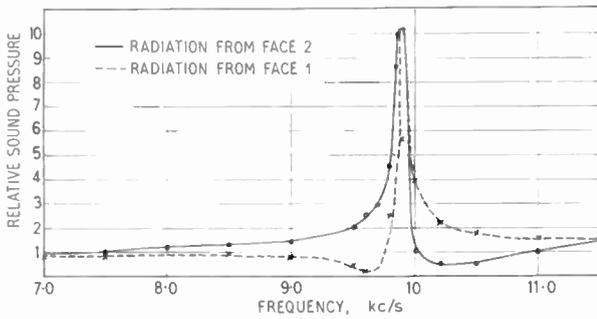
Fig. 12. (contd.) Radiation diagrams from piston source.

Fig. 13. Sound pressure from piston source.

γ is defined in a similar way only this time the YZ plane is considered.

If only the radiation in the XZ plane is required then γ in equation (3) will be $\pi/2$ for all values of α. Thus the radiation sound pressure reduces to

$$P_p = \frac{ja b \omega \rho_0 v_0}{2\pi R} \exp j\omega \left(t - \frac{R}{c}\right) \frac{\sin\left(\frac{\pi b}{\lambda}\cos\alpha\right)}{\frac{\pi b}{\lambda}\cos\alpha} \quad \ldots\ldots(4)$$

The first term gives the instantaneous value of the sound pressure at time t, the second term gives the shape of the polar diagram in the XZ plane. This function is plotted in Fig. 12 for frequencies between 7 kc/s and 16 kc/s. Also shown are photographs of the sound pressure distribution taken experimentally from limb 1 of an FX 1412 core, the two halves glued together with a synthetic resin glue.

For these measurements the flux swing was 2000 gauss peak to peak, and the d.c. component was maintained constant at 1000 gauss, thus simulating the actual flux conditions found in a conventional type of line transformer.

A comparison of the two displays reveals some very interesting results. In the region of 10 kc/s there is a considerable discrepancy between the calculated and experimental results. Above and below this frequency however, it can be concluded that the face of the core from which these photographs were taken is vibrating essentially in an extensional mode, i.e. the amplitude and phase along its length are constant. In the region of 10 kc/s this is not the case. The discrepancy at this frequency suggests that the mode of vibration is no longer extensional but is considerably modified from this condition.

Figure 13 shows the relationship between sound pressure and frequency, under the same flux conditions, taken along an axis normal to the limbs 1 and 2 of the core. These curves show that in the region where the photographs did not agree with the calculated results a severe resonance is present.

4.3. Nature of Core Vibration at Resonance

4.3.1. Analysis of core vibration in the region of resonance

The two curves in Fig. 13 show similar characteristics. The asymmetry about resonance however is reversed in the radiation from the two faces. This suggests that the two sides of the core are not vibrating in exactly the same way. Before the shape of these two curves can be explained it is necessary to know the mode of vibration at resonance. The core was therefore mounted on rubber feet positioned at the extreme corners of the assembly in order to introduce as little damping as possible. Again the flux conditions were maintained the same as those previously used. In order to measure the amplitude of vibration a crystal pick-up, of the type normally used for record reproduction was used. Although it did not give very accurate results, this device was sufficiently precise to give an indication of the type of vibration at resonance. The pick-up was mounted in a micro-manipulator so that the length of each limb could be explored with a reasonable degree of accuracy. The results obtained from this experiment are shown in Fig. 14.

The relative amplitude of vibration is plotted against distance along each limb of the core. From this it is clear that the core is resonant in a flexural mode with antinodes of vibration at the centre of each limb. By comparing the phase of the vibrations on limbs 1 and 2 it was also apparent that the orthogonal limbs of the transformer core were moving in antiphase. This
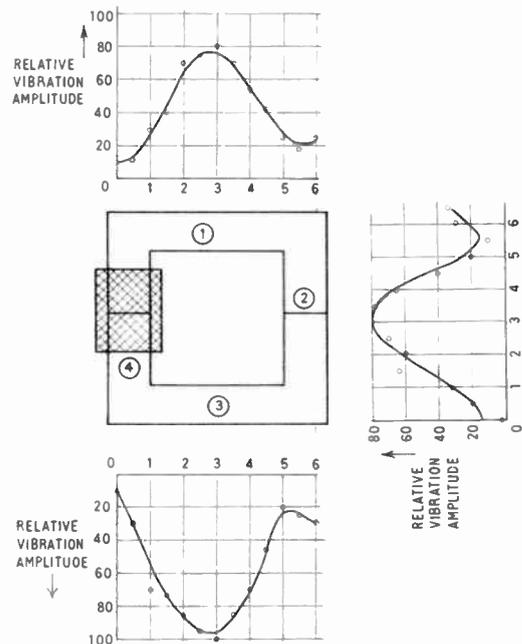

Fig. 14. Amplitude of vibration along each limb of a transformer core.

means that if at a given instant in time limbs 1 and 3 are moving outwards from the centre of the core, the limbs 2 and 4 are moving inwards. This can best be illustrated by means of the diagram shown in Fig. 15.

From the knowledge that the core is vibrating in a flexural mode, a more accurate analysis can be made of the radiation diagrams at and near flexural resonance.
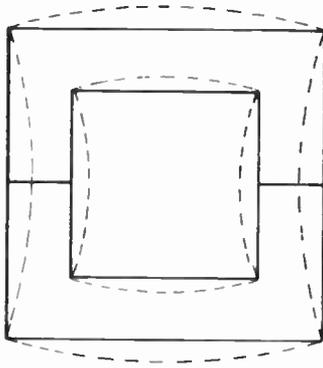

Fig. 15. Mode of vibration at flexural resonance.

Comparison between the calculated radiation diagram for the extensional mode (Fig. 12(d)) and that obtained from the polar plotter at the same frequency, shows that due to flexure of the limb the side lobes are considerably reduced. This can be verified by a theoretical analysis, assuming the limb to be flexing.

In equation (2) the velocity v_0 is assumed constant over the surface area of the piston, i.e. the piston is moving with constant amplitude and phase. If the piston is flexing along the X axis only, then the velocity will be a function of x. For the flexural mode let the velocity distribution along the x axis be given by $v_0 = v \cos \pi x/b$. Thus, substituting this in eqn. (2),

$$P_p = \frac{j\omega\rho_0 v}{2\pi R} \exp j\omega \left(t - \frac{R}{c}\right) \int_{-b/2}^{+b/2} \cos\frac{\pi x}{b} \times$$

$$\times \exp j\frac{\omega}{c}(x\cos\alpha)\,dx \int_{-a/2}^{+a/2} \exp j\frac{\omega}{c}(y\cos\gamma)\,dy$$

$$\ldots\ldots(5)$$

From Appendix 2, the resultant expression for P_p is given by

$$P_p = \frac{j2ab\rho_0 vc}{\pi\lambda R} \exp j\omega\left(t - \frac{R}{c}\right) \left[\frac{\cos\left(\dfrac{\pi b}{\lambda}\cos\alpha\right)}{1 - \dfrac{4b^2}{\lambda^2}\cos^2\alpha}\right] \times$$

$$\times \left[\frac{\sin\left(\dfrac{\pi a}{\lambda}\cos\gamma\right)}{\dfrac{\pi a}{\lambda}\cos\gamma}\right] \quad \ldots\ldots(6)$$

If the radiation pattern is required only in the XZ plane then γ will be $\pi/2$ for all values of α. Thus the last term in eqn. (6) will tend to unity.

The shape of the radiation pattern will be given by

$$R_a = \frac{\cos\left(\dfrac{\pi b}{\lambda}\cos\alpha\right)}{1 - \left(\dfrac{2b}{\lambda}\cos\alpha\right)^2}$$

This function is plotted in Fig. 12(d) for 9·9 kc/s, the frequency at which the core is in a flexural resonant mode. Comparison of this diagram with the photograph of the sound pressure distribution at the same frequency confirms that the limb is vibrating in a flexural mode. The amplitude of vibration at this frequency is many times that of the extensional mode. However, a few hundred cycles away from resonance the amplitudes of the flexural and extensional vibrations become of the same order, and the resultant motion of the face in this region will be the vector sum of these two types of vibration.

4.4.2. Effect of flexural resonance on radiation diagram distribution

The asymmetry in the shape of the resonance curves shown in Fig. 13 can be explained by considering them in conjunction with the radiation diagrams at various frequencies.

The phase of the extensional displacement relative to the driving force is substantially constant over the range for which the core is resonant in a flexural mode. This is the case because the extensional resonant frequency occurs outside the audible range, an approximate value for the lowest extensional resonant frequency can be found by considering the total length of the U-core to be the same as the wavelength of sound in ferroxcube at the resonant frequency. With an FX 1412 the total length is 20 cm, which gives a value of 25 kc/s for the lowest extensional resonant frequency. Associated with the flexural resonant condition however, the phase of the displacement relative to the driving force undergoes a change of approximately π radians in the region of resonance. This rate of change of phase will be a function of the mechanical Q of the system, the higher the Q the more rapid will this phase change be.

The phase of the flexural displacement relative to the extensional displacement will thus be changing fairly rapidly in the region of flexural resonance. Since the orthogonal limbs of the core are in antiphase, (Fig. 15), the resultant displacement due to the vector sum of extensional and flexural vibrations will be different on limbs 1 and 2 of Fig. 7. If the two types of vibration are substantially in phase then no marked change will be apparent in the radiation diagram; the shape will change slightly due to the different

distribution along the length of the limb, but will always have a maximum of radiation along the normal to the vibrating surface. If however the two types of vibration are in antiphase then the radiation diagram can be considerably changed from that due either to the extensional or flexural vibrations.
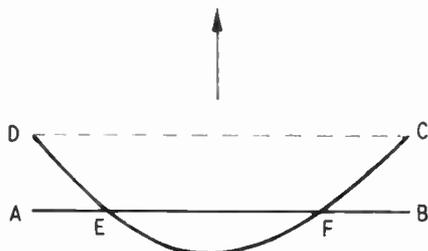
Fig. 16. Displacement of each transformer limb.

This can best be explained by reference to Fig. 16. If the line AB is the normal position of the surface of the undeflected beam, then D C can be considered as the line of maximum displacement of the extensional vibration. The flexural vibration, if in antiphase, will result in a deflection of the beam as indicated by the line D E F C. Under these conditions it can be seen that the resultant displacement due to the two types of vibration will result in the points of zero displacement occurring at E and F. If the displacement in the direction of the arrow is considered as being positive then the beam is vibrating in three distinct parts. Sections DE and FC have positive displacements, however, the centre section of the beam E F has a negative displacement. Under these conditions it is possible to get complete cancellation of the radiation along a normal to the surface. The photograph shown in Fig. 12(e) was taken at a frequency of 10·2 kc/s and clearly shows the minimum of radiation along the normal. This condition is critically dependent on frequency since both the amplitude and phase of the flexural displacement relative to the extensional displacement are changing fairly rapidly in the region where this condition is satisfied.

The minima in the sound pressure frequency curves of Fig. 13 are due to this effect. It will be noted that cancellation occurs along the normals on opposite sides of resonance for faces 1 and 2, as would be expected since the phase of the flexural vibrations on these two limbs are opposite.

From the preceding analysis the sound pressure, frequency curves can be divided into four main sections.

(a) Below the flexural resonant frequency the amplitude of vibration is almost entirely due to forced extensional vibrations.

(b) At resonance the vibration changes from extensional to flexural, the extensional mode being very much smaller in amplitude.

(c) On either side of resonance, since both the extensional and flexural vibrations are of the same order of amplitude, the resultant motion will be the vector sum of both.

(d) Above resonance the vibrations are again extensional.

5. Factors Influencing Frequency and Amplitude of Flexural Resonance

From the previous analysis it is clear that the noise produced by the core of the line output transformer can be magnified many times due to flexural resonance. The main concern of the time-base engineer when designing the mechanical arrangement of the line transformer, are the steps to be taken to ensure that the resultant assembly is as quiet as possible. This involves a knowledge of the main factors on which the frequency and amplitude of resonance depends. In order to provide this information each of the main factors will be considered separately.

5.1. Effect of Adhesive used in the Gap

Since the mode of vibration at resonance results in an antinode of vibration at the centre of each limb, it is reasonable to suppose that the rigidity of the glue used would have a profound effect on the frequency of the flexural resonance.

Figure 17 shows the effect of changing the rigidity of the glue used in the gap. In this experiment three FX 1412 U-cores were assembled, each with different glues. A rubber-based impact adhesive was used as the most pliable, cellulose acetate glue as a more rigid adhesive, and a synthetic resin was used as a very rigid glue. The effect of these three glues can easily be seen from the curves.
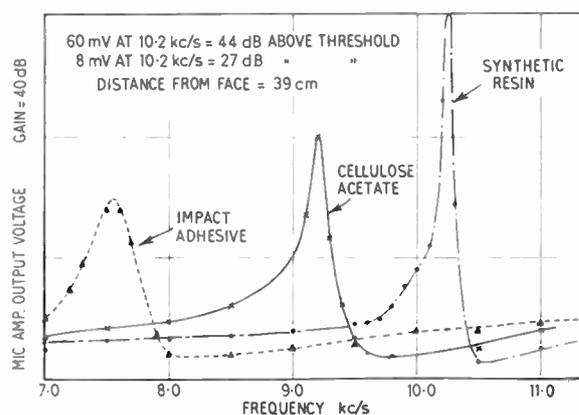
Fig. 17. Effect of gap adhesive on flexural resonance.

The results of this experiment show that as the rigidity of the adhesive used in the gap increases the resonant frequency also increases. The limit to this increase will be when the rigidity of the glue approaches that of the original material, at which point the
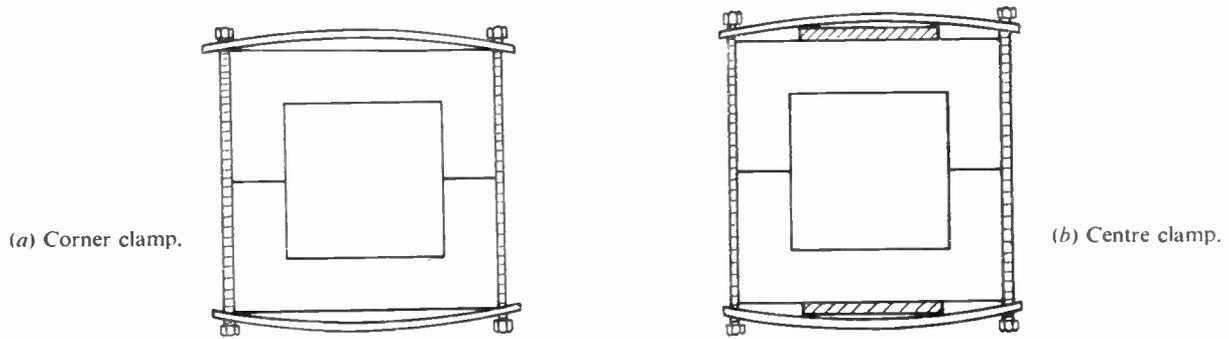
(a) Corner clamp.

(b) Centre clamp.

Fig. 18. Methods of clamping transformer core.

resonant frequency will approach that of a solid core. It is interesting to note that with a soft rubbery type of glue the resonant frequency is moved far away from 10·125 kc/s, and no magnification of sound is produced at line frequency. This is undoubtedly the cheapest and most effective way of preventing flexural resonance near 10·125 kc/s.

In order to check the repeatability of the above results several FX 1412 and modified FX 1412 cores with the gap at the end of the side limb were measured using synthetic resin and cellulose acetate glues on the same core. In this way it is possible to determine the percentage change in the frequency of flexural resonance between the two types of glue and core.

Table 2

Comparison of frequency of flexural resonance for two types of core and glue.

(a) FX 1412 Cores

Core No.	synthetic resin (f_0)	cellulose acetate (f_0)	% reduction
1	10·1 kc/s	8·9 kc/s	11·9
2	10·2 kc/s	8·75 kc/s	14·2
3	9·8 kc/s	8·7 kc/s	12·25

(b) Modified FX 1412 Cores

Core No.	synthetic resin (f_0)	cellulose acetate (f_0)	% reduction
1	12·0 kc/s	11·7 kc/s	2·5
2	11·9 kc/s	11·3 kc/s	5·05
3	12·0 kc/s	11·5 kc/s	4·2

The results obtained are given in Table 2 and indicate that the change in frequency is greater in the case of the FX 1412 than with the modified FX 1412 core. This is to be expected since in the case of the FX 1412, the position of the gap coincides with an antinode of vibration at resonance. In the case of the modified core the gap is situated at a nodal point.

5.2. *Effect of Different Types of Clamping on Flexural Resonance*

The normal method of clamping the line transformer is shown in Fig. 18(a). With this method, due to the bending of the clamps in the centre, little force is exerted at the mid-point of the transformer limb. The majority of the force is exerted at the corners. Figure 19 shows the effect of clamping at the corners. Curve (1) is the sound pressure measured normally to the line of the transformer core without any form of clamping. Curve (2) shows the effect of clamping at the corners. It can be seen that with end-clamping the amplitude at resonance is considerably increased. Alternatively, if the clamping is exerted at the centre of the limb, as shown in Figure 18(b), then the amplitude at resonance is very considerably decreased.
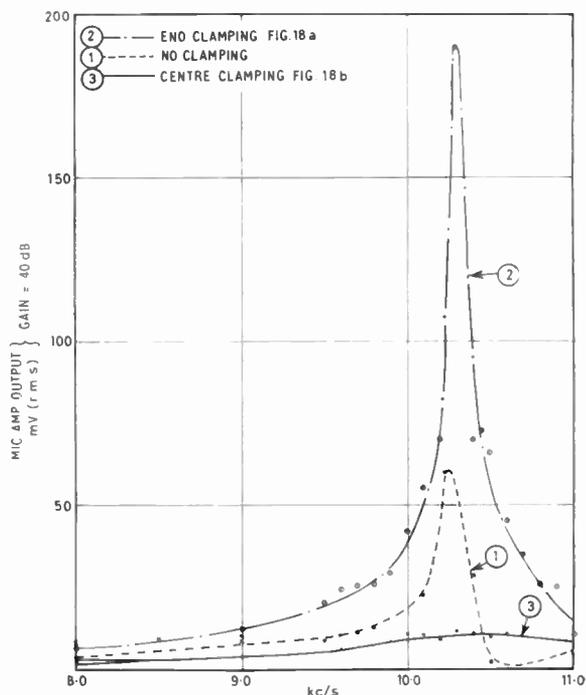

Fig. 19. Effect of clamping on flexural resonance.

curve (3). These measurements were carried out with the peak value of flux density the same in each case, i.e. 2000 gauss. It is interesting to observe that the sound pressure away from resonance, say at 8 kc/s, is not the same under the three conditions of clamping. This is due to the fact that the type of clamping modifies the radiation diagram and thus these values cannot be directly compared. In order to find the effect of clamping on the sound energy radiated from the core it would be necessary to integrate the sound pressure around a sphere surrounding the core and thus find a value for the total radiated sound energy. This measurement is extremely difficult since a very large number of measurements have to be made in order to obtain a reasonably accurate result. In order to observe the effect away from resonance radiation diagrams were plotted at 8 kc/s for the three conditions of clamping (Fig. 20). It can be seen that in each case
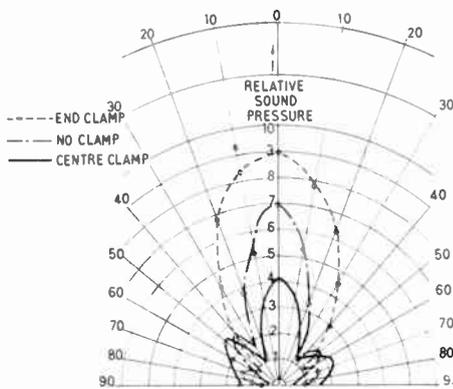

Fig. 20. Effect of clamping on polar distribution of radiation.

the radiation patterns are different. With the clamping force at the end of the limb the side-lobes are reduced. The cause of this is probably due to flexing of the limb. It will also be seen from these radiation diagrams that with end-clamping the angle between the side-lobes and main lobes is greater, which would be accounted for by flexing of the core. The effect of flexure on the polar diagram can be seen by reference to Fig. 12(d). In the case of the piston source flexing, the side-lobes are considerably reduced.

In order to calculate the flexural resonant frequency for the transformer core it is necessary to know the conditions existing at the corners. The resonant frequency of a beam in flexure is largely dependent on these conditions. The exact behaviour of the core at the corners is very complex since the cross-section at this point changes. However a simplified calculation can be done in order to illustrate the factors on which the resonant frequency depends.

If the sides of the core are considered as a beam simply supported at each end, then the resonant

frequency is given by[3]

$$f = \frac{1}{2\pi} \sqrt{\frac{48 \cdot 7\, EI}{L^3\, 0 \cdot 5\, M_B}}$$

From this relationship it can be seen that the frequency of flexural resonance is largely determined by the length of the beam. In order to verify the application of this formula a solid core with a square cross-section was made. Each limb had a cross-section measuring $0 \cdot 515$ in $\times 0 \cdot 515$ in the length was $2 \cdot 53$ in. The calculated value from the above equation is 12 kc/s. This value is of the same order as that found from measurement, i.e. $11 \cdot 4$ kc/s.

From the above simplified analysis it can be stated that if the window size of the core is decreased without changing the cross-sectional area then the resonant frequency will be higher. If at the same time as decreasing the window size the second moment of area is also reduced then the resonant frequency may not change by a substantial amount. This is illustrated by the resonant frequency of the FX 1452 core which has a smaller window area but a higher resonant frequency.

The resonant frequencies of several types of U-core were measured, in each case the cores were glued with a synthetic resin glue. The results are shown in the Table 3. Resonance curves for the three most popular cores are shown in Fig. 21, together with the resonance curve for an experimental core with a very much smaller window size. The dimensions are given in Table 1.
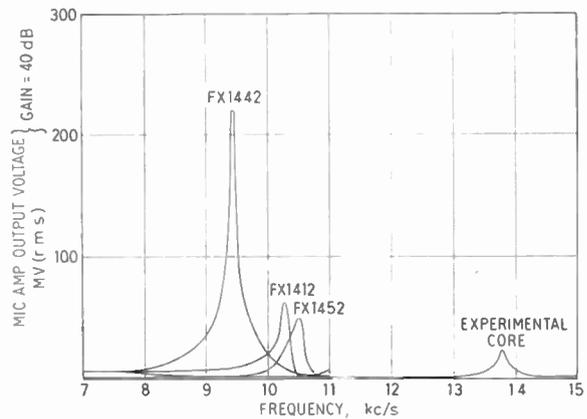

Fig. 21. Flexural resonance curves for different cores.

Table 3

Type FX No.	FX 1412	FX 1452	FX 1442	FX 1374	FX 1036	Experimental core	Modified FX 1412 with end gap
Frequency kc/s	10	10·6	9·5	12·5	12·7	13·8	11·6

6. Relationship Between Amplitude of Vibration and Flux Density for Different Materials

From eqn. (3) the peak value of sound pressure normal to the vibrating surface when the mode of vibration is extensional is given by:

$$P_{pn} = \frac{abcv_0\rho_0}{\lambda R} \qquad \ldots\ldots(10)$$

(By putting $\alpha = \gamma = \pi/2$)

From this relationship the displacement of the vibrating surface corresponding to a given sound pressure can be found.

The choice of frequency at which the sound pressure is measured is important since resonant conditions would considerably increase the sound pressure. Under these conditions the displacement would be a function of the external damping and not an intrinsic property of the material. For this reason the frequency selected for this measurement must be such that the core is not influenced by flexural resonance. At the same time the frequency cannot be very low because the performance of the anechoic enclosure would influence the results. For the above reasons, since the resonant frequency for most types of core used at the present time is above 10 kc/s when a resin adhesive is used, the frequency selected for the measurement of displacement was 8 kc/s.

In order to assess the magnetostriction characteristics of a core it is necessary to measure the displacement of the vibrating core face as a function of the peak flux density. From eqn (10) it is possible to find the velocity of the vibrating surface from a measurement of sound pressure. If the fundamental component only of the sound pressure is measured and the flux density is unidirectional with the flux swing from zero up to the peak value, it is possible to plot fundamental strain against flux density for different core materials. For the prevention of noise the value of fundamental strain should be as small as possible.

Figure 22 shows the measured results obtained on FX 1412 and FX 1452 samples in A2 material. Figure 23 shows the results of a similar measurement on A9 material.

Static measurements carried out on experimental materials indicated that the amount of magnetostriction was small in the range of flux densities used in line transformer U-cores.

Several FX 1412 U-cores were made using the same chemical compositions and firing cycles as these materials. From a batch of 12 of each type, two sets of U-cores were assembled. The results obtained from measurements on these cores are shown in Fig. 24. Figure 25 shows the results obtained on the original samples, measured by static methods.
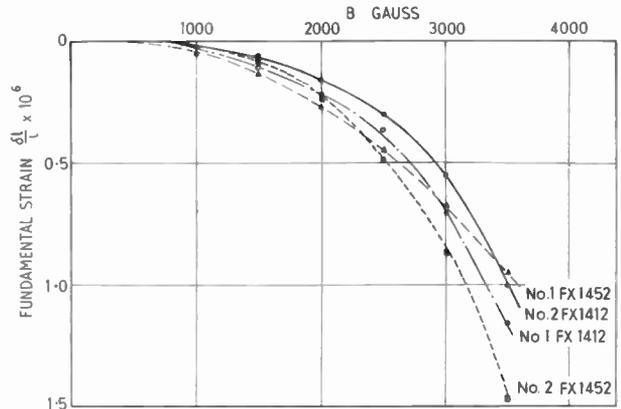
Fig. 22. Fundamental strain curves for A2 material.
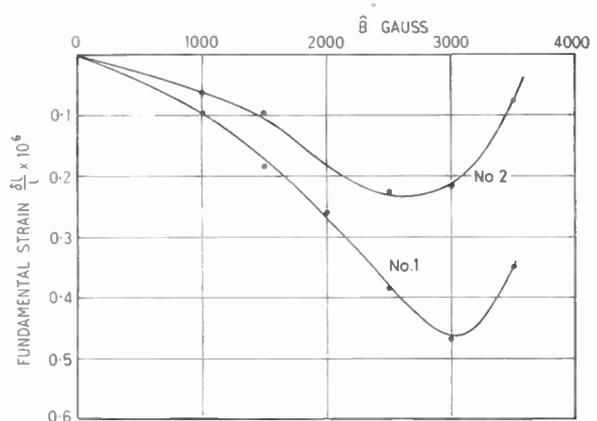
Fig. 23. Fundamental strain curves for A9 material.

7. Results

7.1 Results from Acoustic Measurements at Resonance

The first part of this paper shows that a considerable increase in noise can be obtained when the core is resonant in a flexural mode. With the three cores shown in Fig. 21, i.e. FX 1412, FX 1442 and FX 1452, the measured increase in sound pressure level due to the magnification of resonance is shown by Table 4. The figures given are based on 0·002 dynes/cm^2 as the reference sound pressure, which is the threshold of audibility at 10 kc/s.[1] The calculations assume a flux swing of 2000 gauss and a steady component of 1000 gauss. The material is A2.

From the results shown in Table 4 it can be seen that the difference between the sound pressure level at resonance and under forced vibration is approximately 20 dB. This constitutes a considerable increase in noise and no doubt accounts for the complaints received about excessive noise produced by some television sets. From the curves shown in Fig. 17 it can be seen that effective methods are available to control the frequency of this flexural resonance. If a
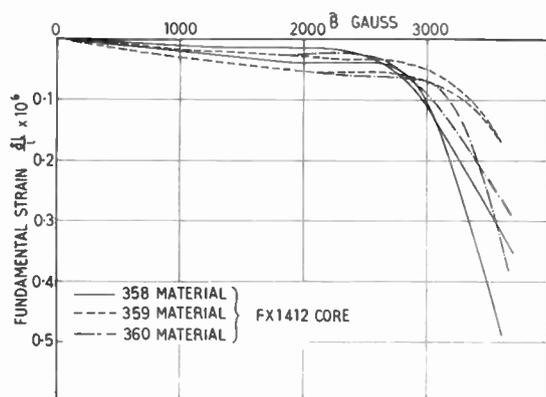
Fig. 24. Fundamental strain curves for materials with low magnetostriction.
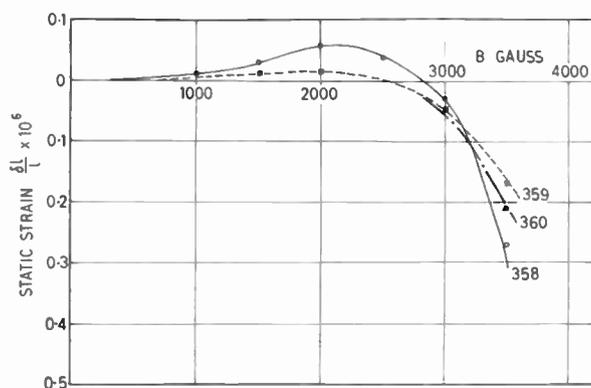
Fig. 25. Static strain curves for materials with low magnetostriction.

Table 4

Sound pressure level at 39 cm from back limb of FX 1412, FX 1442 and FX 1452 core.

Type of Core	S.P.L. above 0·002 dynes/cm² (forced)	S.P.L. above 0·002 dynes/cm² (resonant)
FX 1412	24 dB	45 dB
FX 1442	27 dB	56 dB
FX 1452	23 dB	43 dB

very pliable type of glue is used as the adhesive for securing the two U-cores together, a considerable frequency shift is possible and this is controllable by the rigidity of the glue. An alternative method of preventing this resonance is by clamping the core in a particular way. Several types of clamping were tried, shown in Fig. 18 and the results obtained from measurements on these cores are shown in Fig. 19. The sound pressure level again relative to 0·002 dynes/cm² for each type of clamping at resonance was found to be as follows:

(1) End clamping 55 dB
(2) No clamping 44 dB
(3) Centre clamping 18 dB

These figures were again taken at 39 cm from the vibrating face. To some extent the results will be modified by the size and shape of the clamp used. This is evident from the change in shape of the radiation pattern from the vibrating surface. The type of vibration along the surface will also be a function of clamping and this will also change the radiation pattern. The above figures show that if the clamps are operating at the corners of the assembled line transformer, then a considerable increase in noise can be obtained. Under these conditions of clamping the core is readily excited in a flexural mode, and excessive noise would be produced. This method of clamping line transformers has been used extensively throughout the industry with, in some cases, rather disastrous results. The most effective method of clamping seems to be the type shown in Fig. 18(b) where the clamping force is exerted near the centre of the back limb of the line transformer. In this experiment the packing material used was "Neoprene", although any plastic or similar material would be satisfactory.

With this method of clamping the core, the reduction in sound pressure level over the end clamping system is 37 dB.

7.2. Results of Dynamic Displacement Measurements on Different Materials

By measurement of the fundamental amplitude of sound pressure at a given distance from the transformer core, it is possible, provided the type of vibration along the limb is known, to determine the equivalent peak to peak amplitude of vibration at the source, and hence the fundamental strain at this vibration amplitude. This gives a direct comparison between materials for the amount of noise produced at a given flux swing. This is a most important factor when selecting suitable materials for line output transformers.

Reference to Fig. 1 will show that the static strain curves against flux density for ferrite materials are very non-linear. This means that in order to obtain a relationship between actual strain and flux density from an acoustical measurement the harmonic content of the acoustic noise would have to be analysed. If the fundamental frequency of measurement is, say, 8 kc/s, this means that harmonics at 16 kc/s, 24 kc/s and possibly higher frequencies would have to be measured with a reasonable accuracy, and related in phase to the fundamental. Hence only fundamental strain curves are given in this paper. Comparison between the strain curves measured by static methods and those given in this paper show reasonable agreement.

It is interesting to observe that the new material A9 has a turnover in the fundamental strain curves, (Fig. 23). This reduction in fundamental amplitude can be accounted for by the fact that the static strain curves have a similar changeover of direction of magneto-striction as in the case of the special cores 358, 359 and 360. In the case of the new material, A9, this changeover is more pronounced. The effect of the changeover in the 358–360 materials results not in a decrease of noise at high inductions but a levelling of the curves in the region of 1000–2000 gauss.

A comparison of materials is shown in Table 5. This is based on the peak-to-peak amplitude of vibration at 3000 gauss with 1500 gauss steady component when the core is vibrating in a forced condition. The sound pressure level shown in the last column of this table assumes that the size of the source is the same in each case.

Table 5
Fundamental strain and sound pressure levels for different core materials.

Type of core	Material	Fundamental strain $\times 10^6$	S.P.L. above 0·002 dynes/cm² 39 cm from rectangular source 1·6 cm × 6·5 cm
FX 1452	A2	0·88	37 dB
FX 1452	A9	0·46	31 dB
FX 1412	358	0·12	19·5 dB
FX 1412	359	0·06	13 dB
FX 1412	360	0·08	16 dB
FX 1452	A6055	0·26	26 dB

It can be seen that the material used in the line transformer has a marked effect on the level of noise produced by this component. The figures for sound pressure level in the last column of Table 5 are taken at only 39 cm from the source. This means that the sound level, when the line transformer is mounted in a television cabinet, will be reduced from these figures. Comparison between the noise measured at a given point in a free sound field and that measured say from a line transformer mounted in a cabinet at the same distance will bear very little relation to each other. This is due to multiple reflection effects which take place within the cabinet and room. From the values shown in Table 5, however, a comparison can be obtained between materials and the effect of the choice of material on the level of sound produced.

8. Conclusions
It has been shown that the ferrite core used in the line output transformer of a television receiver can mechanically resonate in a flexural mode. The frequency of this resonance is determined by two main factors, size of core and type of glue used in the gap.

With certain combinations of core size, clamping method, and type of glue, considerable magnification of the acoustic noise can be produced at 10·125 kc/s, the line frequency of the 405-line system. The variety of reports received from users of ferrite cores have shown that the level of noise can vary very considerably. The reason for this could be explained by the shift in the resonant frequency due to tolerances in core size and variations in consistency of the adhesive used.

Increases in sound pressure levels, due to resonance, of 30 dB have been measured. From measurements made, two methods can be suggested, both of which result in a substantial change in the frequency of resonance, which will effectively prevent resonance occurring near 10 kc/s. The first solution involves changing the size of the core. From Fig. 21 it can be seen that by reducing the size of the core the resonant frequency can be raised quite considerably above 10 kc/s. This change, however, could not be carried out purely for prevention of noise since the size of core is governed largely by other design requirements. The second solution which is both effective and cheap involves changing the rigidity of the glue used to cement the two U-cores together. By this method it is possible to change the resonant frequency by approximately 7 kc/s. The more rigid glue gives the higher resonant frequency. Since with a synthetic resin glue the resonant frequency of all the round leg U-cores falls in the range 9·5–10·5 kc/s, this type of adhesive is not recommended.

It has been established that incorrect clamping methods can increase the magnification at resonance considerably, and that corner clamping of the transformer should not be used. The most satisfactory method of reducing the amplitude of vibration at resonance is by centre clamping as shown in Fig. 18(b). This results in a reduction of 37 dB over the corner clamped core.

Finally it has been shown that the amplitude of sound pressure under conditions of forced vibration is determined by the type of material used. Measured results indicate that with a sinusoidal flux swing of 3000 gauss peak to peak, the fundamental strain varies between $0·06 \times 10^{-6}$ for the best material, experimental batch number R359, and $1·0 \times 10^{-6}$ for the standard A2 material. The difference in sound pressure level corresponding to this difference is 24 dB. Thus it is clear that in the development of future materials the magnetostriction properties should be carefully considered in conjunction with other requirements.

The author would also like to express thanks to Mr. K. Freeman (Mullard) for his assistance in this work, and to Mr. W. C. Copeland (National Physical Laboratory) for helpful suggestions received regarding the measurement of acoustic noise.

10. References

1. "Noise Measurement Techniques", Notes on Applied Science No. 10. D.S.I.R. National Physical Laboratory, (H.M.S.O., 1955).
2. G. W. Swenson, "Principles of Modern Acoustics", p. 112, (Macmillan, 1953).
3. R. G. Manely, "Fundamentals of Vibration Study", p. 96, (Chapman and Hall, 1948).

11. Appendix 1

Derivation of sound pressure at any point p distance R from a rectangular piston of length b and breadth a when all parts of the piston are vibrating with the same amplitude and phase.

$$P_p = \frac{j\omega\rho_0 v_0}{2\pi R}\exp j\omega\left(t-\frac{R}{c}\right)\int_{-b/2}^{+b/2} dx \times$$

$$\times \int_{-a/2}^{+a/2}\exp\left[j\frac{\omega}{c}(x\cos\alpha+y\cos\gamma)\right]dy$$

This may be written in the form

$$P_p = S\int_{-b/2}^{+b/2} dx\int_{-a/2}^{+a/2}\exp\left[j\frac{\omega}{c}x\cos\alpha\left[\exp\right]j\frac{\omega}{c}y\cos\gamma\right]dy$$

where

$$S = \frac{j\omega\rho_0 v_0}{2\pi R}\exp j\omega\left(t-\frac{R}{c}\right)$$

$$P_p = S\int_{-b/2}^{+b/2}\exp\left[j\frac{\omega}{c}x\cos\alpha\right]dx\int_{-a/2}^{+a/2}\exp\left[j\frac{\omega}{c}y\cos\gamma\right]dy$$

$$= S\int_{-b/2}^{+b/2}\exp\left[j\frac{\omega}{c}x\cos\alpha\right]dx\left[\frac{\exp\left[j\frac{\omega}{c}y\cos\gamma\right]}{j\frac{\omega}{c}\cos\gamma}\right]_{-a/2}^{+a/2}$$

Evaluating the integral summation and putting $\omega = 2\pi f$ and $\lambda = c/f$, gives

$$P_p = S\int_{-b/2}^{+b/2}\exp\left[j\frac{2\pi fx}{c}\cos\alpha\right]dx \times$$

$$\times a\left[\frac{\exp\left[j\frac{\pi a}{\lambda}\cos\gamma\right]-\exp\left[-j\frac{\pi a}{\lambda}\cos\gamma\right]}{(2j)\frac{\pi}{\lambda}a\cos\gamma}\right]$$

$$= Sa\left[\frac{\sin\left(\frac{\pi a}{\lambda}\cos\gamma\right)}{\frac{\pi a}{\lambda}\cos\gamma}\right]\left[\frac{\sin\left(\frac{\pi b}{\lambda}\cos\alpha\right)}{\frac{\pi}{\lambda}\cos\alpha}\right]$$

Therefore the complete solution is

$$P_p = \frac{j\omega ab\rho_0 v_0}{2\pi R}\exp j\omega\left(t-\frac{R}{c}\right)\left[\frac{\sin\left(\frac{\pi a}{\lambda}\cos\gamma\right)}{\frac{\pi a}{\lambda}\cos\gamma}\right]\times$$

$$\times\left[\frac{\sin\left(\frac{\pi b}{\lambda}\cos\alpha\right)}{\frac{\pi b}{\lambda}\cos\alpha}\right]$$

which is eqn. (3).

The value of sound pressure along the normal to the surface ($\alpha = \gamma = \pi/2$) is

$$P_{pn} = \frac{fab\rho_0 v_0}{R}\exp j\omega\left(t-\frac{R}{c}\right)$$

which has the peak value

$$P_{pn} = \frac{abf\rho_0 v_0}{R} = \frac{abc\rho_0 v_0}{\lambda R}$$

which is eqn. (10).

12. Appendix 2

The pressure distribution in the flexural mode is, from eqn. (5), given by

$$P_p = \frac{j\omega\rho_0 v}{2\pi R}.\exp j\omega\left(t-\frac{R}{c}\right)\times$$

$$\times\underbrace{\int_{-b/2}^{+b/2}\cos\frac{\pi x}{b}.\exp\left[j\frac{\omega}{c}(x\cos\alpha)\right]dx}_{I_1}\times$$

$$\times\underbrace{\int_{-a/2}^{+a/2}\exp\left[j\frac{\omega}{c}(y\cos\gamma)\right]dy}_{I_2}$$

I_1 is of the form

$$\int\cos mx.e^{nx}dx$$

which has the solution

$$\frac{e^{nx}(n\cos mx+m\sin mx)}{n^2+m^2}$$

Therefore:

$$I_1 = \left[\frac{\exp j\frac{\omega}{c}\cos\alpha . x \left(j\frac{\omega}{c}\cos\alpha\cos\frac{\pi x}{b} + \frac{\pi}{b}\sin\frac{\pi x}{b} \right)}{\frac{\pi^2}{b^2} - \frac{\omega^2}{c^2}\cos^2\alpha} \right]_{-b/2}^{+b/2}$$

$$= \frac{1}{\frac{\pi^2}{b^2} - \frac{\omega^2}{c^2}\cos^2\alpha} \left[\exp j\frac{\omega}{c}\cos\alpha . x . j\frac{\omega}{c}\cos\alpha\cos\frac{\pi x}{b} + \right.$$

$$\left. + \exp j\frac{\omega}{c}\cos\alpha . x . \frac{\pi}{b}\sin\frac{\pi x}{b} \right]_{-b/2}^{+b/2}$$

$$I_1 = \frac{1}{\frac{\pi^2}{b^2} - \frac{\omega^2}{c^2}\cos^2\alpha} \left[\frac{\pi}{b}\exp j\frac{\omega}{c}\cos\alpha . \frac{b}{2} - \right.$$

$$\left. - \left(-\frac{\pi}{b}\exp - j\frac{\omega}{c}\cos\alpha . \frac{b}{2} \right) \right]$$

therefore

$$I_1 = \frac{\pi/b}{\frac{\pi^2}{b^2} - \frac{\omega^2}{c^2}\cos^2\alpha} \left[2\cos\left(\frac{\omega b}{2c}\cos\alpha \right) \right]$$

Now $\lambda = c/f$, therefore

$$I_1 = \frac{\pi/b}{\frac{\pi^2}{b^2} - \frac{4\pi^2}{\lambda^2}\cos^2\alpha} \left[2\cos\left(\frac{\pi b}{\lambda}\cos\alpha \right) \right]$$

$$= \left[\frac{\cos\left(\frac{\pi b}{\lambda}\cos\alpha \right)}{1 - \frac{4b^2}{\lambda^2}\cos^2\alpha} \right] \frac{2b}{\pi}$$

Now $\qquad I_2 = \displaystyle\int_{-a/2}^{+a/2} \exp j\frac{\omega}{c}(y\cos\gamma)\,dy$

This integral is the same as that found in Appendix 1 and is given by

$$a \left[\frac{\sin\left(\frac{\pi a}{\lambda}\cos\gamma \right)}{\frac{\pi a}{\lambda}\cos\gamma} \right]$$

Thus the final expression for the sound pressure P_p at a distance r from the piston in the flexural mode is given by

$$P_p = \frac{j2\pi f\rho_0 v}{2\pi R}\exp j\omega\left(t - \frac{R}{c} \right) \left[\frac{\cos\left(\frac{\pi b}{\lambda}\cos\alpha \right)}{1 - \frac{4b^2}{\lambda^2}\cos^2\alpha} \right]\frac{2b}{\pi} \times$$

$$\times a \left[\frac{\sin\left(\frac{\pi a}{\lambda}\cos\gamma \right)}{\frac{\pi a}{\lambda}\cos\gamma} \right]$$

which yields

$$P = j\frac{2ab\rho_0 vc}{\pi\lambda R}\exp j\omega\left(t - \frac{R}{c} \right) \left[\frac{\cos\left(\frac{\pi b}{\lambda}\cos\alpha \right)}{1 - \frac{4b^2}{\lambda^2}\cos^2\alpha} \right] \times$$

$$\times \left[\frac{\sin\left(\frac{\pi a}{\lambda}\cos\gamma \right)}{\frac{\pi a}{\lambda}\cos\gamma} \right]$$

which is eqn. (6).

Stabilization of a Variable Quantity with Respect to a Single Valued Reference

By

D. M. MAKOW,

Dr.Sc.Techn., Dipl.-Ing. †

Summary: A feedback system consisting of two interacting loops is studied, which stabilizes an output variable using a single valued reference. The deviation of the output quantity caused by an external disturbance depends on the equality of the two loops, and can be made to approach zero by suitable adjustment of system parameters.

Results of the theory were confirmed experimentally using a system of two variable frequency oscillators and a quartz crystal as a reference.

1. Introduction

Feedback control systems required to stabilize a variable value of the output in the presence of external disturbances use as a reference a quantity which can be varied. The value of the output corresponds then to the setting of the reference, and the feedback minimizes the error between the two. For example, the required speed of a motor can be approached in the presence of load and supply voltage fluctuations using as a reference an output voltage of a potentiometer, set to a corresponding value. The stability of the potentiometer output voltage must be better than the stability required from the controlled output.

A voltage source as a reference is convenient, because it can be easily varied. The error introduced by the potentiometer, however, may be excessive and its resolution inadequate in some applications. For example, the frequency stability and accuracy of setting required from a variable oscillator may exceed the resolution and stability of a potentiometer in the presence of disturbances.

Very stable elements are found in nature which are suitable as references. These are, for example, some crystals (quartz) displaying well defined frequencies of electro-mechanical resonance, or gases and solids (ammonia or caesium) with properties of molecular resonance. These elements, however, are single valued and cannot be used for stabilization of a variable output. Continuously variable stable references are not available in nature, and the additional means used to provide continuously-variable properties usually degrade the overall stability.

In this paper a feedback system is described and investigated, which permits stabilization of a variable quantity with respect to a single valued reference. The system provides two output quantities, obtained from similarly constructed elements of a two-loop feedback circuit. These quantities can be varied so

that when the value of the first is increased the value of the second is decreased so that their sum remains constant. The value of the reference equals then the sum and thus no error is fed back. External disturbances will, however, tend to shift the values of the outputs in the same direction since the elements in the two forward paths of the system are of similar construction. The sum of the outputs will differ then from the reference, and the feedback will tend to re-establish the original condition.

2. Theory

2.1. *The Stability of the Output Quantities C_1 and C_2*

The block diagram of the system is shown in Fig. 1. The output quantities are C_1 and C_2. They may be varied in such a manner that when C_1 decreases C_2 increases so that the sum $C_3 = C_1 + C_2$ obtained in the adder is constant. The sum C_3 is subtracted from the reference C_0, which is assumed to be very stable. The difference is applied to the δ-circuit, which generates the error voltage H. The latter is then superimposed on the two control voltages R, which determine the initial values of C_1 and C_2, and is applied to the μ_1 and μ_2 circuits to correct for any deviation of C_1 and C_2 from their initial settings.

The μ and δ circuits are essentially non-linear, but operate in a small region of their characteristic which
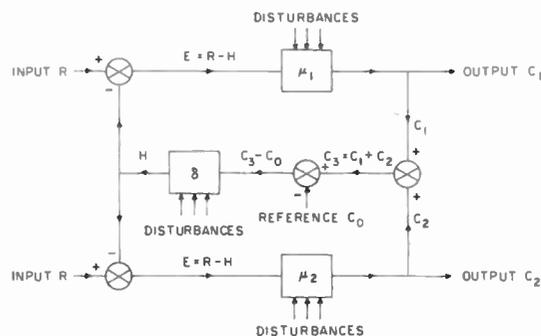
† National Research Council, Radio and Electrical Engineering Division, Ottawa, Canada.

Fig. 1. Block diagram of the two-loop feedback system for stabilization of a variable quantity.

can be assumed linear for the purpose of analysis. It has been found necessary to define their transfer functions, μ and δ, not in the conventional manner, but as the ratio of the relative deviations of the outputs to the inputs. This makes it possible to obtain non-dimensional expressions for the transfer functions and to include implicitly the operating points of the output quantity which is variable.

The outputs are in general non-linear functions of the voltage E and of the transfer factors μ

$$\left.\begin{array}{l} C_1 = F_1(\mu_1, E) \\ C_2 = F_2(\mu_2, E) \end{array}\right\} \qquad \ldots\ldots(1)$$

The above notation is useful as it does not restrict C to be zero when $\mu = 0$ or $E = 0$, as the case would be, using a linear relationship. The deviation in C from its initial value caused by a deviation in μ and in E, as a result of an external disturbance (for example, changes in supply voltage, in temperature, etc.) is found by partial differentiation.

$$\left.\begin{array}{l} \dfrac{\Delta C_1}{C_1} = v_1 \dfrac{\Delta \mu_1}{\mu_1} + \mu_1 \dfrac{\Delta E}{E} \\[3mm] \dfrac{\Delta C_2}{C_2} = v_2 \dfrac{\Delta \mu_2}{\mu_2} + \mu_2 \dfrac{\Delta E}{E} \end{array}\right\} \qquad \ldots\ldots(2)$$

The factors v are the slopes of the $C = f(\mu)$ characteristic at the operating point, multiplied by μ/C. They can be measured or obtained from available data of the system component. Similarly, the factors μ are the slopes of the $C = f(E)$ characteristic, multiplied by E/C.

The voltage H is a function of δ and C_3, and is zero when $C_3 = C_0$

$$H = F(\delta, C_3) \qquad \ldots\ldots(3)$$

Then the voltage E and its relative derivative are

$$E = R - H = R - F(\delta, C_3)$$

$$\frac{\Delta E}{E} = -\psi \frac{\Delta \delta}{\delta} - \delta \frac{\Delta C_3}{C_3} \qquad \ldots\ldots(4)$$

The factor ψ is the slope of the $E = f(\delta)$ characteristic, multiplied by δ/E, and the factor δ is the slope of the $E = f(C_3)$ characteristic multiplied by C_3/E. Both refer to values at the operating point and can be measured or obtained from available data.

Since C_3 is the sum of C_1 and C_2 one finds

$$\frac{\Delta C_3}{C_3} = \frac{1}{1+K} \frac{\Delta C_1}{C_1} + \frac{K}{1+K} \frac{\Delta C_2}{C_2} \qquad \ldots\ldots(5)$$

where

$$K = \frac{C_2}{C_1} \qquad \ldots\ldots(6)$$

The effect of an external disturbance on system components is represented by the values

$$\frac{\Delta \mu_1}{\mu_1}, \frac{\Delta \mu_2}{\mu_2}, \text{ and } \frac{\Delta \delta}{\delta};$$

these will be different for different types of disturbance. The resulting deviation in C_1 and C_2 is obtained by substituting (5) and (4) into (2) and solving the latter for

$$\frac{\Delta C_1}{C_1} \text{ and } \frac{\Delta C_2}{C_2}.$$

(It is assumed that $R = $ constant or zero; the regulator case.)

$$\frac{\Delta C_1}{C_1} = \frac{1}{1 + \delta\left(\mu_1 \dfrac{1}{1+K} + \mu_2 \dfrac{K}{1+K}\right)} \left[v_1 \frac{\Delta \mu_1}{\mu_1} + \frac{K}{1+K} \delta\left(\mu_2 v_1 \frac{\Delta \mu_1}{\mu_1} - \mu_1 v_2 \frac{\Delta \mu_2}{\mu_2}\right)\right] -$$

$$- \frac{\mu_1 \psi}{1 + \delta\left(\mu_1 \dfrac{1}{1+K} + \mu_2 \dfrac{K}{1+K}\right)} \cdot \frac{\Delta \delta}{\delta} \qquad \ldots\ldots(7)$$

$$\frac{\Delta C_2}{C_2} = \frac{1}{1 + \delta\left(\mu_1 \dfrac{1}{1+K} + \mu_2 \dfrac{K}{1+K}\right)} \left[v_2 \frac{\Delta \mu_2}{\mu_2} + \frac{1}{1+K} \delta\left(\mu_1 v_2 \frac{\Delta \mu_2}{\mu_2} - \mu_2 v_1 \frac{\Delta \mu_1}{\mu_1}\right)\right] -$$

$$- \frac{\mu_2 \psi}{1 + \delta\left(\mu_1 \dfrac{1}{1+K} + \mu_2 \dfrac{K}{1+K}\right)} \cdot \frac{\Delta \delta}{\delta} \qquad \ldots\ldots(8$$

The relative deviation in the sum C_3 is found from (5):

$$\frac{\Delta C_3}{C_3} = \frac{1}{1 + \delta\left(\mu_1 \dfrac{1}{1+K} + \mu_2 \dfrac{K}{1+K}\right)} \left[\frac{1}{1+K} v_1 \frac{\Delta \mu_1}{\mu_1} + \frac{K}{1+K} v_2 \frac{\Delta \mu_2}{\mu_2}\right] - \frac{\left(\dfrac{1}{1+K} \mu_1 + \dfrac{K}{1+K} \mu_2\right)\psi}{1 + \delta\left(\mu_1 \dfrac{1}{1+K} + \mu_2 \dfrac{K}{1+K}\right)} \cdot \frac{\Delta \delta}{\delta} \qquad \ldots\ldots(9)$$

The following is of interest:

Case 1: When there is no feedback ($\delta = 0$) equations (7) and (8) reduce to

$$\frac{\Delta C_1}{C_1} = v_1 \frac{\Delta \mu_1}{\mu_1} \qquad \ldots\ldots(10)$$

$$\frac{\Delta C_2}{C_2} = v_2 \frac{\Delta \mu_2}{\mu_2} \qquad \ldots\ldots(11)$$

Case 2: For $\mu_2 v_1 \frac{\Delta \mu_1}{\mu_1} = \mu_1 v_2 \frac{\Delta \mu_2}{\mu_2}$ and with feedback, the reduction of the relative frequency deviation is inversely proportional to the sum of the gains in the two loops.

Case 3: As seen from equations (7) and (8), a condition is possible when the large bracket expression equals zero. In such a case C_1 and C_2 are not influenced by changes in the μ portions of the system and theoretically perfect stability is possible. Inspection of these two equations will reveal, however, that the large bracket expressions cannot be made to equal zero for both equations simultaneously. If this were possible, the relative deviation $\Delta C_3/C_3$ could be made also to equal zero, which is not the case as seen from (9). The sum C_3 can be stabilized only by the factor of the loop gain, whereas C_1 or C_2 can exceed the stability of C_3. This system provides, therefore, due to the combination of its balancing and feedback properties, a means of stabilization by a factor exceeding that possible in a conventional feedback circuit.

The deviation in C_1 or C_2 caused by a deviation in the δ-circuit is not reduced by the feedback. The δ-circuit is often passive and is made very stable; the value of $\Delta \delta/\delta$ is therefore small and its effect on C_1, C_2 and C_3 usually negligible.

2.2. *Case 4:* $\mu_2 v_1 \dfrac{\Delta \mu_1}{\mu_1} \neq \mu_1 v_2 \dfrac{\Delta \mu_2}{\mu_2}$

Equations (7) and (8) show that the deviation in C_1 and C_2 depends on the value of the large bracket expressions, which is determined by the properties of the two loops. It is desirable to rewrite the above equations in terms of quantities which can be easily measured. The following substitutions are made:

$$\delta \mu_1 \frac{1}{(1+K)} = G_1 \qquad \ldots\ldots(12)$$

$$\delta \mu_2 \frac{K}{(1+K)} = G_2 \qquad \ldots\ldots(13)$$

G_1 and G_2 are the open loop transfer functions of each loop. They are defined by the ratio of the incremental deviations of the output to the input of one loop opened at one point, with conditions in the other loop remaining constant. Also, since δ is assumed stable and $\Delta K/K$ small, it is

$$\frac{\Delta \mu_1}{\mu_1} = \frac{\Delta G_1}{G_1} \qquad \ldots\ldots(14)$$

and

$$\frac{\Delta \mu_2}{\mu_2} = \frac{\Delta G_2}{G_2} \qquad \ldots\ldots(15)$$

Then equations (7) and (8) are given by (16) and (17)

$$\frac{\Delta C_1}{C_1} = \frac{1}{(1+G_1+G_2)} (1+\gamma_1 G_2) v_1 \frac{\Delta G_1}{G_1} = W_1 v_1 \frac{\Delta G_1}{G_1}$$
$$\ldots\ldots(16)$$

$$\frac{\Delta C_2}{C_2} = \frac{1}{(1+G_1+G_2)} (1+\gamma_2 G_1) v_2 \frac{\Delta G_2}{G_2} = W_2 v_2 \frac{\Delta G_2}{G_2}$$
$$\ldots\ldots(17)$$

The factors γ_1 and γ_2, called the inequality factors, are defined by (18) and (19). They are a measure of the inequality between the two loops.

$$G_2 v_1 \frac{\Delta G_1}{G_1} - K G_1 v_2 \frac{\Delta G_2}{G_2} = \gamma_1 G_2 v_1 \frac{\Delta G_1}{G_1} \ldots(18)$$

$$G_1 v_2 \frac{\Delta G_2}{G_2} - \frac{1}{K} G_2 v_1 \frac{\Delta G_1}{G_1} = \gamma_2 G_1 v_2 \frac{\Delta G_2}{G_2} \ldots(19)$$

It can be shown that the relationship between γ_1 and γ_2 is given by (20) and Fig. 2,

$$(1-\gamma_1)(1-\gamma_2) = 1 \qquad \ldots\ldots(20)$$

The factors W_1 and W_2, called the reduction factors, express the improvement in stability of C due to feedback for a given disturbance.
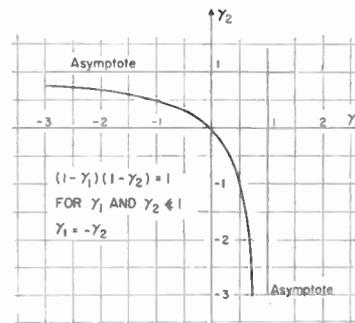
Fig. 2. Relationship between the inequality factors γ_1 and γ_2.

The equation (16), $W_1 = f(\gamma_1)$ is shown in Fig. 3 with the gain G as parameter, and assuming $G_1 \simeq G_2 = G$. An identical function can be drawn for $W_2 = f(\gamma_2)$. It is seen that for $\gamma_1 = 0$ the reduction factor W_1 is inversely proportional to the gain factor G. Also when $\gamma_1 = 0$, $\gamma_2 = 0$ as seen from (20). Therefore, W_2 is also inversely proportional to G at the same time. However, if $\gamma_1 \neq 0$, γ_2 will have a value given by (20), and W_1 will be different from W_2. In particular, for $\gamma_1 = -1/G_2$, a value of $W_1 = 0$
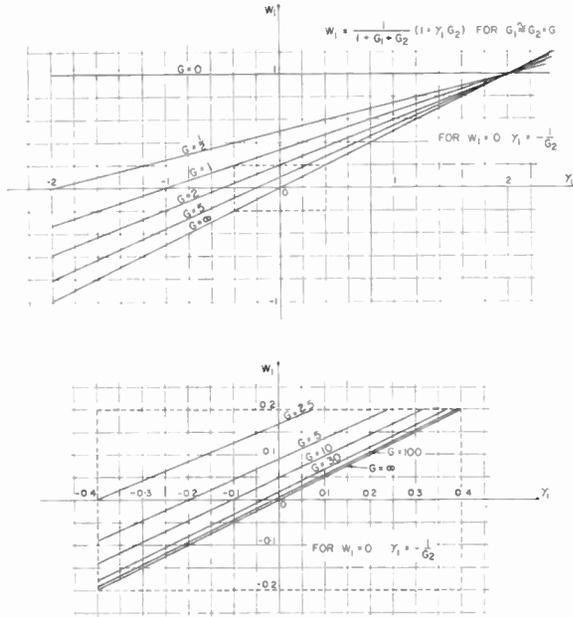
Fig. 3. The relationship between the reduction factor W_1 and inequality factor γ_1 for several values of loop gain G.

is obtained. Then, the corresponding value of $\gamma_2 = 1 - 1/(1-\gamma_1)$ leads to a reduction factor W_2 greater than zero. The condition $W_1 = 0$ can be obtained at any value of $G_2 > 0$, by suitable adjustment of γ_1, which fulfils the condition $\gamma_1 = -1/G_2$. This would indicate that high loop gain is not essential in order to realize the value $W_1 = 0$. It is seen that for $G = 0$ the reduction factor W is always equal to unity and not dependent on γ, which describes the condition when there is no feedback.

High loop gain is, however, desirable for several reasons. First, as follows from the above, small values of W_1 and W_2 can be obtained simultaneously for a given value of γ_1 or γ_2, when the loop gain is high. Second, when by appropriate choice of G_1 or G_2, $\Delta C_1/C_1$ or $\Delta C_2/C_2$ was made zero, small deviations in G_1 and G_2, which may take place after this condition has been established, will influence W_1 and W_2 to a considerably lesser extent when the loop gain is high. Third, satisfactory feedback correction can be obtained for amplitudes of disturbance, which at a low loop gain would have caused $C_3 = C_1 + C_2$ to shift beyond the range of feedback correction and therefore to terminate the operation of the system.

The inequality factors γ_1 and γ_2 describe also the effect of varying C_1 and C_2 expressed by the factor K. Suppose that the loop gain G_1 or G_2 was adjusted so that $\Delta C_1/C_1$ or $\Delta C_2/C_2$ is equal to zero for a value of $K = K_c$, at the centre of the range. Then, assuming that G_1, G_2, their relative derivatives and the factors v

are constant with the setting of C_1 and C_2, it can be shown that $\Delta C_1/C_1$ and $\Delta C_2/C_2$ at a value of K off centre the range, are given by

$$\frac{\Delta C_1}{C_1} = \frac{1}{1+G_1+G_2}\left[1 - \frac{K}{K_c} + G_2\left(1 - \frac{K}{K_c}\right)\right]v_1\frac{\Delta G_1}{G_1}$$
$$= W_{1K}v_1\frac{\Delta G_1}{G_1} \quad ...(21)$$

and

$$\frac{\Delta C_2}{C_2} = \frac{1}{1+G_1+G_2}\left[1 - \frac{K_c}{K} + G_1\left(1 - \frac{K_c}{K}\right)\right]v_2\frac{\Delta G_2}{G_2}$$
$$= W_{2K}v_2\frac{\Delta G_2}{G_2} \quad ...(22)$$

The reduction factors W_{1K} and W_{2K} are now functions of the off-centre setting K/K_c.

3. Applications and Experimental Results

3.1. A Variable Frequency Oscillator

The principle of stabilization of a variable quantity, analysed above, has been applied to frequency stabilization of a variable oscillator. The μ_1 and μ_2 circuits consist then of two oscillators O1 and O2 (see Fig. 4) associated with two reactance stages R1 and R2. The input to R1 and R2 is the voltage E and the outputs of O1 and O2 are the frequencies f_1 and f_2 respectively, which are equivalent to the output quantities C_1 and C_2 in Fig. 1. The adder is a mixer M producing the sum $f_3 = f_1 + f_2$. The δ circuit consists of a crystal filter and phase detector. The centre frequency of the crystal filter provides the reference $f_0 \simeq f_x$ and the phase detector generates an error voltage proportional to the magnitude and polarity of the frequency error $f_3 - f_0$. The grid-bias voltages of the reactance stages are the input voltages R shown in Fig. 1.

The circuit of this oscillator was built for the purpose of checking experimentally the relationships derived in the preceding sections. The ranges of the oscillators O1 and O2 are 47 to 50 kc/s and 53 to 50 kc/s respectively. The tuning range of each oscillator was split into six ranges controlled with a selector switch. Each range is 500 c/s wide with some overlap and is tunable with a precision dial coupled to accurate variable capacitors which form a part of the resonant capacitance. The reactance stages are of conventional design. The outputs of the oscillators O1 and O2, having the frequencies f_1 and f_2 respectively, are connected to the tuned mixer M where the sum frequency f_3, approximately 100 kc/s, is obtained. The latter is applied to the crystal discriminator which consists of a crystal filter and a phase detector. The crystal filter employs a 100-kc/s quartz crystal in a bridge circuit which compensates the parallel capacitance of the crystal and thus eliminates its parallel resonance. The crystal acts then as a series
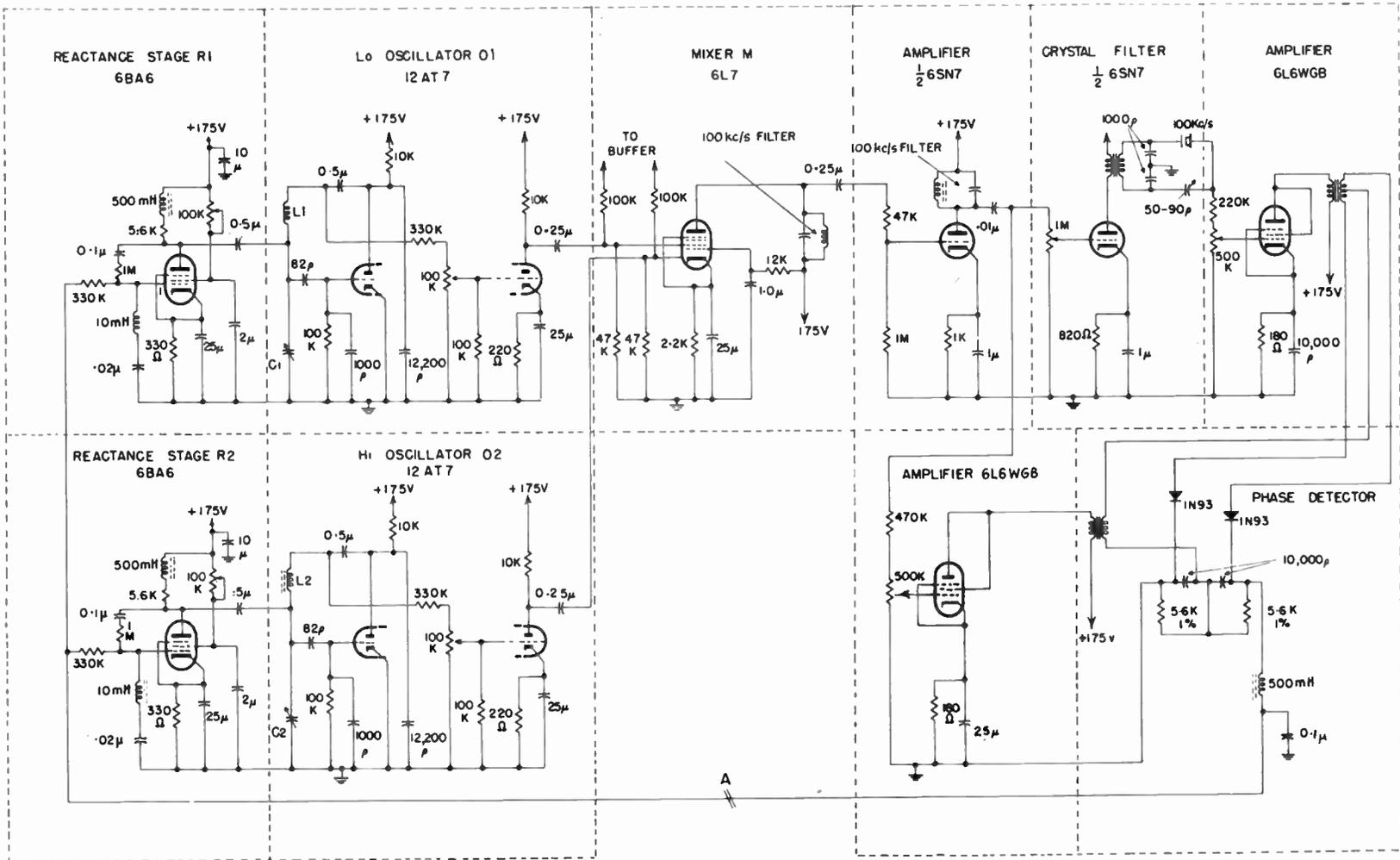
Fig. 4. Circuit diagram of the variable oscillator feedback system used for experimental analysis.

Fig. 5. The calculated and measured values of the relative frequency deviation and the reduction factors W_1 and W_2, as a function of the inequality factors γ_1 and γ_2 respectively. Low loop gain case.

resonant circuit having a Q of about 6300 and it introduces a negative phase shift at frequencies below its resonance frequency f_0 and a positive phase shift above. The voltage of the frequency f_3, shifted in phase according to whether f_3 is larger or smaller than f_0 is applied to one input of the phase detector. The same voltage, but not shifted in phase, is applied directly to the second input of the phase detector. The phase detector generates then a d.c. voltage, which is proportional in magnitude and polarity to the phase difference of its two input voltages. This d.c. error voltage is then fed back to the grid circuits of the reactance stages.

The two oscillators and the two reactance stages are designed to be almost identical. Therefore, any outside disturbance such as changes in temperature, humidity, CO_2 content in the air, power supply variations or mechanical vibrations will shift the frequencies f_1 and f_2 in the same direction and almost by the same amount. The resulting error frequency in the sum f_3, available as an error voltage H at the output of the discriminator, is applied to the two reactance

stages and shifts the frequencies f_1 and f_2 to their original values. Tuning of f_1 and f_2 to desired values is accomplished by shifting these frequencies in opposite directions so that the sum f_3 remains constant and no feedback correction takes place.

3.2. Frequency Stability as a Function of the Inequality Factor γ

The relative frequency stability $\Delta f_1/f_1$ and $\Delta f_2/f_2$ is expressed by equations (7) and (8) for a relative change $\Delta\mu_1/\mu_1$ and $\Delta\mu_2/\mu_2$ in the μ_1 and μ_2 circuits. In these equations the output variables C_1 and C_2 are identical with the output frequencies f_1 and f_2. The equations (16) and (17) describe the stability as a function of the inequality factor γ_1 and γ_2. These factors, defined by (18) and (19), are functions of the loop gain G_1 and G_2, of the relative derivatives of the latter, of the factors v_1 and v_2 and of the factor $K = f_2/f_1$ which describes the relative frequency relationship of the two oscillators. The reduction factors W_1 and W_2 for a given disturbance, defined in (16) and (17), are then a function of γ_1 and γ_2 respectively.
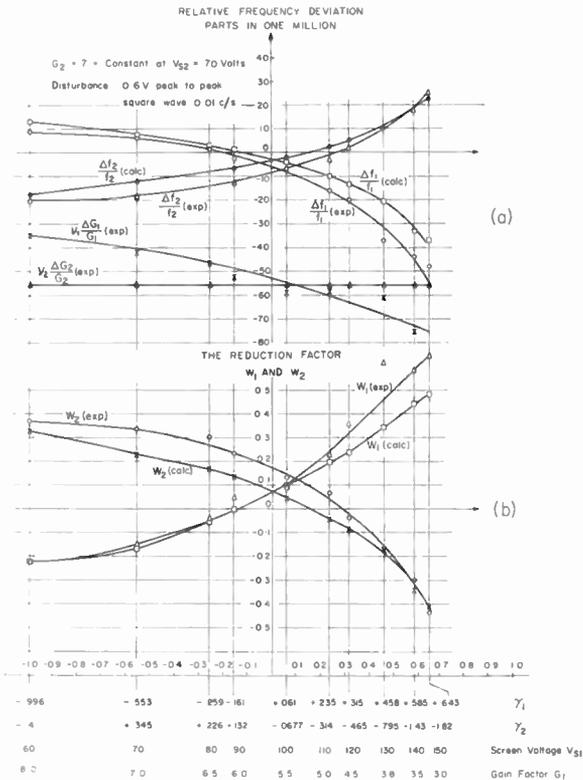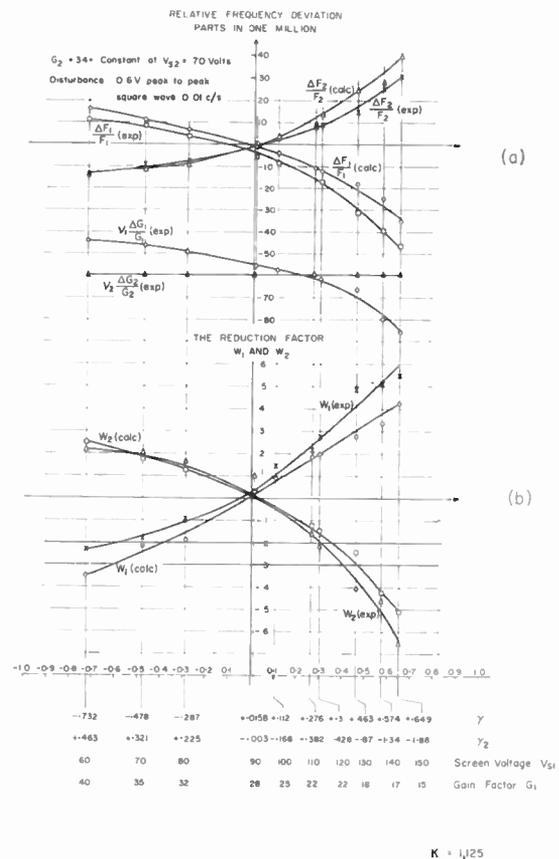

Fig. 6. The calculated and measured values of the relative frequency deviation and the reduction factors W_1 and W_2 as a function of the inequality factors γ_1 and γ_2 respectively. High loop gain case.

The reduction factors W_1 and W_2 can be evaluated by measuring the deviation $\Delta f_1/f_1$ and $\Delta f_2/f_2$ caused by a disturbance applied to both oscillators simultaneously, when the feedback line is connected, as well as the frequency deviation $v_1 \Delta G_1/G_1$ and $v_2 \Delta G_2/G_2$ for the same disturbance when the line is disconnected. The applied disturbance was in the form of a capacitance change across C_1 and C_2. This was done by changing the output capacitance of the reactance stages with a 0·6 volt peak to peak square voltage waveform, frequency 0·01 c/s, which was applied to suppressor electrodes of the reactance tubes R1 and R2. The factors γ_1 and γ_2 have been varied most conveniently by changing G_1 whereas G_2 was fixed at all times. The loop gain G_1 could then be set to several values by suitable adjustment of the screen voltage on the reactance stage R1.

In Figs. 5 and 6 the values shown for $\Delta f_1/f_1$, $\Delta f_2/f_2$, $v_1 \Delta G_1/G_1$ and $v_2 \Delta G_2/G_2$ as a function of γ_1 were measured with an electronic counter. In Fig. 5 the gain factor G_2 was fixed and equal to 7 for the screen voltage $V_{s2} = 0$ volts, and in Fig. 6 G_2 was equal to 34 at $V_{s2} = 70$ volts. The higher gain in the latter case was obtained by increasing considerably the input signal to the phase detector. Also, the relative frequency deviation $\Delta f_1/f_1$ and $\Delta f_2/f_2$ as well as the reduction factors W_1 and W_2 were calculated by means of equations (16) and (17) and were plotted on the same graphs, curves a and b respectively. The corresponding values for γ_2, G_1 and V_{s1} are indicated on the abscissa. It is seen that in Figs. 5 and 6 a reasonably good agreement with the theoretically evaluated values has been obtained.

In the vicinity of the points where the W_1 and W_2 curves cross the abscissa, the reduction factor is very small for a reasonable variation in the loop gain, as seen in Figs. 5 and 6. The crossover points themselves represent perfect stability. These points do not coincide for the W_1 and W_2 curves and they are further apart for the low loop-gain curves than for the high loop gain. Also for γ_1, or $\gamma_2 = 0$, W_1 and

W_2 are larger in the low loop-gain case. This behaviour is also apparent from the curves calculated from theory shown in the above figures.

The possibility of obtaining a minimum deviation for $\Delta f_1/f_1$ or $\Delta f_2/f_2$ in this system, by suitable adjustment of V_{s1} or V_{s2}, is very convenient. A minimum deviation can be obtained in this way for any type of a disturbance. For example the influence of supply voltage variations which affect the two oscillators unequally or the influence of non-equal temperature coefficients of the components of the two oscillators can be balanced in this way.

3.3. Frequency Stability Across the Tunable Range of the Oscillators

When the frequencies f_1 and f_2 of the oscillators O1 and O2 respectively are varied, the inequality factors γ_1 and γ_2 will be affected, as these factors are functions of the factor $K = f_2/f_1$, as seen in equations (18) and (19). As a result, $\Delta f_1/f_1$ and $\Delta f_2/f_2$, which are then functions of K, will be influenced to an extent given by equations (21) and (22). Thus, for example, if the system is compensated by means of V_{s1} so that $\Delta f_1/f_1 = 0$ is obtained at 48·5 kc/s, which is the centre of the band O1, ($K = K_c = 1·06$), the value for $K = K_E$ at 47 kc/s, which is the edge of the band, is $K_E = 1·125$. Then, the values of the reduction factors at the edge of the band can be computed from (21) and (22) and are found to be $W_{1K} = -0·028$ and $W_{2K} = 0·035$ for $G_1 = 34$, $G_2 = 30$, $K_E/K_c = 1·06$. The average values W_{1K} and W_{2K} are then $-0·014$ and $0·018$ respectively.

The corresponding experimental values across the range of the two oscillators are shown in Fig. 7. The above were obtained using a disturbance in the form of a 1·2 volt peak to peak square wave, applied in an identical manner as in the foregoing section. The system was balanced for best stability at the centre of the band of the oscillator O1 at about 48·5 kc/s. It is seen that there is little change in stability with feedback off the centre of the band. The average deviation with feedback is about 2 to 3 parts per million and that without feedback 100 parts per million, which corresponds to an average reduction factor of about 0·02 to 0·03. This is close to the average values W_{1K} and W_{2K} calculated above. The linear relationship as given by (21) and (22) has not been obtained, probably due to the fact that G_1, G_2 and their derivatives and the factors v are not constant with frequency.

3.4. The Special Case $\gamma = 1$

The value of $\gamma = 1$ represents the case when the disturbance is applied to one oscillator only, as seen from inspection of equations (18) and (19). This case was investigated experimentally by applying a disturbance in the form of a 0·6 volt peak-to-peak square
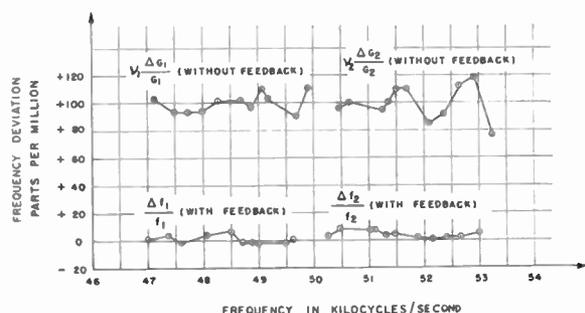

Fig. 7. The relative frequency deviation across the tunable range of the oscillator O1 and O2 for a given disturbance. The values with feedback and without feedback are compared.

Table 1

The calculated and measured values of the relative frequency deviation and the reduction factors W_1 and W_2 for $\gamma_1 = 1$ and $\gamma_2 = 1$ respectively.

|	G_1	G_2	$v_1\dfrac{\Delta G_1}{G_1}$ in 10^{-6}	$v_2\dfrac{\Delta G_2}{G_2}$ in 10^{-6}	$\dfrac{\Delta f_1}{f_1}$ (exp.) in 10^{-6}	$\dfrac{\Delta f_2}{f_2}$ (exp.) in 10^{-6}	$\dfrac{\Delta f_1}{f_1}$ (calc.) in 10^{-6}	$\dfrac{\Delta f_2}{f_2}$ (calc.) in 10^{-6}	W_1 (exp.)	W_2 (exp.)	W_1 (calc.)	W_2 (calc.)
Disturbance applied to G_1	28	28	$-36 \cdot 1$	0	$-21 \cdot 6$	$17 \cdot 6$	$-18 \cdot 2$	$15 \cdot 8$	$0 \cdot 60$	∞	$0 \cdot 50$	∞
Disturbance applied to G_2	28	28	0	$-39 \cdot 6$	$24 \cdot 5$	$-24 \cdot 5$	$21 \cdot 9$	$-20 \cdot 2$	∞	$0 \cdot 62$	∞	$0 \cdot 51$

wave to the suppressor grid of one reactance stage only, whereas the suppressor grid of the other reactance stage was grounded, and vice versa. The measured and the calculated values of the frequency change $v_1 \Delta G_1/G_1$ or $v_2 \Delta G_2/G_2$ without feedback and the values $\Delta f_1/f_1$ or $\Delta f_2/f_2$ with feedback as well as the corresponding reduction factors W are shown in Table 1. A reasonably good agreement has been obtained between the experimental and calculated values.

In the above experiment the disturbance was applied to one oscillator only, in the form of a capacitance variation using the reactance stage. The same effect can be accomplished by shifting the dial settings on oscillator O1 while leaving the dial on oscillator O2 unchanged. The corresponding shift in the frequencies f_1, f_2 and $f_3 = f_1 + f_2$ is plotted in Fig. 8. It is seen that $\Delta f_1 = 264$ c/s, $\Delta f_2 = -247$ c/s and $\Delta f_3 = 17$ c/s. When the feedback was disconnected and the experiment repeated the corresponding shifts were $\Delta f_1 = 558$ c/s, $\Delta f_2 = 0$ and $\Delta f_0 = 558$ c/s. The frequencies f_1 and f_2 change in opposite direction so that f_3 remains almost constant and the shift Δf_1 without feedback is approximately twice the corresponding shift with feedback.

3.5. Frequency Stability with Changes in the Supply Voltages

In the experiments described in the foregoing three sections the disturbance which was applied to the system was changing the capacitance of the tuned circuit. In actual operation of the system such a change can be caused by variations in temperature, humidity, power supply or by vibrations. The influence of power supply voltage variations on the frequency of oscillation was investigated. The screen voltages V_{s1} and V_{s2} were adjusted to values such that the frequency deviation $\Delta f_1/f_1$ and $\Delta f_2/f_2$ when the
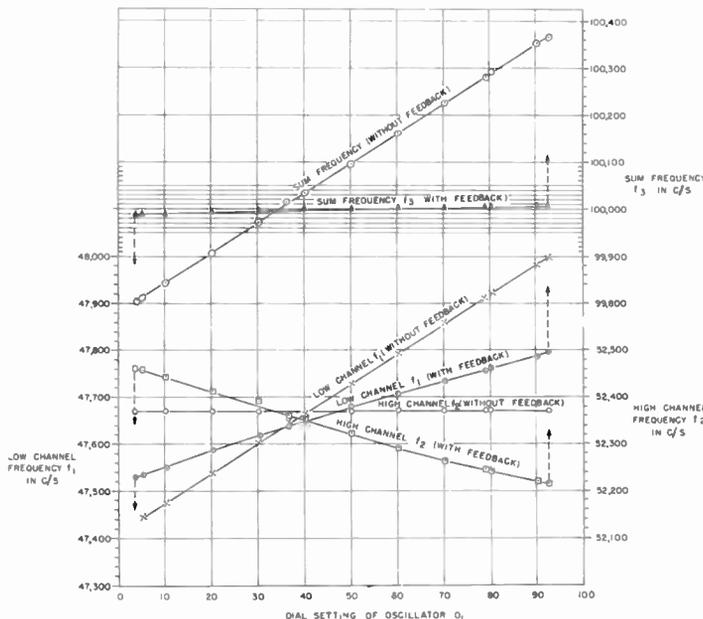
Fig. 8.

Frequency f_1, f_2 and f_3 versus dial setting of the oscillator O1 with the dial setting on the oscillator O2 fixed.
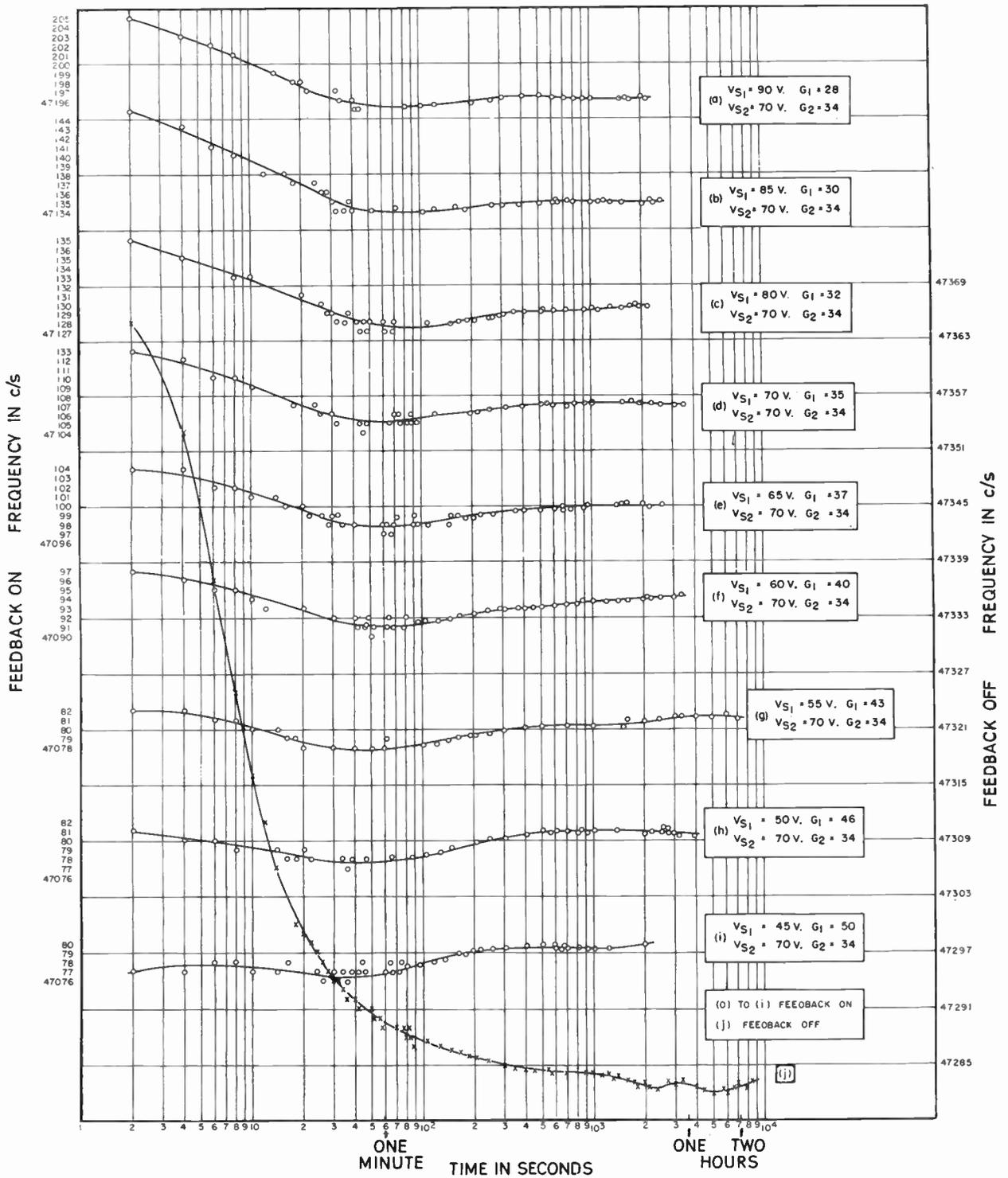
Fig. 9. The frequency drift during the warm-up period of the oscillator. The values with feedback and without feedback are compared.

feedback was connected were close to a minimum when the anode voltage on the whole system was changed by 10%. The values for the frequency deviation in the vicinity of such a minimum were found to be $\Delta f_1/f_1 = 6\cdot4 \times 10^{-6}$ and $\Delta f_2/f_2 = 3\cdot8 \times 10^{-6}$. The corresponding values without feedback were found to be $v_1 \Delta G_1/G_1 = 185 \times 10^{-6}$ and $v_2 \Delta G_2/G_2 = 90 \times 10^{-6}$. The reduction factors are then: $W_1 = 0\cdot0346$ and $W_2 = 0\cdot0423$. Without any further adjustment on the screen voltages the corresponding frequency deviations caused by a 10% change in the filament voltage were:

$$\frac{\Delta f_1}{f_1} = 42\cdot5 \times 10^{-6}$$

$$\frac{\Delta f_2}{f_2} = 43\cdot2 \times 10^{-6}$$

$$v_1 \frac{\Delta G_1}{G_1} = 550 \times 10^{-6}$$

$$v_2 \frac{\Delta G_2}{G_2} = 340 \times 10^{-6}$$

and the reduction factors were $W_1 = 0\cdot0763$ and $W_2 = 0\cdot127$. It is seen that the reduction factors are larger here as the filament variations do not produce identical effect as anode voltage variations, and no adjustment on V_{s1} was carried out for this case.

3.6. *The Frequency Drift during the Warming-up Period of the System*

The ability of the system to correct for changes in temperature was studied by measuring the initial frequency drift when the equipment was switched on. This frequency drift is due mainly to the inductance of the resonant circuit, which changes its value during this period as a result of heating. In Fig. 9 the frequency drift measured during the warming-up period is shown for the unstabilized (feedback off) and stabilized oscillator (feedback on). A series of drift curves is shown for the latter case each for a different gain value G_1 and G_2 = constant. As G_1 increases, the drift decreases, it reaches a minimum for $G_1 = 46$ and it reverses its direction for $G_1 > 46$. This minimum represents the condition when $\gamma_1 = -1/G_2$ for a given disturbance in temperature. It is seen that the total frequency drift is reduced in the curve (i) by a factor of about 25 and the period required to reach the desired frequency value is also reduced considerably when the feedback is on.

4. Conclusion

The two-loop feedback system described stabilizes a continuously variable quantity with respect to a single valued reference. As a result of the balancing properties of the system, the degree of stabilization is determined not only by the loop gain, but also by the gain relationship in the two loops. Theoretically, perfect stabilization can be obtained which is approached experimentally by suitable adjustment of the parameters.

In certain applications, where the range of one variable output is adequate for the application under consideration, duplication of components for the two-loop feedback is disadvantageous and must be weighed against the merits of this system. In other applications, where both outputs can be utilized, for example in variable oscillators, this need not be the case.

5. Acknowledgment

6. Appendix: Discussion of Feedback Stability

The open loop transfer functions G_1 and G_2, as defined in equations (12) and (13) are functions of the complex frequency of disturbance $s = \sigma + j\omega$. In the example discussed in section 3 these functions can be represented by third order systems with three poles and one zero.

$$G_{1(s)} = \delta\mu_1 \frac{1}{(1+K)} = \frac{DU_1 \dfrac{1}{(1+K)} (s\tau_{D0}+1)}{(s\tau_{D1}+1)(s\tau_{D2}+1)(s\tau_1+1)} \quad (23)$$

and

$$G_{2(s)} = \delta\mu_2 \frac{K}{(1+K)} = \frac{DU_2 \dfrac{K}{(1+K)} (s\tau_{D0}+1)}{(s\tau_{D1}+1)(s\tau_{D2}+1)(s\tau_2+1)} \quad (24)$$

where D is the magnitude of δ, and U_1 and U_2 are the magnitudes of μ_1 and μ_2 respectively. The values τ_1, τ_2, τ_{D1} and τ_{D2} are the lagging time-constants and τ_{D0} the leading time-constant of these functions. The μ_1 and μ_2 transfer functions are characterized by the τ_1, τ_{D0}, τ_{D2} and τ_2, τ_{D0}, τ_{D2} time-constants respectively and the δ function by τ_{D1}. The μ_1 and μ_2 transfer functions were assumed here to differ only at the high-frequency end, that is $\tau_1 \neq \tau_2$.

The overall transfer function $G_{T(s)}$ is then the sum of (23) and (24). Assuming that

$$U_2 = \varepsilon U_1 = \varepsilon U$$

and

$$\frac{1}{\tau_2} = \frac{\eta}{\tau_1} = \frac{\eta}{\tau}$$

where ε and η are respectively the inequalities in gain and time-constants by which the two functions differ from each other, it is

$$G_{T(s)} = \frac{\frac{1}{2}DU\,\dfrac{\tau_{D0}}{\tau_{D1}\tau_{D2}\tau}\left(s+\dfrac{1}{\tau_{D0}}\right)\left[\left(s+\dfrac{\eta}{\tau}\right)+\varepsilon\eta\left(s+\dfrac{1}{\tau}\right)\right]}{\left(s+\dfrac{1}{\tau_{D1}}\right)\left(s+\dfrac{1}{\tau_{D2}}\right)\left(s+\dfrac{1}{\tau}\right)\left(s+\dfrac{\eta}{\tau}\right)} \quad\ldots\ldots(25)$$

The value ε includes here the effect of setting C_1 and C_2 to different values as expressed in equations (7) and (8) by the quantity K.

The steady-state error E is a function of the factor ε

$$E = \frac{1}{1+G_{T(s)(s\to 0)}} = \frac{1}{1+\frac{1}{2}DU(1+\varepsilon)} \quad\ldots\ldots(26)$$

The effect of the factors ε and η on feedback stability and on the response to a periodic and transient disturbance can be studied conveniently using the root locus diagram. The bracketed expression in the numerator of equation (25) can be replaced by a leading term $s - s_0$ having a zero s_0 given by

$$s = -\frac{1+\varepsilon}{\dfrac{1}{\eta}+\varepsilon}\cdot\frac{1}{\tau} = -\frac{F}{\tau} \quad\ldots\ldots(27)$$

where F will be called the error factor. It is seen that F is mainly affected by η and when $\eta = 1$, F is not influenced by ε and is equal to unity.

In the root locus diagram shown in Fig. 10 the zeros and poles of the system are marked on the negative real axis and the root locus is found by methods described in the literature. The values of the poles and zeros correspond to those measured in an actual system discussed in Section 3.1. The root locus consists of a first portion on the real axis between $-1/\tau_{D0}$ and $-1/\tau_{D1}$, a second portion on the real axis between $-1/\tau_{D2}$ and $-\eta/\tau$, a third portion on the real axis between $-F/\tau$ and $-1/\tau$ and a curved portion asymptotically reaching $\pm\infty$. The zero $s_0 = -F/\tau$ is always found between $-1/\tau$ and $-\eta/\tau$ and its location, for a given η, is a function of ε. For $\varepsilon \ll 1$ (very small gain in one channel) s_0 approaches $-\eta/\tau$; for $\varepsilon \gg 1$, s_0 approaches $-1/\tau$. The location of the asymptote is given by the expression

$$\frac{\sum \text{pole values} - \sum \text{zero values}}{n} \quad\ldots\ldots(28)$$

where n = number of poles minus number of zeros. For $\varepsilon < 1$ the asymptote moves to the left thus improving the stability margin and for $\varepsilon > 1$ it moves to the right reducing the stability margin. When η

Fig. 10. The root locus diagram showing positions of the open and closed loop poles and zeros in the complex plane.

approaches unity, s_0, $-1/\tau$ and $-\eta/\tau$ coincide and the asymptote moves to the left crossing the real axis approximately in the centre between $-1/\tau_{D2}$ and $-1/\tau$.

From the root locus diagram one concludes that the system is unconditionally stable because the root locus does not cross the $j\omega$ axis. However, an actual system will usually have additional open loop poles having values smaller than $-1/\tau$, as a result of a further decrease of the gain response at higher frequencies. Therefore, the root locus will not continue asymptotically for higher $j\omega$ values as indicated in Fig. 10, but it will curve to the right and cross the $j\omega$ axis at a value of the loop gain for which the system will become unstable.

In Fig. 10 the closed loop poles have been evaluated for the gain value, 70. The closed loop poles which are given by the values $s_{1,2} = -\sigma \pm j\omega$, $s_3 = -\sigma_3$ and $s_4 = -\sigma_4$ determine the damping and the oscillatory component of the response. The poles s_3 and s_4 should be as large as possible without causing excessive losses and the poles $s_{1,2}$ should result in a value of the damping factor between $0\cdot4$ and 1.

Automatic Force Balance Check Weigher

By

P. A. JASSOY †

Summary: The high speed check weigher was developed to replace the sampling methods previously employed. These methods were not absolutely positive in detecting underweight articles. Besides eliminating the manual labour employed, the check weigher with electrical output enables the average weight to be indicated continuously and in "real time".

1. Introduction

Control of weight is crucial in many industries—especially when the consumer product is packaged in standard containers. The law demands that most foods and other packaged goods should be sold by weight, and strict penalties can be incurred if errors in measurement are not discovered. Furthermore, significant material savings can be achieved by tighter weight control. It is obvious, therefore, that there has been a considerable incentive to weighing machine manufacturers to develop techniques for automatic check weighing.

Modern production lines operate at speeds of 50–250 containers per minute and, since the weighing operation must be synchronized with the filling and closing machines, automatic weighers must be capable of handling these articles at these speeds. The handling devices must not only be able to stand the wear and tear of high speed running, but must not damage or contaminate the cartons in any way. Moreover, the environment under which these machines must operate may include steam cleaning, corrosive atmospheres and other hazards. Generally speaking, of course, maintenance is not possible except when the production line is halted—and skilled personnel are few and far between.

2. Design Considerations

Against this background the design considerations were mainly mechanical. Due to the wide variety of sizes and shapes of containers, it was at first considered that they should be allowed to pass through the machine without constraint. Early experiments showed that without built-in marshalling arrangements the articles could not be presented to the weigher with the necessary precision for accurate measurement. Under variable operating conditions of temperature, humidity and moisture, and with inconsistent package dimensions and shape, friction drive proved to be unreliable. It was decided, therefore, to design machines which controlled the container throughout its movement.

Basically, two types of handling arrangements were developed—an in-line unit for rectangular packets, and a rotary unit for dealing with round cans. Detailed discussion of the second unit will follow.

The design of the weighing mechanism preceded development of the mechanics, the original concept having been initiated in 1952 by a team of engineers in the Unilever group.‡ The required speed of weighing (approximately 100 ms weighing time at 200 cans/min) militated against a simple mechanical balance technique§ and it was decided to use a force balance method. Though the restoring force could have been provided by pneumatic or hydraulic means, the possibility of generating an electro-magnetic force by simple, controllable techniques led to the adoption of this principle.

3. Weigher Development

In the first design of weight transducer the weight of the container was supported almost entirely by the force balance coil (see Fig. 1). The position of the coil was detected by a capacitor which was part of one arm of a bridge circuit energized from a 20 kc/s oscillator. The output from the bridge circuit was amplified and rectified to produce the current which supplied the force coil. The load shaft on which the coil was mounted was supported by a pair of parallel diaphragm springs, and the servo stiffness (0·001 in/lb) was high enough to make the effect of the spring restraint negligible. Since this was an a.c. system there were no problems with amplifier drift. However, the high gain of the system made it very sensitive to vibration—and special anti-vibration mountings had to be designed. These filtered out most of the external noise, but had their own resonances. The large weight range (0–2 lb) and correspondingly limited electrical output (4 volts/ounce) resulted in a differential signal between accept and reject of only 120 mV. D.c. amplification of this error voltage was necessary in

---

† Elliott Brothers (London) Ltd., Lewisham, London, S.E.13.

‡ Patent 701325.

§ A. L. Hendon and G. C. Chapman, "Weighing techniques for automation production lines", *Trans. Soc. Instrum. Tech.*, **11**, pp. 154–59, September 1959.
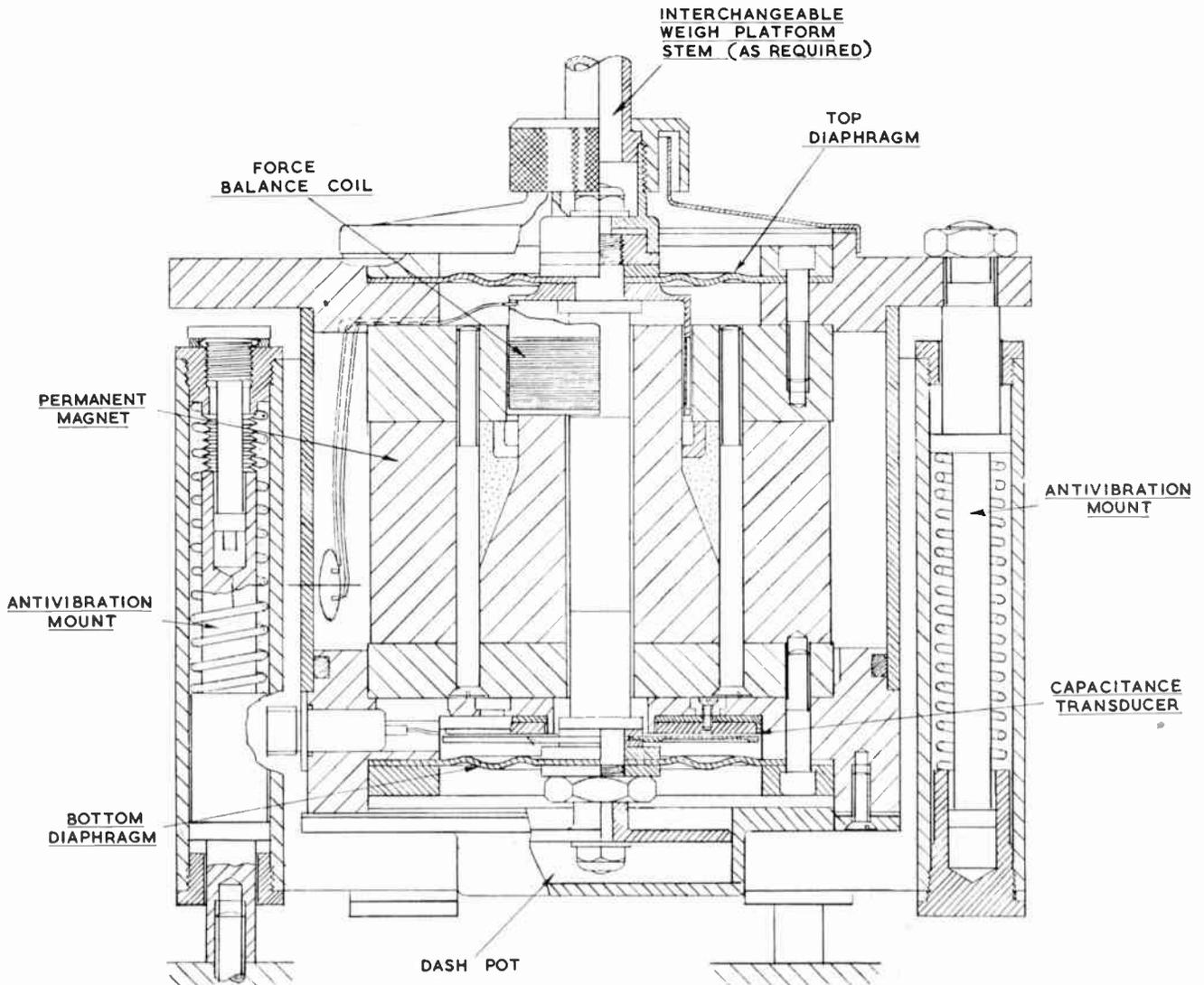
Fig. 1. Cross-section of the check weigh head.

order to operate the output relays—thus increasing complexity and cost. Furthermore, the servo required large power reserves in order to generate the required deceleration forces—resulting in a fairly large unit.

The inherent technical difficulties mentioned above resulted in the adoption of a new design. This transducer, though developed on similar basic principles, utilized a partial mass-balance system. Since the electrical force balance system then had a much smaller load it was reduced in size—and the balanced arrangement resulted in a better signal/noise ratio. The mechanical system was developed round a parallel Roberval linkage, using cross spring pivots (see Fig. 2)—thus eliminating knife-edges or other types of friction bearing. Balance was achieved at the gross weight of the packet and some mechanical amplifica-

tion of the deflection was designed into the position pick-off. This resulted in a mechanical advantage which, added to the increase in sensitivity resulting from the decreased servo range (± 2 ounces), gave a five-fold increase in output signal over the previous design. Mechanical stops prevented overloads on the lever system and pivots—and limited the deflection to that within the linear range of the servo. The position pick-off was a differential capacitor, and a velocity pick-off (a small magnet attached to the moving system and operating as the core of a fixed coil) was also incorporated to facilitate damping.

4. Servo Amplifier and Weight Discriminator

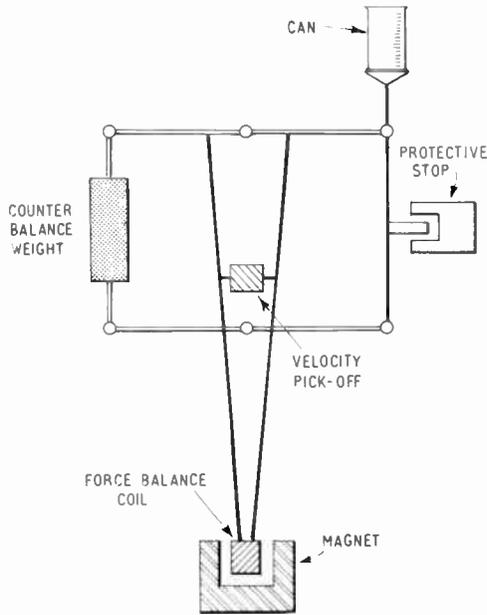The servo amplifier and discriminator circuits are shown in Fig. 3. Conventional techniques are used,

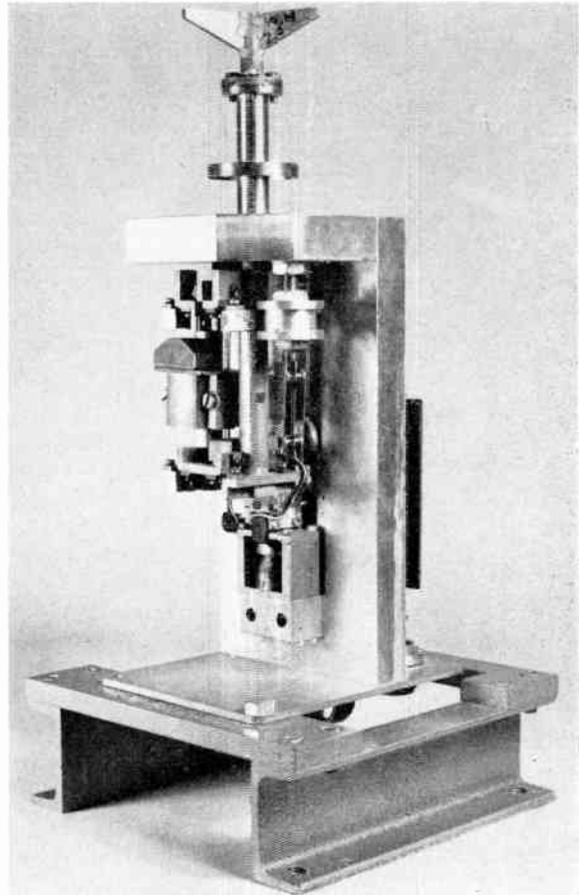Fig. 2(a). Schematic diagram of the check weigh head.

but some interesting detail points should be noted. The 50 kc/s output signal from the transducer is detected by a special phase-sensitive detector. The d.c. output is mixed with the velocity signal in a simple resistive network and then passed to the power amplifier. This amplifier uses a novel push-pull circuit consisting of a pair of cathode-coupled cascade stages. The force coil is connected (in series with a precision resistor) directly between the two anodes. The voltage across the resistor is an accurate measure of the difference in weight between the container and the counter balance weight. This voltage charges a

Fig. 2(b). The check weigh head.

"memory" capacitor via relay contacts. The time-constants of the charging circuit are arranged to give the maximum noise filtering action consistent with speed of response and accuracy. As the error must not
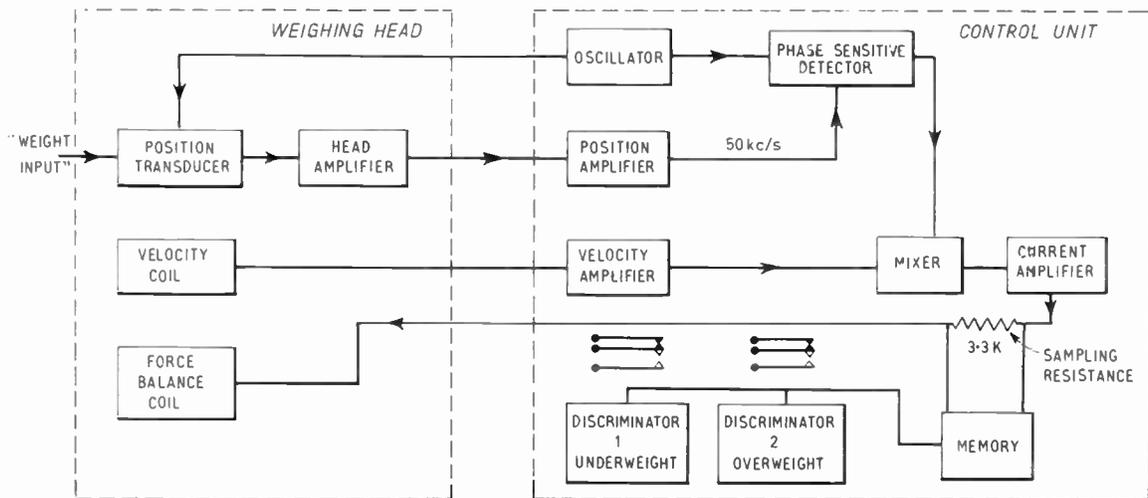
Fig. 3. Servo amplifier and discriminator block diagram.

exceed 0·1%, the time-constant is limited to approximately 1/7 of the shortest weighing period—i.e. 8–9 ms. This in turn implies a loop frequency response which is flat to 20 c/s. The output of the servo amplifier was 20 volts/ounce, the deflection being 0·001 in/ounce. Since the desired weighing accuracy (15 grains; 0·972 grammes) was equivalent to 600 mV, and the drift did not exceed 120 mV, the balanced system has proved to be satisfactory. The signal on the memory capacitor is passed to the discriminator circuits via a cathode follower. These decision circuits are simple Schmitt triggers, each driving a relay. Any number of these circuits can be provided. The power supply for the amplifier output stages and the trigger bias circuits is common and though the h.t. supply is stabilized it is not critical, and no special reference supply is required. The memory capacitor is discharged between each weighing cycle so that a reference level at zero volts is established. This level is equivalent to correct weight.

The output contacts of the discriminator relays control the mechanical gating devices which route the container to the appropriate output channel. Further relays, gated by photo-electric detectors on the handling machine, inhibit the operation of the reject device when no container is present, and control the output sampling relay.

5. Mechanical Design

The handling mechanisms were designed to accept containers of one basic shape, but of varying dimensions. The practical speed limit is determined by the container dimensions in the flow direction—and by the height/diameter ratios (see Fig. 4).

As stated previously, it was decided to design mechanisms which *index* the container through the machine. Apart from the problems referred to earlier. the weighing accuracy would be improved if there was minimum vibration—and if the kinetic energy of the package was *not* transferred to the weighing element. It was assumed that the articles would arrive at random—and means had to be provided to queue them and then phase them into the weighing cycle. Further means had to be supplied for routing them to the appropriate output paths.

As shown in Fig. 4, the containers are synchronized with the machine cycle by a mechanical stop and a star-wheel. The star-wheel indexes them serially into a rotating turret where they are gripped and carried round to the weighing station. At this point they are released on to a grid which lowers them onto the weigh platform. At the end of the weighing period the grid

Fig. 4. Handling mechanism used with the check weigher.

is raised, the container is gripped, and then carried to the appropriate output belt. The turret is driven by a special gearbox which generates a harmonic motion, thus providing smooth acceleration and deceleration forces. During the weighing period all parts of the machine are stationary except for the motor. The handling time is approximately twice as long as the weighing time, i.e. 133 ms at 150 cans/min.

The whole machine is normally mounted on anti-vibration mountings to reduce floor-borne noise, and detailed attention has been paid to the sealing of motors, gears, bearings—and the weight transducer itself. All parts in contact with the containers are manufactured of stainless steel or aluminium to minimize contamination problems. The electronic units can be mounted on the machine or remotely.

6. Conclusions

As a result of the development of the check weigher it is now possible to supply statistics to production managements of through-put, reject rate, machine utilization, weight distribution and material usage. Future trends will involve feedback of the weight information to the filling machines—thus making possible greater savings of raw material.

The possibility of incorporating the weigher into the filling machine has been considered—but since most high speed fillers have multiple heads, this would be extremely expensive. However, such a development could eliminate the need for check weighing.
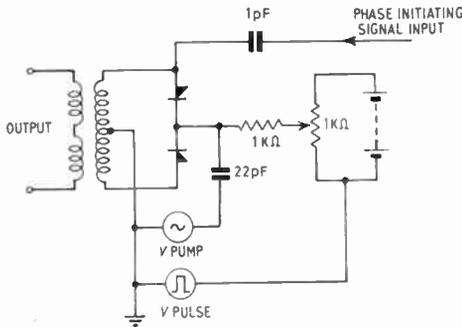
Fig. 4. First experimental balanced bridge circuit using abrupt junction diodes.

type. The inductor resonated with the total series capacitance of the two diodes at a frequency of about 5·7 Mc/s. The Q of the coil was 65 at this frequency and the parametric output was developed across a coil tightly coupled to the main winding. The pump frequency was varied between 11 and 12 Mc/s.

3.1. Measurements

The pertinent measurements fall under two main headings:—

(a) steady-state conditions,

and (b) switched conditions.

(a) *Steady-state conditions.* Referring to the circuit of Fig. 4, steady-state measurements were obtained with the negative terminal of the bias supply returned directly to earth (i.e. no pulse input), and with no phase-initiating input applied. With a pump frequency of 11·2 Mc/s an output frequency below the

resonant frequency of the tuned circuit would be expected. On increasing the pump amplitude from zero, no output is observed until a critical point A is reached (Fig. 5(a)).

At this point the parametron starts to oscillate in either of its two possible phases. As the pump amplitude is increased, the output rises to a maximum. Increasing the pump amplitude still further causes diode conduction, consequent increased circuit damping and a reduction of output voltage. Finally at point B excessive diode damping stops the oscillation altogether.

When the pump voltage is reduced, the curve retraces its original path. However, oscillation does not stop until critical point C, which corresponds to an input level below that of point A, is reached. The circuit thus displays a hysteresis effect. Repeating these measurements at a higher pump frequency shows a narrowing of this hysteresis loop (Fig. 5(b)), until at the highest frequency at which the circuit will operate, the loop disappears entirely (Fig. 5(c)). Figure 6
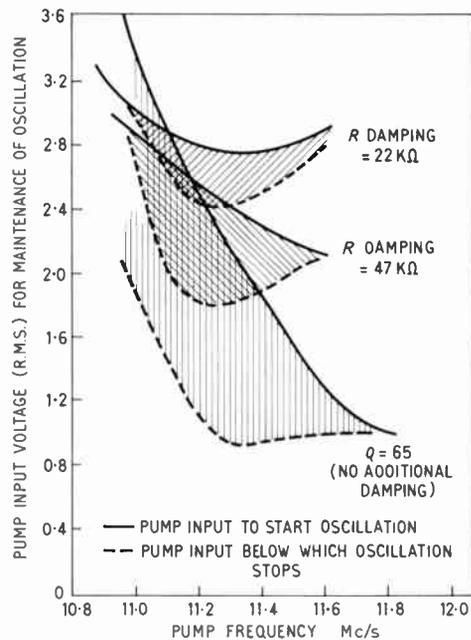

Fig. 6. Variation of hysteresis effects with pump frequency.

shows the range of pump voltage over which hysteresis effects are observed (i.e. between points A and C of Fig. 5). The three cross-hatched areas indicate the limits for three conditions of external damping. These curves demonstrate that

(i) As the frequency is lowered a larger pump voltage is required to cause oscillation.

and (ii) The greater the damping imposed on the tuned circuit, the larger is the required pump voltage to make the circuit oscillate.

Fig. 5. Steady state input/output characteristic.

(b) *Switched conditions.* When operating under switched conditions the phase-initiating signal must be applied before, and must overlap with, the pump voltage. However, for experimental purposes the initiating signal can be continuous, and the parametric output may be switched off by applying to the diodes a pulse of sufficient amplitude that the consequent change in capacitance causes the oscillation to cease.
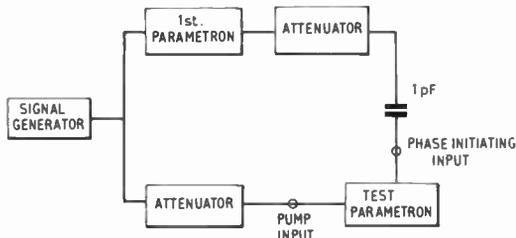

Fig. 7. Block diagram of test circuit.

The initiating signal should be related in phase to the pump signal of the parametron under test. This may be achieved by feeding the output of another parametron (operating at a similar frequency) via a capacitor of 1pF into the initiating input of the "test parametron". A common pump source may then be applied to the inputs of the two parametrons. For test purposes attenuators are provided in each of the inputs of the "test parametron" (Fig. 7). The time taken for the oscillation to build up to its final amplitude as a function of the phase-initiating voltage is shown in Fig. 8 for two values of the pump voltage.
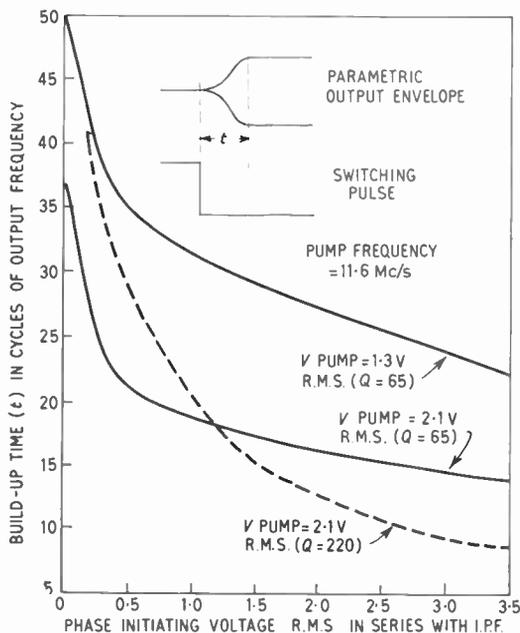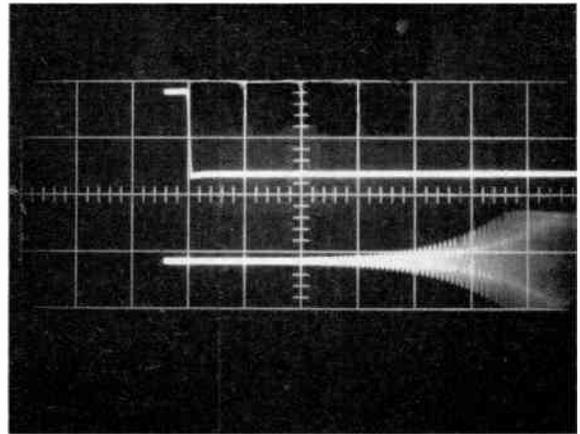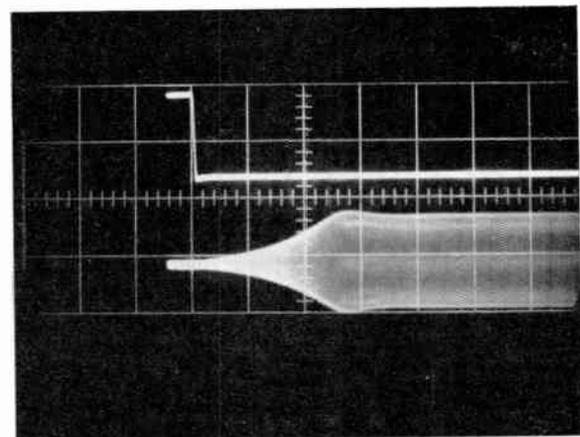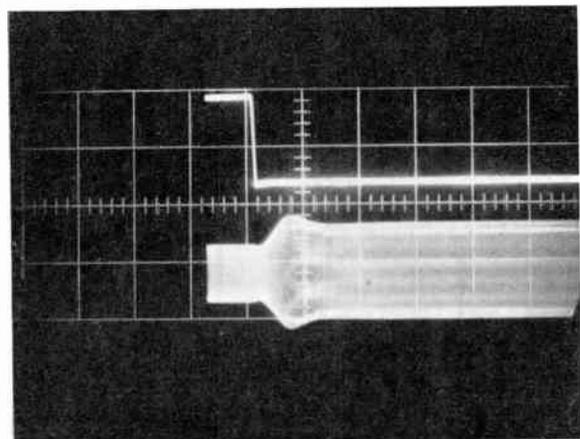

Fig. 8. Build-up time as a function of phase initiating voltage for the balanced bridge circuit shown in Fig. 4.

(a) Phase initiating voltage = <50 mV r.m.s.

(b) Phase initiating voltage = 400 mV r.m.s.

(c) Phase initiating voltage = 4 V r.m.s.

Fig. 9. Oscillograms showing build-up time of parametric output for a pump input voltage = 2·1 V r.m.s. (Horizontal scale = 2 μs/cm).
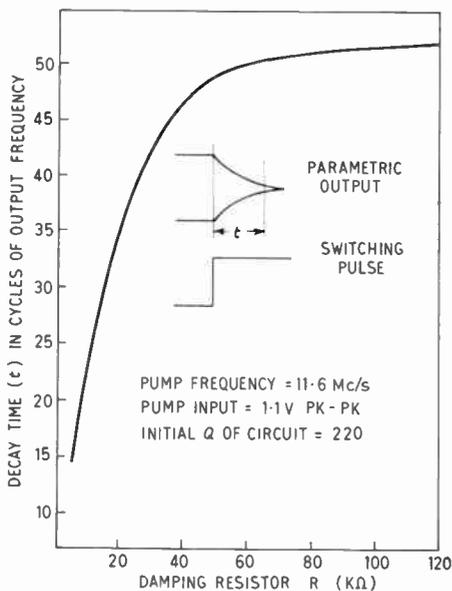
Fig. 15. Decay time to 10% of maximum amplitude—with damping.

voltage is V_2, we have

increase in energy $= \frac{1}{2}(C_2 V_2{}^2 - C_1 V_1{}^2)$

and assuming there is ideally no change in charge during this period (with a capacitance change of the form shown in Fig. 1(b)), then

$$C_1 V_1 = C_2 V_2$$

and increase in energy per cycle is

$$\frac{1}{2}\left(\frac{C_1}{C_2} - 1\right) C_1 V_1{}^2 \text{ joules}$$

Therefore pump power $= \frac{1}{2} C_1 V_1{}^2 \left(\frac{C_1}{C_2} - 1\right) \times 2f \text{ watts}$

$$......(6)$$

where $2f$ is the pump frequency.

The theoretical pump power required, as evaluated from the above expression, is 0·7 mW. This compares favourably with the results of between 0·8 and 1·2 mW. Powers of this order have been reported by other experimenters, but it is interesting to note that earlier figures quoted for microwave experiments[9] have been in the region of 30–50 mW, the difference presumably being accounted for by the high loss of the strip transmission lines employed in these tests. More recently,[10] microwave measurements have yielded pump powers of about 6 mW, when waveguide techniques were used.

4.3. Effect of Damping on the Minimum Input for Oscillation

Since increasing the damping on the circuit increases the total conductance G_t, given by expression (3), the magnitude of the negative conductance of expression

(2) must also increase to maintain the condition for oscillation given by eqn. (4). This implies that the pump voltage must increase, and is confirmed by the curve of Fig. 12.

4.4. Build-up Time

It has been shown[5] that the minimum number of cycles of the output frequency required for a growth factor e (i.e. time-constant) is given by

$$\frac{2}{\pi n}\left(\frac{V_0/V_r}{V_0/V_r - 1}\right)\left(1 + \frac{C_s}{C_0}\right) \qquad ......(7)$$

where $V_0 = (\phi - V_{dc})$
$V_r = (\phi - V_p)$
C_s = total stray capacitance.

It is more convenient to measure the total time from the instant of switching on the pump to that when the parametric output builds up to its final value. The total build-up time clearly depends on the amplitude of the initiating signal and is longest for zero applied initiating voltage. Under these conditions the oscillation builds up from noise and therefore takes many times the value given by eqn. (7). In order to correlate the results given in the curve (Fig. 13) to the theoretical results of eqn. (7), it is necessary to deduce the difference in the number of cycles of build-up time for two fixed voltages of initiating input, the amplitude of one of the initiating voltages being e times the other. The results of Fig. 13 show that with a pump voltage of 1·1 V and an initiating voltage of 2·7 V, build-up is complete in 6 cycles. With an initiating voltage of $2·7 \times 1/e = 1$ V, 11 cycles are required and therefore the number of cycles for growth factor e equals $11 - 6 = 5$ cycles.

Substituting the appropriate values in expression (7) gives a theoretical value for build-up of 4·4 cycles. The experimental results show good correlation with this figure.

It is recognized that the build-up time is a minimum when the pump amplitude is large enough to be just below the conduction point of the diodes.

Hilibrand and Beam have shown[5] that a theoretical minimum rise time of 1·3 cycles (using an abrupt junction diode) is possible. Practical values of 3 to 6 cycles at a frequency of 3·5 Mc/s have been reported from the United States.[7]

5. Practical Applications of the Parametron

In this type of circuit, information is conveyed by the phase of the signal only. The parametron is essentially a bi-directional device and cannot differentiate between its input and output circuits. Unidirectional transfer of the signal is achieved by employing the three-phase clock pulse system.[11, 12] This method
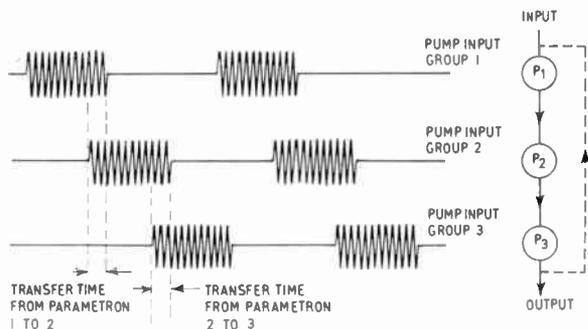
Fig. 16. Three-phase modulated pump system of information transfer.

requires three parametrons per bit. Referring to Fig. 16 a parametron is represented by a circle and each parametron is fed from a pump signal which is modulated by a three-phase generator of rectangular waveform. The parametrons are split into three groups or parts. P_1 is fed with the modulated pump signal, P_2 with the same signal but with a phase-lag of $2\pi/3$ radians and overlapping P_1 in terms of time. P_3 is fed with a similar signal with a further phase-lag of $2\pi/3$ radians and overlapping P_2. If now we consider that certain phase information is stored in a P_1 device it cannot be passed on to a P_2 device until both pump signals are simultaneously present—hence the overlap in time. Since, however, P_3 is not energized at this time, the information cannot proceed any further. Eventually the pump signals will be simultaneously present on P_2 and P_3 devices and the information will propagate from P_2 to P_3 circuits but not to P_1 circuits as these will not be energized at this time. Transfer from P_3 to P_1 circuits will only occur during the overlap of time of their pump signals.

Feeding the output of a P_3 parametron to the input of a P_1 parametron is a convenient method of producing a signal of reference frequency and phase. Dynamic flip-flop circuits can also be constructed in this manner.

Since it takes a finite time to transfer a signal from one parametron to another, groups of such circuits may be connected in tandem to form delay-lines.

5.1. *Logical Circuits*

In Fig. 17 information x, y, z is fed as either of two phases to the parametrons X, Y, Z and U and may be represented by digits "0" or "1".

The output phase is determined by the phase of the majority number of inputs and, therefore, there must always be an odd number of inputs. This is known as the "majority decision principle".[13] If x is always constant and equals the phase corresponding to the digit 1 it will be seen that the circuit possesses the property of an OR gate. If, on the other hand x corresponds to the digit 0, the logic results in the circuit acting as an AND gate.

Simple reversal of the signal will produce an inverter or NOT function. Circuits can be built around these and other logical bricks to perform the usual functions of a computer. Thus, in this type of circuit, one parametron will have to feed a number of similar parametrons. It has been shown that the properties of this circuit are adversely affected if the loading is increased beyond a certain value. This, therefore, sets a limit to the maximum number of circuits that any one parametron may feed.

6. Conclusions

1. The measurements have been confined to low-frequency operation. Since the time for the oscillation to build up to its final amplitude is inversely proportional to the output frequency, it is reasonable to assume that switching times will bear the same relationship at greatly increased frequencies. Evidence from the United States supports this theory.

2. The device has demonstrated that it can operate under widely variable circuit conditions.

3. For optimum build-up time the Q factor should be high. Also the pump amplitude should be as large as possible without causing diode conduction.

4. The second arrangement of circuit presented gives an overall improved performance.

7. Acknowledgments

8. References

1. S. Muroga and K. Takashima, "The parametron digital computer Musasino-1", *Trans. Inst. Radio Engrs (Electronic Computers)*, **EC-8**, No. 3, pp. 308–16, September 1959.

IF $x=1$ AND CONSTANT			
x	y	z	U
1	0	0	0
1	1	0	1
1	0	1	1
1	1	1	1

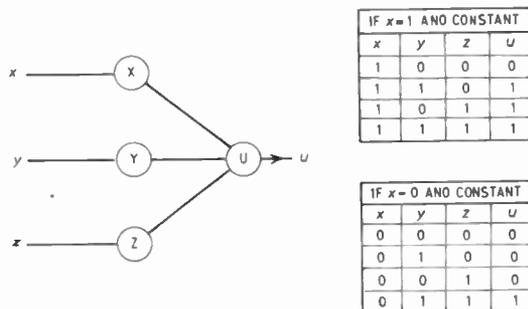| IF $x=0$ AND CONSTANT			
x	y	z	U
0	0	0	0
0	1	0	0
0	0	1	0
0	1	1	1

Fig. 17. Logical OR and AND gates using parametrons.

2. S. Muroga and K. Takashima, "System and logical design of the parametron digital computer Musasino-1", *J. Inst. Elect. Commun. Engrs, Japan*, **41**, pp. 1132–41, November 1958. (D.S.I.R. Translation No. 59–17793.)

3. K. Takashima, S. Muroga and K. Nishida, "Engineering description of the parametron digital computer Musasino-1", *J. Inst. Elect. Commun. Engrs, Japan*, **41**, pp. 1141–9, November 1958. (D.S.I.R. Translation No. 59–17792.)

4. S. Takahashi, "Development of Japanese computers", *Computer J.*, **2**, No. 3, pp. 122–9, October 1959.

5. J. Hilibrand and W. R. Beam, "Semiconductor diodes in parametric subharmonic oscillators", *R.C.A. Rev.*, **20**, No. 2, pp. 229–53, June 1959.

6. J. Hilibrand, C. W. Mueller, R. D. Gold and C. F. Stocker, "Semiconductor parametric diodes in microwave computers", *Trans. Inst. Radio Engrs (Electronic Computers)*, EC-8, No. 3, pp. 287–97, September 1959.

7. L. S. Onyshkevych, W. F. Kosonocky and A. W. Lo, "Parametric phase-locked oscillator—characteristics and applications to digital systems", *Trans. Inst. Radio Engrs (Electronic Computers)*, EC-8, No. 3, pp. 277–86, September 1959.

8. W. Shockley, "The theory of *p-n* junctions in semiconductors and *p-n* junction transistors", *Bell Syst. Tech. J.*, **28**, p. 435, July 1949.

9. F. Sterzer, "Microwave parametric subharmonic oscillator for digital computing", *Proc. Inst. Radio Engrs*, **47**, pp. 1317–24, August 1959.

10. A. H. Solomon and F. Sterzer, "A parametric subharmonic oscillator pumped at 34·3 kMc/s", *Proc. Inst. Radio Engrs*, **48**, p. 1322, July 1960.

11. E. Goto, "The parametron, a digital computing element which utilizes parametric oscillation", *Proc. Inst. Radio Engrs*, **47**, pp. 1304–16, August 1959.

12. J. von Neumann, "Non-linear capacitance or inductance switching, amplifying and memory organs", U.S. Patent No. 2,815,488 (3rd December, 1957).

13. S. Muroga, "Logical elements on majority decision principle and complexity of their circuits", *UNESCO International Conference on Information Processing*, June 1959, Chapter 5. pp. 400–15.

14. E. Goto, "On the application of parametrically excited non-linear resonators", *J. Inst. Elect. Commun. Engrs, Japan*, **38**, pp. 770–5, October 1955.

15. S. Sajiki and K. Togino, "An Application of the Parametron to the Numerical Control of Machine Tools", Government Mechanical Laboratory, Tokyo, October 1958 (27 pages).

16. S. Muroga, "Elementary principles of the parametron", *Datamation*, September/October 1958, pp. 31–4.

17. H. E. Billing and A. O. Rudiger, "The possibility of speeding up computers using parametrons", *UNESCO International Conference on Information Processing*, June 1959, Paper No. K.2.11 (14 pages).

18. J. Wesley Leas, "Microwave solid-state techniques for high speed computers", *UNESCO International Conference on Information Processing*, June 1959, Paper No. K.4 (12 pages).

19. R. L. Wigington, "A new concept in computing", *Proc. Inst. Radio Engrs*, **47**, pp. 516–23, April 1959.

20. F. Sterzer and W. R. Beam, "Parametric subharmonic oscillators", *Solid-State Circuits Conference*, 1959, pp. 86–7.

21. T. Rajchman, "Magnetics for computers", *R.C.A. Rev.*, **20**, No. 1, pp. 121–3, March 1959.

22. "Improvements in logical elements", International Business Machines, British Patent No. 793,799.

23. A. H. Nethercott, Jr., "On the switching time of sub-harmonic oscillators", *IBM J. Res. Development*, **4**, No. 4, pp. 402–6, October 1960.

24. D. B. Day, "Parametric diodes—design and fabrication", *J. Brit.I.R.E.*, **21**, No. 3, pp. 283–6, March 1961.

25. G. J. Lasher, "The dynamics of a subharmonic oscillator with linear dissipation", *IBM J. Res. Development*, **5**, No. 2, pp. 157–61, April 1961.

Directional Distribution of Ambient Sea Noise

By

P. RUDNICK, Ph.D.,†

V. C. ANDERSON, Ph.D.,†

AND

Cdr. B. A. BECKEN‡

Presented at the Symposium on "Sonar Systems", in Birmingham on 9th–11th July 1962.

Summary: Observations of the directional distribution of ambient sea noise are reviewed, for depths of 100 to 1000 feet, in the octave 0·75 to 1·5 kc/s, obtained with a 32-element spherical array yielding 32 simultaneous beams covering all directions in three dimensions. The results are presented diagrammatically. An appendix contains a description of the DIMUS beam-forming system (clipping and shift-register delays) which is employed.

1. Introduction

The Marine Physical Laboratory of the Scripps Institution of Oceanography is conducting an investigation of the directional distribution of ambient noise in the sea with an array and associated equipment which were originally designed and described by Anderson.[1,2] This is believed to be the first attempt to observe a three-dimensional pattern at low frequency. Teer has reported observations at 19 kc/s with a line array[3] and results at lower frequencies with a deep line array have recently appeared.[4,5]

2. Experimental Arrangements

The array used in the present work contains thirty-two non-directional receiving hydrophones arranged in two concentric spheres with radii 4·5 ft and 2·7 ft. Thirty-two conical beams are simultaneously formed, their directions spread uniformly over the sphere. The frequency range at present is the octave 0·75 kc/s to 1·5 kc/s.

The array is suspended with a single armoured coaxial cable, lowered over the side of a small ship, then supported by submerged floats and a spar buoy near the side of the ship but connected with it only by slack cable. The maximum depth thus far is 1000 ft.

Outputs of the individual hydrophones are telemetered over the supporting cable to the ship, where they are available as analogue voltages. Beams are formed by the DIMUS (digital multibeam steering) system,[2] which involves clipping and sampling of individual hydrophone outputs, followed by shift-registers used as delay lines.

Each of the thirty-two beams is rectified and smoothed, and is also available unrectified for aural

---

† University of California, San Diego Marine Physical Laboratory of the Scripps Institution of Oceanography, San Diego 52, California.

‡ U.S. Navy Electronics Laboratory, San Diego 52, California.

monitoring. The rectified outputs are scanned in sequence. The original method of recording was by frame-by-frame photography of an oscilloscope face; more recently eight-bit numbers are punched on paper tape.[6] This tape is in a form which permits immediate entry of data into a Bendix G-15 digital computer, for averaging and other numerical operations. The overall accuracy of beam-to-beam comparison at any instant is believed to be well within 0·5 dB. The customary pattern of observation when photographic recording was used was as follows. The array was held at a fixed depth at one station for a period of one hour, during which time three four-minute camera records were made at half-hour spacing. Frames taken 14 seconds apart were read, giving about 50 sets of beam outputs which were averaged for the given depth-station.

3. Results

The first substantial program of data collection and reduction was carried through by Becken[7] before the digital computer technique was devised. His results, in graphical form, are reproduced in Figs. 1 and 2. Figure 1 shows a representative set of data, taken in sea state 3, plotted to display the dependence of intensity on azimuth. In this figure, θ is a colatitude angle, measured from the vertically downward propagation direction. Elliptical patterns, with the long axis tending to be parallel to the wave-fronts of the swell, were normally observed. In this plot the beam outputs are plotted without adjustment for the response of the beam for directions other than its axis. Figure 2 (a)–(e), on the other hand, present "restored" fields which, when subject to the degeneration resulting from the limited off-axis rejection of the array, correspond to the observed beam intensities, averaged over all azimuths at each elevation.

Becken found these results consistent with the Knudsen[8] data on sea state dependence. He somewhat formally separated the observed patterns into two
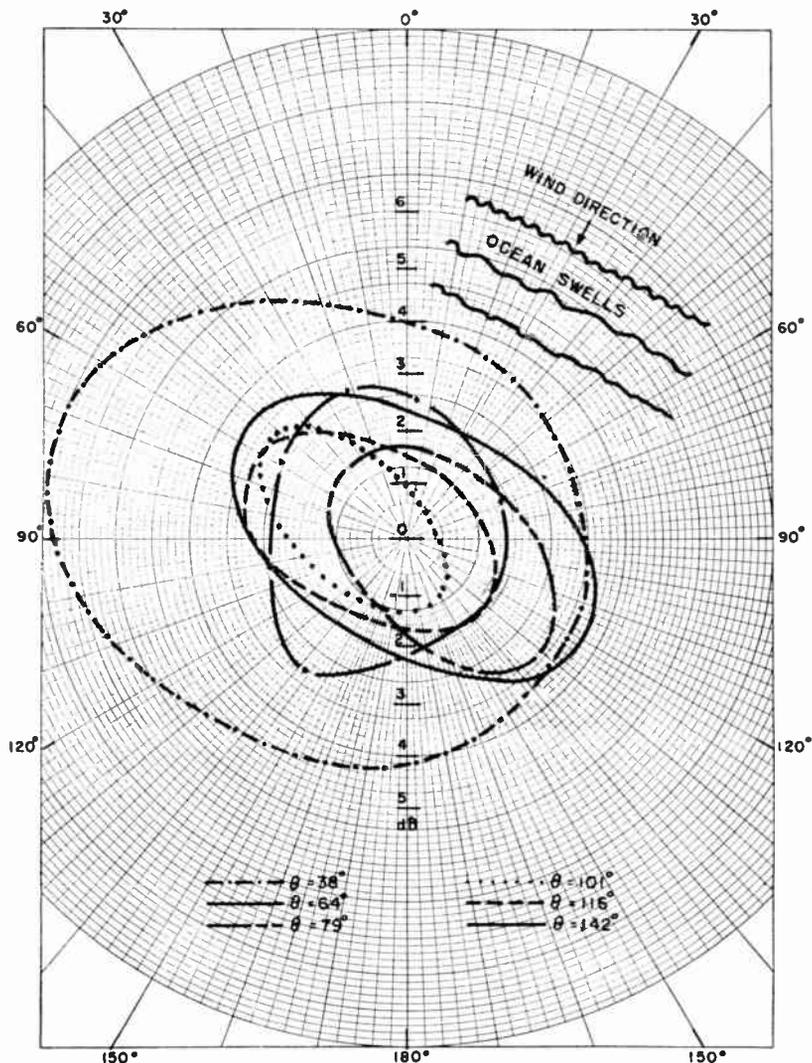
Fig. 1. Ambient noise azimuthal dependence.

additive components, one isotropic and independent of sea state, the other anisotropic and containing the whole of the observed variation with sea state. This latter component he found consistent with a simple model embodying a homogeneous distribution of directional sources on the sea surface, rectilinear propagation with the accepted value of volume absorption, and specular bottom reflection with a reasonable dependence of intensity on angle. The radiated power per unit of surface area was postulated proportional to $(\cos \theta)^n$ with $n = 2$ for $70° \leqq \theta \leqq 90°$ and $n = (90° - \theta)/10$ for $0° \leqq \theta \leqq 70°$, θ being the angle of reflection measured from the normal.

4. Acknowledgments
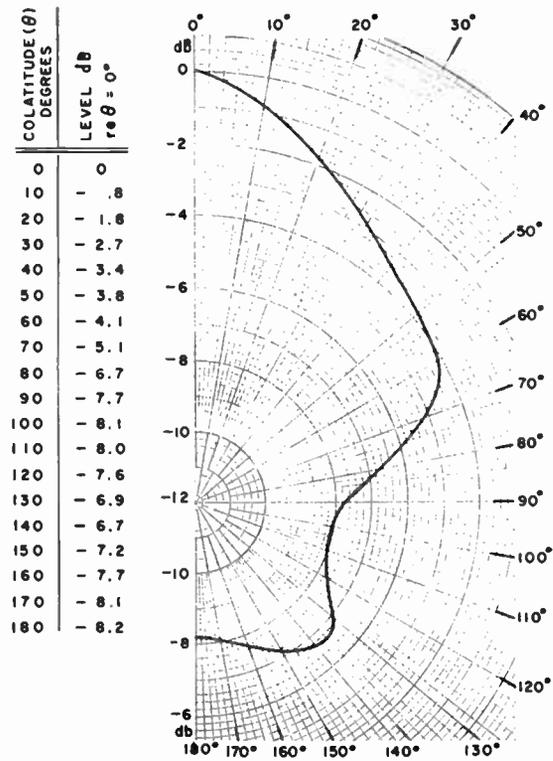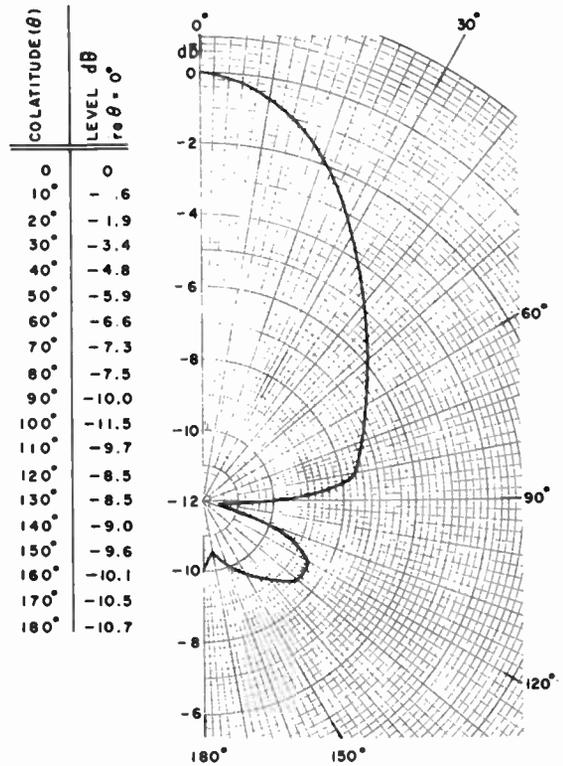
5. References

1. Victor C. Anderson, "Arrays for the investigation of ambient noise in the ocean", *J. Acoust. Soc. Amer.*, 30, No. 5, pp. 470–7, May 1958.

2. Victor C. Anderson, "Digital array phasing", *J. Acoust. Soc. Amer.*, 32, No. 7, pp. 867–70, July 1960.

3. C. A. Teer, H.M. Underwater Detection Establishment Report No. 65, 1949.

4. Carle A. Forster, "Ambient sea-noise directivity", Paper L4, 64th Meeting, Acoustical Society of America, Seattle, Washington, 7 November 1962.

5. Jack G. Watson, "Deep ocean-noise model determined by a deep-line array", Paper L5, 64th Meeting, Acoustical Society of America, Seattle, Washington, 7 November 1962.

6. Earl D. Squier, "Digital encoder and paper tape punch", University of California, San Diego, Marine Physical Laboratory of the Scripps Institution of Oceanography, San Diego 52, California, SIO Reference 63–1, 1 February 1963.
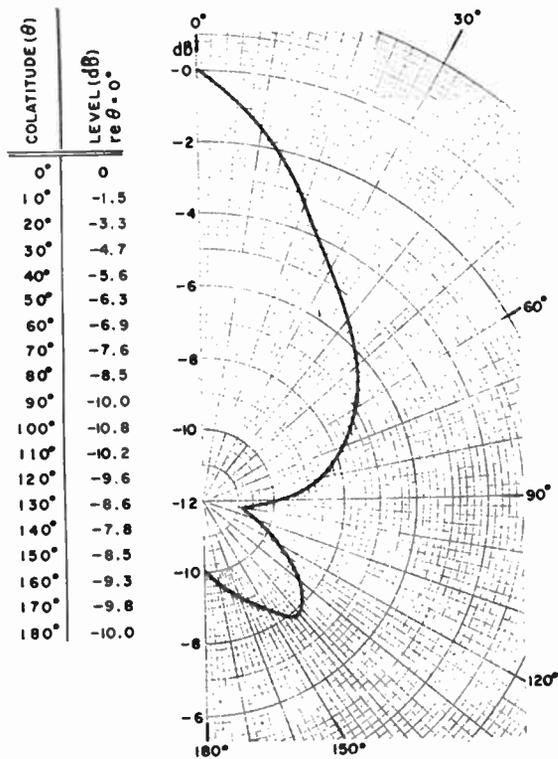
COLATITUDE (θ) DEGREES	LEVEL dB re θ = 0°
0	0
10	− .8
20	− 1.8
30	− 2.7
40	− 3.4
50	− 3.8
60	− 4.1
70	− 5.1
80	− 6.7
90	− 7.7
100	− 8.1
110	− 8.0
120	− 7.6
130	− 6.9
140	− 6.7
150	− 7.2
160	− 7.7
170	− 8.1
180	− 8.2

(a) Sea state 3, array depth 1000 ft.

COLATITUDE (θ)	LEVEL dB re θ = 0°
0	0
10°	− .6
20°	− 1.9
30°	− 3.4
40°	− 4.8
50°	− 5.9
60°	− 6.6
70°	− 7.3
80°	− 7.5
90°	−10.0
100°	−11.5
110°	− 9.7
120°	− 8.5
130°	− 8.5
140°	− 9.0
150°	− 9.6
160°	−10.1
170°	−10.5
180°	−10.7

(b) Sea state 3, array depth 560 ft.

COLATITUDE (θ)	LEVEL (dB) re θ = 0°
0°	0
10°	−1.5
20°	−3.3
30°	−4.7
40°	−5.6
50°	−6.3
60°	−6.9
70°	−7.6
80°	−8.5
90°	−10.0
100°	−10.8
110°	−10.2
120°	−9.6
130°	−8.6
140°	−7.8
150°	−8.5
160°	−9.3
170°	−9.8
180°	−10.0

(c) Sea state 3, array depth 150 ft.

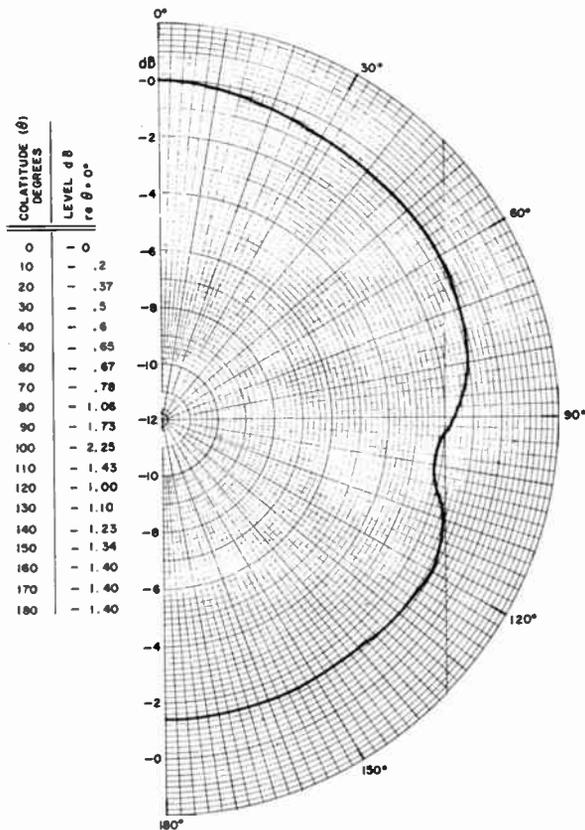| COLATITUDE (θ)	LEVEL (dB) re θ = 0°
0°	0
10°	− 1.1
20°	− 2.1
30°	− 2.9
40°	− 3.3
50°	− 3.6
60°	− 3.7
70°	− 3.8
80°	− 5.3
90°	− 6.5
100°	− 7.6
110°	− 7.0
120°	− 5.8
130°	− 5.1
140°	− 4.8
150°	− 4.7
160°	− 4.8
170°	− 5.2
180°	− 5.7
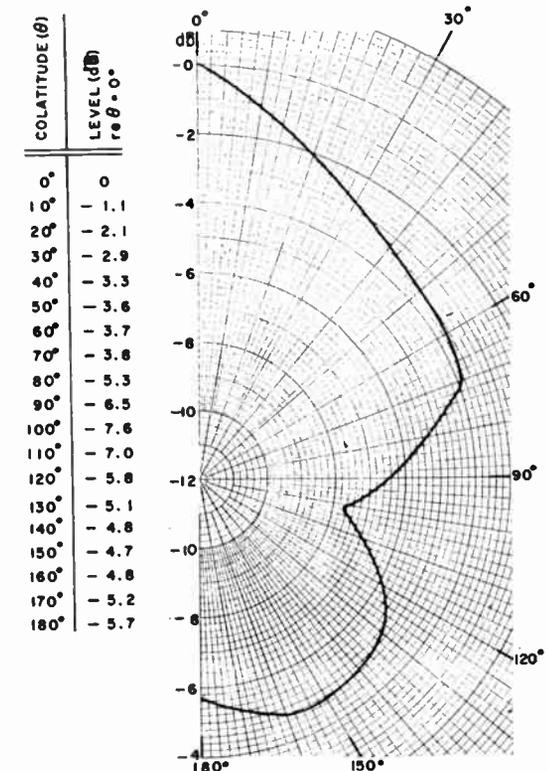
(d) Sea state 1 +, array depth 130 ft.

Fig. 2. True field vertical distribution.

(e) Sea state 1/2, array depth 1000 ft.

7. B. A. Becken, "The directional distribution of ambient noise in the ocean", University of California, San Diego, Marine Physical Laboratory of the Scripps Institution of Oceanography, San Diego 52, California, SIO Reference 61–4, 7 March 1961.

8. V. O. Knudsen, R. S. Alford and J. W. Emling, Rpt. No. 3, NDRC Sec. No. 6. 1, NDRC-1848 (1944).

9. Philip Rudnick, "Small signal detection in the DIMUS array" J. Acoust. Soc. Amer., 32, pp. 871–7. July 1960.

6. Appendix

Description of DIMUS Beam-Forming System

The thirty-two f.m. telemetered hydrophone voltages, after demodulation, are subject to infinite clipping, and each is sampled at a 5-kc/s rate and fed to a 10-stage shift register. The sequence of polarity samples is passed along the register by means of 5-kc/s clocking pulses, and is available at any of 10 output taps, with maximum relative delay of 1·8 ms. A 32 × 32 matrix of isolating resistors is used to add these sequences of polarity samples in the same way that analogue signals would be combined to form the thirty-two simultaneous beams. Each hydrophone contributes with the appropriate time delay to each beam. The output of each beam is quantized in time at the 5-kc/s sampling rate, and quantized in voltage to 33 possible values of which a range of ± 3 just exceeds the standard deviation when the hydrophones receive uncorrelated Gaussian noise.

A detailed analysis has been published[9] comparing this system with the conventional one for the detection of weak plane-wave signals in isotropic Gaussian noise. The effect of clipping is to distort the scale of all correlation coefficients by the well-known arcsin relationship, depressing all small inter-element correlations by a factor $2/\pi$, including those which constitute the signal. The actual loss of detectability is not as great as this, however, for two reasons. A portion of the noise, that arising from inter-element correlations, is similarly depressed, and the clipping extends the spectrum of the noise toward higher frequencies, so that it is more effectively smoothed after rectification. The overall loss in detection threshold ranged from 0·5 to 1·5 dB in particular examples, including effects of delay quantization. This may be regarded as a small price to pay for the substantial equipment advantages, which make feasible large numbers of simultaneous beams.

A second practical effect of clipping is a normalization of the beam output. It is wholly insensitive to changes in absolute noise power; each beam output approximately represents signal-plus-noise/noise-ratio. This is convenient in limiting the range required of a recorder, but in the present experiments made it necessary for absolute noise levels to be obtained by an auxiliary measurement of the analogue voltage of one hydrophone which could be combined with the relative values from the various beams.

Some of the explicit advantages of the DIMUS system are: relief from need of amplitude matching of hydrophones in the array, complete freedom from attenuation and dispersion in the delay lines, and easy availability of indefinitely long delay per section which is useful at low frequencies.

Phenomena During the Growth and Decay of Spread-F

By

M. S. V. GOPALA RAO, Ph.D.†

AND

Professor

B. RAMACHANDRA RAO,

D.Sc. (*Member*)†

Summary: Continuous observations of the ionospheric echoes at the time of the onset of spread-F and during the decay of the same, yielded useful information. Two different types of spread-F onset are described. An attempt is made to find out whether the F-layer drift spreads measured by the three station method on 5·6 Mc/s at 1830 hours l.t. are related to the magnitude of spread-F that is likely to occur later in the night.

1. Introduction

When pulsed radio waves from a vertical pulse sounding ionosphere station are reflected back from an ideally stratified ionosphere, one would naturally expect clear echoes corresponding to a well-defined single virtual height; but on some occasions the ionospheric echo becomes very diffuse with a mountain range of echoes having various time delays. When this condition prevails for the F region echoes, the phenomenon is known as spread-F. This phenomenon is mainly a night-time phenomenon at equatorial and lower middle latitude stations, whereas at higher latitudes it is said to occur even during daylight hours. The $h'F$ record under spread-F conditions will be very diffuse and no definite layer structure can be identified. In fact, when spread-F is highly active, no critical frequency can be obtained and radio propagation over long distance will be affected by the irregularities responsible for spread-F. Although this phenomenon was known for more than two decades, it has not been well understood, particularly in relation to its origin and geomagnetic effects.

2. Experimental Technique

The experimental set-up employed is the conventional vertical pulse-sounding equipment used for ionospheric research. It consists of a 5 kW peak power pulse transmitter radiating r.f. pulses of 100 µs width at the rate of 50 c/s on a frequency of 5·6 Mc/s. The power from the transmitter is fed to one of the crossed delta antennas aligned in a N–S direction. The signals received on the E–W delta antennas are fed to a communications receiver modified for pulse reception, the output of which is fed to the Y plates of one of the three beams of a triple beam oscillograph. Spread-F observations are made using only one beam of the triple beam oscillograph. When the equipment is used for drift recording by the spaced receiver method before onset of spread-F

† Ionospheric Research Laboratories, Andhra University, Waltair, India.

as part of the present investigation, signals from three dipole aerials situated at the corners of a right-angled triangle whose sides are 108 metres, are fed to three identical BC-348 receivers and the output displayed on the three beams of the oscillograph. The fading records of the 1F2 echoes is taken, after isolating them by a suitable slit, on a DuMont camera having 35 mm film moving at the speed of 6·3 cm/min. The records are analysed as usual by the similar-fades method by measuring the time displacements between the fading peaks of the N–S and E–W pair of aerials under a microfilm reader.

3. Phenomenon Observed during Formation of Spread-F

In general, very quick and deep fading preceded the onset of the spread-F phenomenon. There is some suddenness in the development of this quick fading because fading of the echo even 5 to 10 minutes prior to this development never indicated or suggested the tendency to increase. Normally the fading rate increased rapidly from about 2–5 cycles/min to about 30–60 cycles/min or even more. After a few minutes of such violent fading, the echo splits into two or more echoes. After splitting, the fading rates of these split components are reduced. Gradually the echo pattern widens and several other spread echoes appear, making up a continuous patch. In some cases the first split component drifts apart appreciably and rapidly from the main 1F echo and later it spreads covering up the gap and finally envelops the main echo. One typical fading record taken on 9th September 1959 from 1850 hrs to 1856 hrs l.t. on 5·6 Mc/s which shows the rapid increase in the fading rate before the onset of spread-F is reproduced in Fig. 1. The three fading patterns correspond to the three receivers used in the regular ionospheric drift measurements by the spaced receiver method which have been carried out at this station for quite a long time.

On the other hand, it is also observed, on some of the nights, that even prolonged quick and deep fading for about half an hour was not followed by
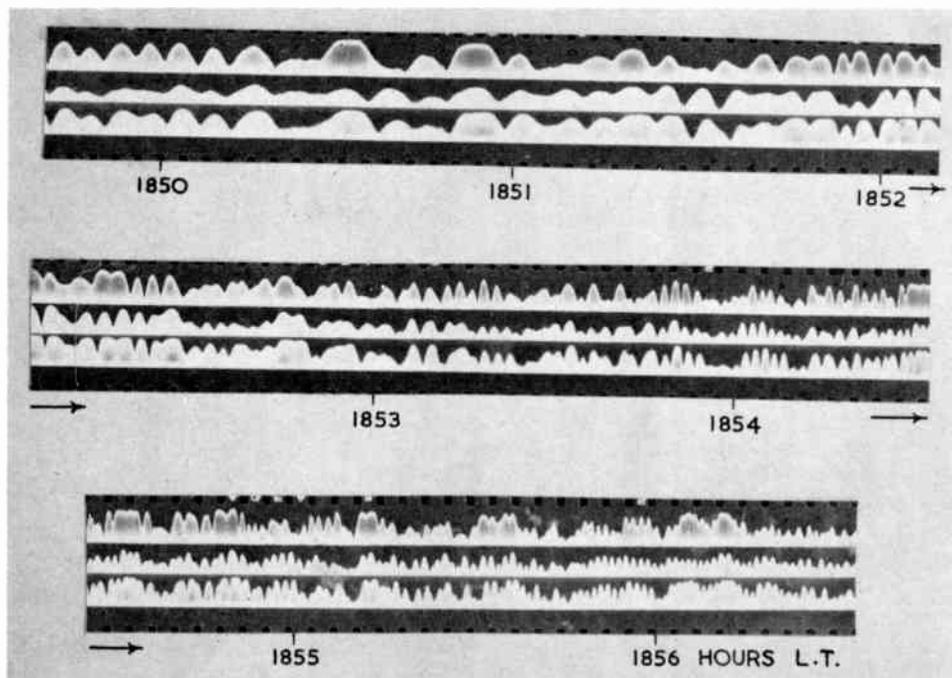
Fig. 1. Rapid increase in the fading rate of the 1F echo prior to the onset of spread-F.

splitting or subsequent formation of spread echoes, appearing as if some inhibiting agency is at work.

In an altogether different type of spread-F onset, no rapid fading is observed to precede the onset of the phenomenon. In these cases a remote patch or a slightly diffused echo appears suddenly at an equivalent height which is about 100 km more than the regular 1F echo. This group gradually spreads on both sides and drifts nearer to and envelopes the 1F echo, which, till then, remains separate and clean without any diffusiveness. Sequences of echo patterns photographed at close time intervals showing the growth of spread-F in different ways are presented in Fig. 2(a), (b) and (c). Each sequence is photographed without disturbing the relative disposition of the 50 km height marks which can be seen just beneath some of the snaps. Sequences (a) and (b) correspond to the first type of spread-F onset which was preceded by quick and deep fading. The sequence (c) corresponds to the second type of onset which was not preceded by quick fading but developed from a remote echo. In this sequence it will be seen that a remote echo which showed no trace at 1835 hrs l.t. appeared at 1840 hrs and while developing gradually into a patch merged with the main 1F echo at 1906 hrs l.t. A study of several of these sequences lead us to believe that in the first type of onset, the required spread-F irregularities have developed locally, while in the second type, the irregularities could have been brought to the overhead point by way of lateral (horizontal) drifts from some

other neighbouring region while they were developing

It is very likely that the quick and deep fading of the single echo occurring just before the first type of spread-F onset is part of the development process of the required irregularities in the ionization density at some unknown level. There is some evidence to show that the incidence of this type of fast fading is almost simultaneous on different frequencies. Further, it is noticed that the fading at this time is not only quick and deep but also, on several occasions, strikingly periodic. This periodic nature of the fading, together with the subsequent splitting of the echo and consequent reduction in the fading rate, is suggestive of the formation of a magneto-ionic split component of spread-F echoes. Some polarization tests made on these splitting echoes confirmed the existence of ordinary and extraordinary echoes under such conditions. It will be noted that a similar splitting of the p'F trace just before the onset of equatorial spread-F has recently been reported by Lyon et al.[2]

4. Spread-F Characteristics during Decay

Continuous observations were similarly made between 2300 hrs and 0100 hrs l.t. to follow the disappearance of the spread-F conditions. The sequence of photographs taken on 24th November 1959 from 2325 hrs l.t. to 0048 hrs shown in Fig. 2(d) illustrates this process clearly. To start with at 2325 hrs l.t. the echo pattern was of type B (severe) according to the classification introduced by Rao and
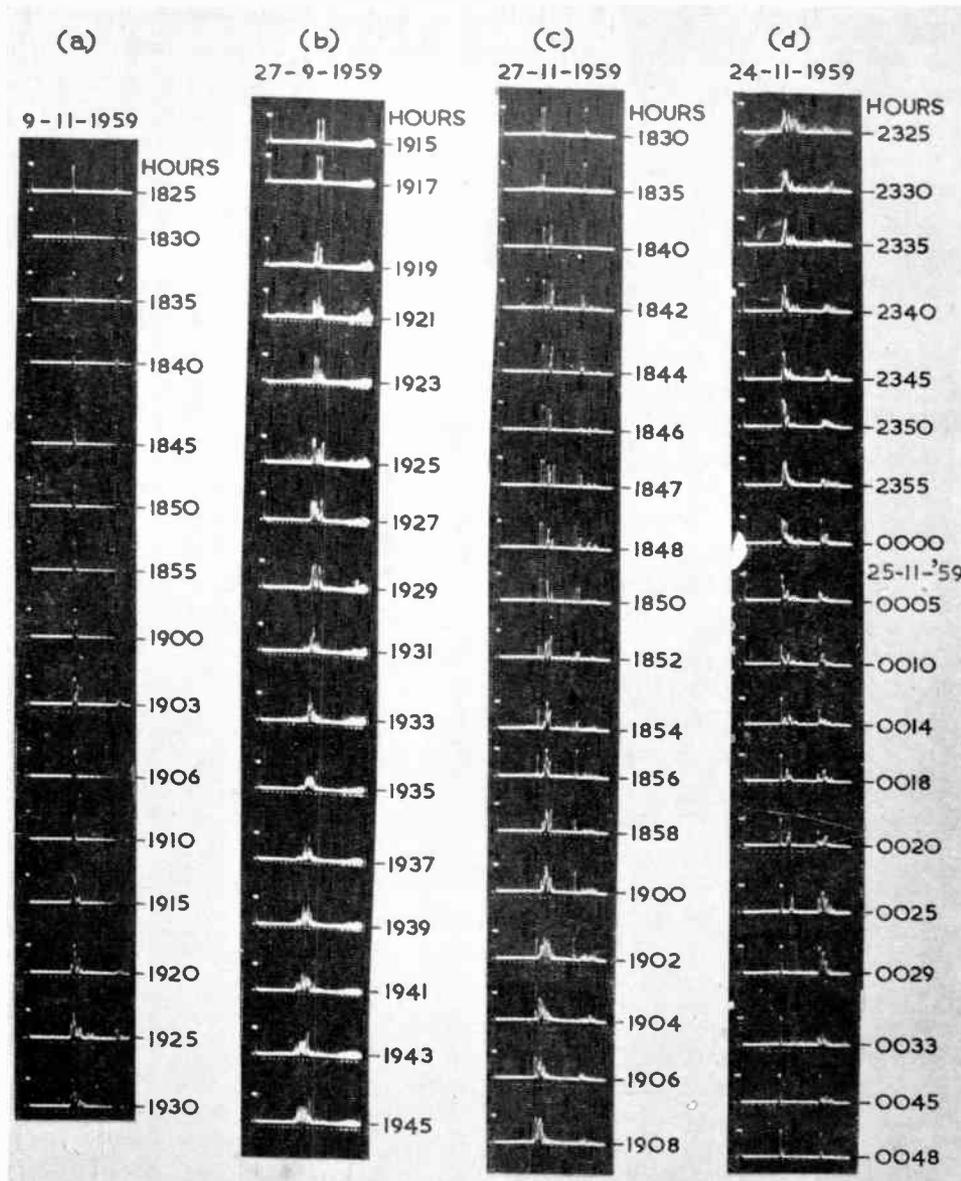
Fig. 2. Sequences of photographs illustrating the growth and decay of spread-F echoes.

Rao.[3] Gradually the pattern changed to type A (less severe) by 2325 hrs and then within 15 to 20 minutes a patch of echoes is seen drifting apart and leaving the main 1F echo separate. At 0029 hrs it is interesting to note that the 1F echo is cleared of spread-F while the 2F echo persists showing spread-F conditions which continued up to 0048 hrs. A nearly similar situation has recently been reported by Booker[4] in his study of the unusual echoes observed in a sequence of ionograms taken after a missile transit through the local F-region. He explained the results by assuming a punched hole in the F-region and suggested the possibility of a similar structure

to produce spread-F echoes. The above result is therefore consistent with such a possibility. Detailed examination into this aspect is however necessary.

The sequences of photographs presented in Fig. 2 were recorded without altering the gain controls of the receiver. It will be seen that the amplitudes of the individual echoes in the fully developed spread-F patch are not appreciably smaller than the original simple overhead echo before spreading. This appears to indicate that several of the echoes in the spread-F patch are received by some scattering or other process than by partial reflections from really different heights. This view is consistent with the results of
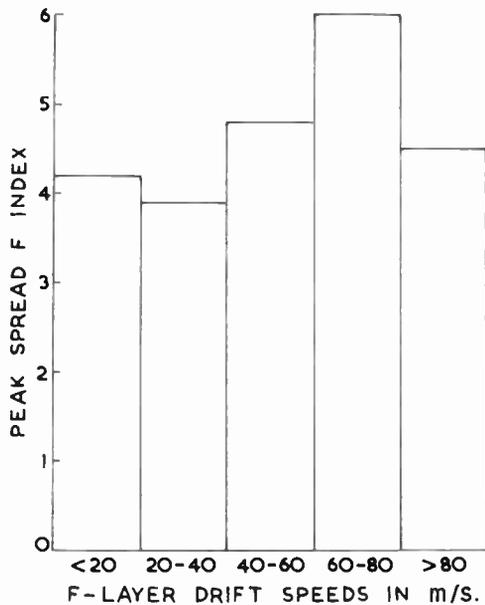
Fig. 3. Diagram showing the F-layer drift speeds in relation to the peak spread-F index.

McNicol *et al.*[5] who have determined the directions of arrival of the spread-F echoes and found them to be generally away from the vertical. The present method of recording the changes in the spread-F phenomenon is somewhat similar but not identical with the "swept-gain" $R' - t$ recording technique used by McNicol *et al.*[5]

5. Spread-F Activity in Relation to F2 Region Drifts

In their systematic study of F2 region drifts at Waltair, Ramachandra Rao and Bhagiratha Rao[6] observed a regular subsidiary maximum in the magnitude of drift speeds at about 2000 hrs l.s.t. in all the seasons. This had been attributed to the increase in the virtual height of the F-layer at this time. As this is also observed to be the time of maximum occurrence and magnitude of spread-F activity, it is of interest to see whether these increased drift speeds are in any way related to the spread-F phenomenon. The inverse correlation of F2 drift speeds with magnetic activity reported for this station by Rao *et al.*[7] is also comparable with the negative correlation between spread-F and magnetic activity at equatorial latitudes.

When spread-F is prevailing at any station the usual closely-spaced receiver method of ionospheric drift measurement will not be applicable. But measurements will be possible before the onset of the quick and deep fading which precedes the onset of spread-F. It is difficult to say whether this quick fading is a manifestation of increased drift speeds. With a view to studying whether the magnitude of drift speed in the F-region observed at 1830 hrs l.s.t.

(which is well before the onset of spread-F) on individual nights, has any relation with the magnitude of spread-F observed on the same nights a series of routine drift measurements were carried out for 5 months from 1st September 1959. F-layer reflections on 5·6 Mc/s were used for this purpose.

For the purpose of analysis the data on drift speeds are divided into groups of magnitudes of < 20; 20 to 40; 40 to 60, etc. The peak spread-F indices attained on individual nights falling into these groups are sorted out and average values of the peak spread-F index corresponding to each of the above groups are obtained. The results are shown in Fig. 3. Some tendency for the increased drift speeds to be associated with larger values of peak spread-F index is clear up to a drift speed of 80 m/s. But there is a fall in the last group which might have resulted by the averaging of insufficient data. It may be noted that Maxwell[8] considered the magnitudes of the F2 drift speeds determined by star scintillation methods in connection with his discussion on the turbulence in the upper atmosphere as a cause for radio star scintillations and spread-F.

6. Acknowledgment

7. References

1. M. S. V. Gopala Rao, B. Ramachandra Rao and P. Rama-chandra Rao Pant, "Correlation of spread-F activity with F-region height changes", *J. Atmos. Terrestr. Phys.*, **17**, p. 345, February 1960.

2. A. J. Lyon, N. J. Skinner and R. W. Wright, "Equatorial spread-F at Ibadan, Nigeria", *J. Atmos. Terrestr. Phys.*, **21**, Nos. 2–3, p. 100, June 1961.

3. M. S. V. Gopala Rao and B. Ramachandra Rao, "Nocturnal and seasonal variations of equatorial spread-F", *J. Atmos. Terrestr. Phys.*, **22**, No. 1, p. 12, September 1961.

4. H. G. Booker, "A local reduction of F-region ionization due to missile transit", *J. Geophys. Res.*, **66**, No. 4, p. 1073, April 1961.

5. R. W. E. McNichol, H. G. Webster and G. G. Bowman, "A study of spread-F ionospheric echoes at night at Bris-bane. I. Range spreading (experimental)", *Aust. J. Phys.*, **9**, No. 2, p. 247, June 1956.

6. B. Ramachandra Rao and E. Bhagiratha Rao, "Study of horizontal drifts in the F1- and F2-regions of the ionosphere at Waltair", *J. Atmos. Terrestr. Phys.*, **14**, Nos. 1–2, p. 94, April 1959.

7. B. Ramachandra Rao, E. Bhagiratha Rao and Y. V. Ramana Murthy, "Effect of magnetic activity on drifts of the F2-region", *Nature (London)*, **183**, p. 667, 7th March 1959.

8. A. Maxwell, "Turbulence in the upper ionosphere", *Phil. Mag.*, **45**, p. 1247, December 1954.

Microwave Branching Systems

By

M. V. O'DONOVAN

(Associate Member)†

Summary: In multi-channel microwave radio relay systems it is sometimes necessary to have a number of transmitters and receivers simultaneously utilizing the same aerial. This is advisable from economic considerations because of the saving entailed in feeder and aerial costs. To achieve this a complex branching system is necessary. The object of this paper is to describe the design and development of such a branching system in the 7000 Mc/s frequency band.

The branching system contains a number of branching units connected in cascade. Each unit consists of a number of microwave band-pass filters and 3 dB short-slot couplers in a suitable configuration. By means of detailed experimental investigation and theoretical analysis a design procedure for band-pass filters in waveguide is derived and normalized design curves are plotted. Filter characteristics calculated on a theoretical basis are compared with those obtained from experimental prototypes. The design data for broad-band short-slot couplers is derived. On the basis of the information obtained a prototype 3 dB coupler is developed and its characteristics measured. The operation of a branching unit is described. Finally, the specification of the complete branching system is outlined and a prototype constructed. A description is given of the tests carried out on it and the results of these tests.

1. Introduction

A number of excellent papers have already been written on the design of microwave filters. The branching system described here utilizes maximally-flat filters and this is the only type of filter dealt with in this paper. The author has found, however, that insufficient attention has been paid in the past to fundamental cavity design, i.e. to determine on a theoretical basis the exact physical dimensions of a resonant cavity having prescribed electrical characteristics. This particular aspect of filter design is dealt with at length and accurate design curves are plotted.

In the case of the 3 dB short-slot coupler the design data are derived from an initial consideration of the different modes sustained in the coupling section.

2. Microwave Filter Design

2.1. Circuit Theory

If a resonant branch in a filter is connected between a generator and a load, each of resistance R, its loaded Q can be defined in terms of the resulting insertion loss in the following manner:

$$\frac{P_0}{P_L} = 1 + Q_L^2 \left(\frac{f}{f_0} - \frac{f_0}{f}\right)^2 \qquad \ldots\ldots(1)$$

where P_0 = power available from generator

P_L = power delivered to the load

f_0 = resonant frequency of branch

f = frequency at which insertion loss is measured.

† Pye Telecommunications Ltd., Cambridge.

If the power delivered to the load is -3 dB of the available power at a frequency f_c then

$$\frac{P_0}{P_L} = 2 \quad \text{and} \quad Q_L = \frac{1}{\dfrac{f_c}{f_0} - \dfrac{f_0}{f_c}} \qquad \ldots\ldots(2)$$

As the 3 dB bandwidth is normally specified in the design of maximally-flat filters it follows that the loaded Q of a complete filter can be found from equation (2).

Consider the low-pass lumped element prototype normalized to $R = 1$ and $\omega' = 1$ at the 3 dB points (Fig. 1(*a*)). Cohn[1] has demonstrated that the insertion loss function for such a prototype is

$$A = 10 \log_{10}(1 + \omega^{2n})$$

where n is the total number of branches.

The element values for a maximally-flat response are given by the expression

$$g_K = 2 \sin\left[\left(\frac{2K - 1}{2n}\right)\pi\right] \qquad \ldots\ldots(3)$$

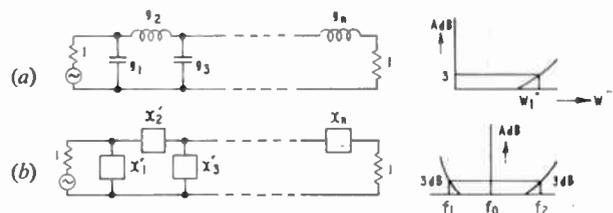where K is the number of the branch from one end of the filter.

Fig. 1. (*a*) Low-pass prototype.
(*b*) Band-pass equivalent.

Transformation to the band-pass equivalent circuit of Fig. 1(b) is achieved by substituting the following expression for ω'

$$\omega' = \frac{\dfrac{\omega}{\omega_0} - \dfrac{\omega_0}{\omega}}{\dfrac{\omega_2}{\omega_0} - \dfrac{\omega_0}{\omega_2}} = Q_L\left(\frac{\omega}{\omega_0} - \frac{\omega_0}{\omega}\right) \quad \ldots\ldots(4)$$

Transforming the reactance of the series branch of the low-pass prototype, $j\omega'g_2$ to the band-pass equivalent

$$x'_2 = j\omega g_2 \frac{Q_L}{\omega_0} - j\omega_0 g_2 \frac{Q_L}{\omega}$$

$$= j\omega \frac{g_2 Q_L}{\omega} + \frac{1}{j\omega \dfrac{1}{\omega_0 g_2 Q_L}} \quad \ldots\ldots(5)$$

It follows, therefore, that x'_2 is a series resonant circuit with an inductive element $L'_2 = g_2 Q_L/\omega_0$ and capacitive element $C'_2 = 1/\omega_0 g_2 Q_L$.

The Q of a series resonant circuit can be defined as

$$Q = \frac{\omega_0 L}{2R}$$

Therefore

$$Q_2 = \frac{g_2 Q_L}{2R}$$

Transforming any one of the shunt branches of the low-pass prototype gives a similar result. The general case can, therefore, be expressed as

$$Q_K = \frac{g_K Q_L}{2R} \quad \ldots\ldots(6)$$

Substituting for g_K in equation (3) gives

$$Q_K = Q_L \sin\left[\left(\frac{2K-1}{2n}\right)\pi\right] \quad \ldots\ldots(7)$$

Transforming the insertion loss function

$$A = 10\log_{10}\left\{1 - \left[Q_L\left(\frac{f}{f_0} - \frac{f_0}{f}\right)\right]^{2n}\right\} \text{ dB} \quad \ldots(8)$$

2.2. Inclusion of V.S.W.R. in Design Formulae

In the design of microwave filters for multi-channel radio relay systems one of the most important specifications is the maximum v.s.w.r. that can be tolerated within the pass-band. It is imperative, therefore, that this is included in the design formulae.

Consider a transmission line which contains a discontinuity.

Let ρ_P = power reflection coefficient

ρ_V = voltage reflection coefficient

S = v.s.w.r.

If unit power is fed into this line a power reflection ρ_P occurs at the discontinuity and $(1-|\rho_P|)$ is the power left for transmission.
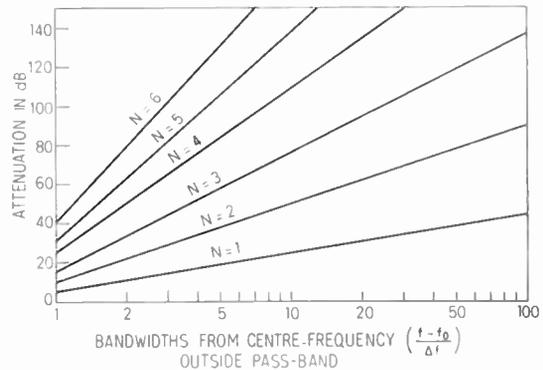

Fig. 2. Bandwidths from centre frequency outside pass-band.

Regarding the reflecting discontinuity as a source of power loss we have

$$\text{transmission loss} = 10\log\left(\frac{1}{1-|\rho_P|}\right) \text{ dB}$$

but

$$|\rho_P| = |\rho_V|^2 = \left(\frac{1-S}{1+S}\right)^2$$

Therefore

$$\text{transmission loss} = 10\log_{10}\left[\frac{1}{1 - \left(\dfrac{1-S}{1+S}\right)^2}\right]$$

$$= 10\log_{10}\left[\frac{(1+S)^2}{4S}\right] \text{ dB} \quad \ldots(9)$$

If a microwave filter is composed entirely of purely reactive elements and if it is terminated in Z_0 then the relationship given in equation (9) will hold.

Expressing equation (9) as a ratio gives

$$\frac{P_0}{P_L} = \frac{(1+S)^2}{4S} \quad \ldots\ldots(10)$$

Referring to equation (1) and taking the case of a complete filter containing n branches

$$\frac{P_0}{P_L} = 1 + \left[Q_L\left(\frac{f}{f_0} - \frac{f_0}{f}\right)\right]^{2n}$$

where Q_L = loaded Q of complete filter.

From equation (10)

$$\frac{(1+S)^2}{4S} = 1 + \left[Q_L\left(\frac{f}{f_0} - \frac{f_0}{f}\right)\right]^{2n}$$

Therefore

$$\left[Q_L\left(\frac{f}{f_0} - \frac{f_0}{f}\right)\right]^{2n} = \frac{(S+1)^2}{4S} - 1 = \frac{(S-1)^2}{4S}$$

$$Q_L = \frac{\left[\dfrac{(S-1)^2}{4S}\right]^{1/2n}}{\left(\dfrac{f}{f_0} - \dfrac{f_0}{f}\right)} \quad \ldots\ldots(11)$$

where S = v.s.w.r. within pass-band 2 $(f-f_0)$.

2.3. *Rejection Properties*

The first step in designing a filter is to choose the number of branches necessary to give a desired rejection in the nearest adjacent channel. This can be done by solving for n in equation (8). To avoid lengthy calculations normalized insertion loss curves have been calculated and plotted for $n = 2, 3, 4, 5$ and 6. (Fig. 2.)

3. Cavity Design

3.1. *Susceptance Formulae*

Marcuvitz[2] has shown that, for a symmetrically located post of circular cross-sectional area aligned parallel to the electric field (H_{10} mode), at the reference plane T and for $x = a/2$ (Fig. 3(a)) the equivalent circuit will be of the form shown in Fig. 3(b).

(a) Inductive post in waveguide.   (b) Equivalent circuit.
Fig. 3.

The normalized reactances of the shunt conductance x_a, and the series capacitance x_b, are given by the relations

$$2x_a - x_b = \frac{a}{\lambda_g}\left[S_0 - \left(\frac{\pi d}{2\lambda_0}\right)^2 - \frac{5}{8}\left(\frac{\pi d}{2\lambda_0}\right)^4 \right] \quad \dots(12)$$

$$x_b = \frac{a}{\lambda_g}\frac{\left(\dfrac{\pi d}{a}\right)^2}{1 + \dfrac{1}{2}\left(\dfrac{\pi d}{\lambda_0}\right)^2\left(S_2 + \dfrac{3}{4}\right)} \quad \dots\dots(13)$$

where a = internal broad dimension of guide

d = post diameter

λ_0 = wavelength in free space

λ_g = wavelength in the guide.

$$S_0 = \log_e \frac{4a}{\pi d} - 2 +$$
$$2\sum_{n=3,5,7,\cdots}^{\infty}\left[\frac{1}{\sqrt{n^2 - \left(\dfrac{2a}{\lambda_0}\right)^2}} - \frac{1}{n} \right]$$

$$S_2 = \log_e \frac{4a}{\pi d} - \frac{5}{2} + \frac{11}{3}\left(\frac{\lambda_0}{2a}\right)^2 -$$
$$- \left(\frac{\lambda}{a}\right)^2 \sum_{n=3,5,7}^{\infty}\left[\sqrt{n^2 - \left(\frac{2a}{\lambda_0}\right)^2} - n + \frac{2}{n}\left(\frac{a}{\lambda_0}\right)^2 \right]$$

He states that these formulae are accurate for values of $d/a < 0.2$.

3.2. *Comparison of Accurate and Approximate Design Formulae*

Certain approximations were made to these formulae in work done at 4000 Mc/s by Potok.[3] The susceptances of a number of posts were calculated at 7000 Mc/s using both the accurate and approximate formulae. These are compared graphically (Fig. 4) with each other and with the susceptances measured experimentally using the nodal shift technique.[3]

As can be seen from Fig. 4 the values of susceptance found experimentally are in very close agreement with those calculated from the accurate formula of Marcuvitz and the approximate formula is inadequate except in the calculation of very small susceptances.
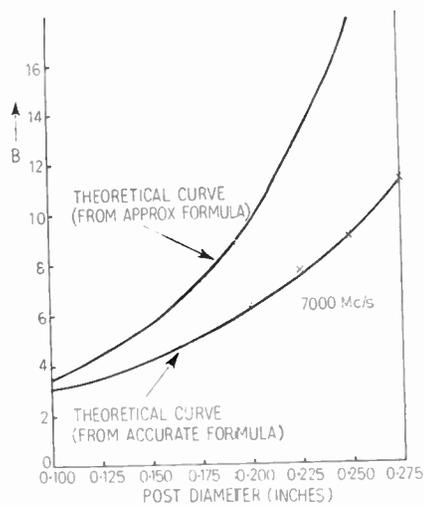

Fig. 4. Susceptance as a function of post-diameter.

Potok[3] has shown that assuming the equivalent circuit of Marcuvitz the expression for the cavity length necessary for resonance becomes

$$l_0 = \frac{\lambda_g}{2\pi}\tan^{-1}\left[\frac{-2(x_a - x_b)}{1 + x_b(2x_a - x_b)} \right] \quad \dots\dots(14)$$

putting $x_b = 0$ this becomes

$$l_0 = \frac{\lambda_g}{2\pi}\tan^{-1}(-2x_a) \quad \dots\dots(14a)$$

which is the simplified solution of Mumford.[4]

3.3. *Calculation of Necessary Design Data*

Using equation (14) cavity lengths were calculated for a number of post diameters at 7000 Mc/s. The resonant frequencies of a number of experimental prototypes were found to be in close agreement with theoretical expectations. Experimental and theoretical values of $l_0/\lambda_{g0} \,(= \theta)$ are plotted as a function of susceptance B in Fig. 5 and (B) is plotted as a function of post diameter in Fig. 6.
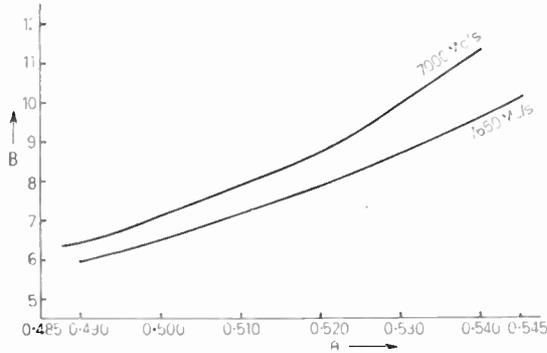
Fig. 5. Susceptance as a function of cavity length $\theta \ (= l_0/\lambda_{g0})$.

The selectivity of a properly terminated resonant branch in a transmission line obeys the relationship

$$Q_L = \frac{\dfrac{2\pi l}{\lambda_{g0}}}{\dfrac{2\pi l}{\lambda_{g0_1}} - \dfrac{2\pi l}{\lambda_{g0_2}}} \qquad \ldots\ldots(15)$$

where λ_{g0} is the wavelength at resonance

λ_{g0_1} and λ_{g0_2} are the wavelengths at the half power points.

This relationship can be expressed in terms of the normalized susceptance.[4]

$$\frac{Q_L}{\left(\dfrac{\lambda_g}{\lambda_0}\right)^2} = \pi \left(\frac{B^2}{4} + \frac{1}{2}\right) \left[1 - \frac{1}{\pi}\tan^{-1}\frac{2}{B}\right] \quad \ldots(16)$$

The theoretical $\dfrac{Q_L}{\left(\dfrac{\lambda_g}{\lambda_0}\right)^2}$ is plotted as a function of

B and compared with the experimentally measured Q_L of a number of prototype cavities (Fig. 7). As can be seen from the graph the experimental points agree to close approximation with the calculated curve.

Finally, using single post obstacles a spacing between individual cavities in a filter of about $3\lambda_g/4$ is used.

If l_1 and l_2 are the resonant lengths of adjacent cavities then the spacing between them

$$l_{12} = \frac{l_1 + l_2}{2} + \frac{\lambda_g}{4} \qquad \ldots\ldots(17)$$

4. The Design of a Complete Prototype Filter

4.1. *Design Procedure*

The first step in designing a filter is to choose the number of branches to give the minimum allowable rejection in the nearest adjacent channel. This information can be ascertained from Fig. 2.
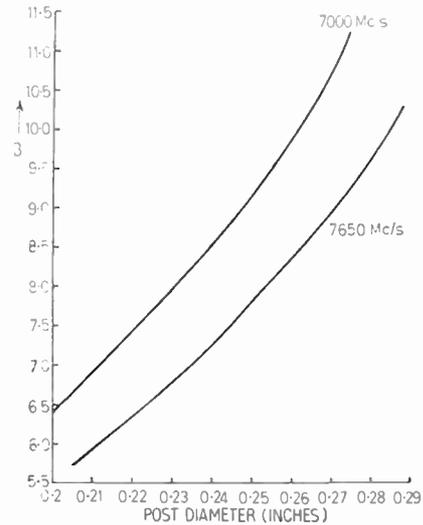

Fig. 6. Susceptance as a function of post diameter.

Having specified the desired pass-band width and the maximum allowable v.s.w.r. within the pass-band, the Q_L of the complete filter can be derived by using equation (11) in conjunction with Fig. 2. Inserting Q_L into equation (7) gives the Q necessary for individual branches.

Transforming to normalized Q, the appropriate susceptances can be found from Fig. 7. From Figs. 5 and 6 the necessary values of θ and post diameter can be ascertained. Finally, the spacing between each branch can be calculated from equation (17).

A prototype five-cavity filter was designed to have a v.s.w.r. $< 1\cdot03$ within a pass-band of ± 10 Mc/s. Its theoretical and measured characteristics are compared in Fig. 8.
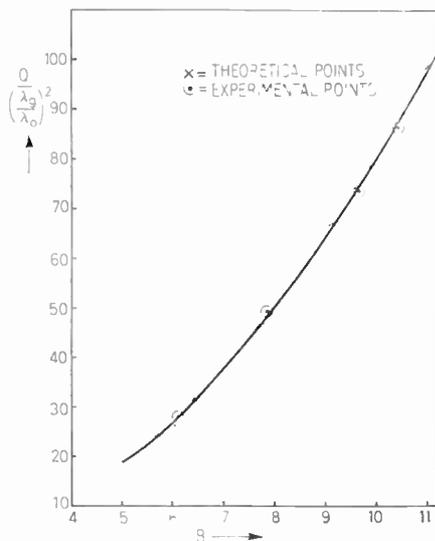

Fig. 7. Q normalized as a function of susceptance.

5. Design of a 3 dB Short-slot Hybrid Junction

5.1. Some General Considerations

Figure 9(a) shows a length of double waveguide in which a portion (length s) of the common wall is cut away. If a signal is applied at terminal 1 a certain amount of it will couple through the slot and can be detected at terminal 4.

No power will be reflected to terminal 2 if the reflected voltages in both the even and odd modes are equal to zero. Riblett[5] has shown that if the condition for complete isolation is satisfied equal power division takes place when the transmitter voltages for the even and odd modes differ from each other by 90 deg. Furthermore, from simple vector arguments concerning the voltages in the even and odd modes the following two facts can be deduced.

(a) The voltage at terminal 4 leads the voltage at terminal 3 by 90 deg.

(b) The voltage at terminal 3 leads by 45 deg the value that it would be if there were no slot in the waveguide.

5.2. Derivation of Design Data

Referring to Fig. 9(a), when a signal is applied at terminal 1 the H_{20} mode is excited in the coupling region due to the effective doubling of waveguide width.

The difference in phase velocity between H_{10} and H_{20} modes in the coupling region can be expressed as follows

$$\frac{2\pi s}{\lambda_{g_1}} - \frac{2\pi s}{\lambda_{g_2}} = \alpha \qquad \ldots\ldots(18)$$

s = length of slot

λ_{g1} = guide wavelength of H_{10} mode,

λ_{g2} = guide wavelength of H_{20} mode,

α = relative phase difference between the two modes within the coupling region of length s.

The cut-off wavelength of any mode propagated in rectangular waveguide can be expressed as a function of waveguide width a in the following manner:
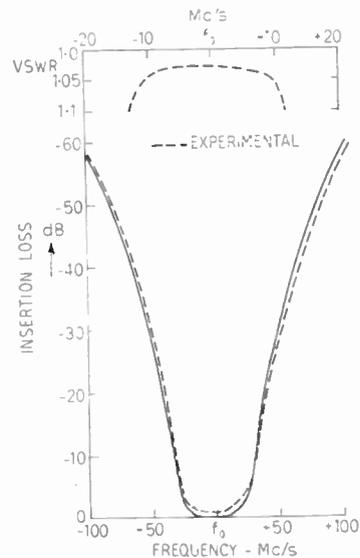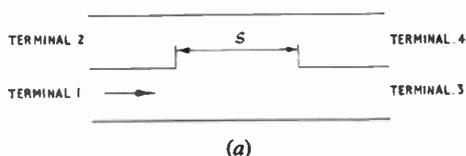
$$(\lambda_c)H_{N0} = \frac{2}{N} a$$

Fig. 8. Prototype filter response.

In the coupling region waveguide width $= 2a$

Therefore $\qquad (\lambda_c)H_{N0} = \frac{4a}{N}$

$(\lambda_c) H_{10} = 4a$ within coupling region

$(\lambda_c) H_{20} = 2a$ within coupling region

Now $\qquad \lambda_g = \dfrac{\lambda_0}{\sqrt{1 - \left(\dfrac{\lambda_0}{\lambda_c}\right)^2}} \qquad \ldots\ldots(19)$

Therefore $\qquad \lambda_{g1} = \dfrac{\lambda_0}{\sqrt{1 - \left(\dfrac{\lambda_0}{4a}\right)^2}} \qquad \ldots\ldots(20)$

and $\qquad \lambda_{g2} = \dfrac{\lambda_0}{\sqrt{1 - \left(\dfrac{\lambda_0}{2a}\right)^2}} \qquad \ldots\ldots(21)$

From equation (18)

$$s = \frac{\alpha}{2\pi} \cdot \frac{1}{\left(\dfrac{1}{\lambda_{g_1}} - \dfrac{1}{\lambda_{g_2}}\right)} \qquad \ldots\ldots(22)$$
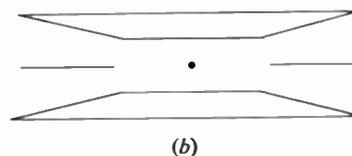
Fig. 9. (a) Theoretical schematic of 3 dB hybrid junction.

(b) Practical schematic of 3 dB hybrid junction.

Substituting equations (20) and (21) in equation (22)

$$s = \frac{\alpha}{2\pi} \left[\frac{1}{\dfrac{\lambda_0}{\sqrt{1-\left(\dfrac{\lambda_0}{4a}\right)^2}} - \dfrac{\lambda_0}{\sqrt{1-\left(\dfrac{\lambda_0}{2a}\right)^2}}} \right] \quad …(23)$$

$$= \frac{\alpha}{2\pi} \left[\frac{1}{\dfrac{\sqrt{1-\left(\dfrac{\lambda_0}{4a}\right)^2}}{\lambda_0} - \dfrac{\sqrt{1-\left(\dfrac{\lambda_0}{2a}\right)^2}}{\lambda_0}} \right] \quad …(24)$$

$$= \frac{\alpha\lambda_0}{2\pi} \cdot \frac{1}{\sqrt{1-\left(\dfrac{\lambda_0}{4a}\right)^2} - \sqrt{1-\left(\dfrac{\lambda_0}{2a}\right)^2}} \quad ……(25)$$

In the special case when 3 dB of the transmitted power is present at terminal 4 the relative phase difference α will be $\pi/2$

Therefore

$$s = \frac{\lambda_0}{4} \cdot \frac{1}{\sqrt{1-\left(\dfrac{\lambda_0}{4a}\right)^2} - \sqrt{1-\left(\dfrac{\lambda_0}{2a}\right)^2}} \quad …(26)$$

5.3. Limiting Conditions

(a) Coupler will function if operating frequency exceeds cut-off frequency of H_{20} mode.

(b) Coupler will not function if operating frequency exceeds cut-off frequency of H_{30} mode.

Now $\quad (\lambda_c)H_{20} = 2a, \quad (\lambda_c)H_{30} = \dfrac{4a}{3}$

within the coupling region.

Therefore the limiting conditions in terms of λ_0 will be

$$\frac{4}{3} < \frac{\lambda_0}{a} < 2 \qquad ……(27)$$

5.4. Practical Aspects of Hybrid Design

So far only the general case has been considered, that is, any length of double waveguide in which a section of the infinitely thin common wall has been cut away. Taking a practical example in W.G.14, it becomes apparent that the wave guide dimensions will have to be modified in order to arrive at a practical design procedure for the proposed hybrid junction.

The effective waveguide width within the coupling region will be $2a$ + thickness of common wall (0·064"). With $a = 1·372$" the H_{30} mode will be propagated at 6300 Mc/s. This means that to design a hybrid in the 7000 Mc/s band the waveguide width within the coupling region will have to be reduced considerably so that the cut-off frequency of the H_{30} mode is very much higher than the required operating frequency.
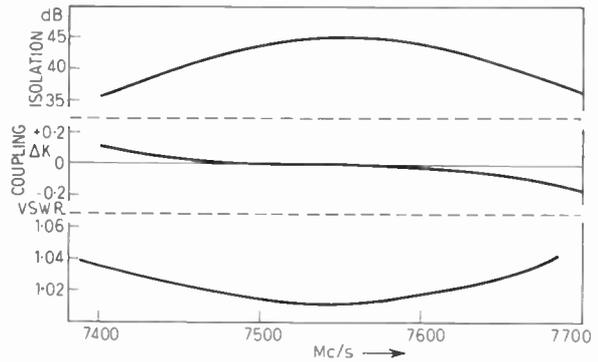

Fig. 10. Characteristics of prototype 3 dB hybrid junction.

Having arrived at a modified value of a the slot length s can be calculated from equation (26). A normalized graph of slot length as a function of wavelength is plotted in Fig. 11.

5.5. Design of Prototype Hybrid Junction

Operating frequency = 7550 Mc/s.

Let (λ_c) $H_{30} = 3·57$ cm $= 1·33a'$

$\qquad a' = 1·054$ in (a' = modified waveguide width)

Inserting a' into equation (26) gives $S = 1·556$".

Figure 9(b) shows the method used to reduce the waveguide width within the coupling section. Measurement carried out on the prototype showed that, while the power division characteristic was excellent over a wide frequency band, the v.s.w.r. characteristic was unsatisfactory.

The coupler was matched by placing a capacitive dome in the coupling region. This necessitated minor adjustments in the dimensions s and a'.

The v.s.w.r. isolation and power division characteristics of the hybrid are plotted in Fig. 10. As can be seen from Fig. 10, the v.s.w.r. is < 1·035 over a bandwidth of 300 Mc/s and the variation from 3 dB power division < ±0·2 dB. As the hybrid is a sym-
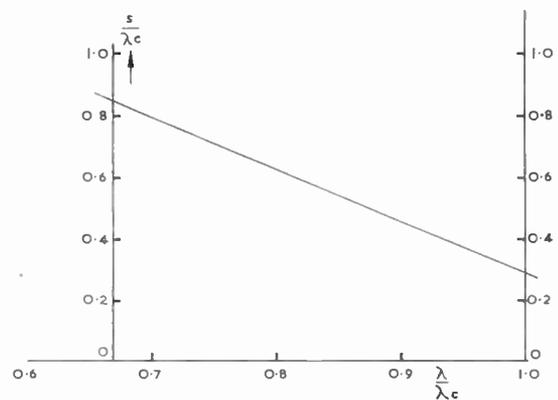

Fig. 11. Slot length as a function of wavelength.

metrical device the isolation can be found by computing the return loss from the measured v.s.w.r. Slight discrepancies between the computed and measured isolation will be due to mechanical asymmetry within the hybrid.

6. Branching Systems

6.1. *Operation of Branching Unit*

The branching unit relies on the fact that when a signal is coupled into the side arm of a 3 dB hybrid junction it gains a phase lead of 90 deg.

A signal f_1 enters the branching unit (Fig. 12(a)). The signal is split into two equal parts A and B in hybrid No. 1, part B leading in phase by 90 deg. Both A and B pass through the filters which are tuned to accept them. In hybrid No. 2 both signals split in half again into A_1, A_2, B_1 and B_2. B_1 gains a further 90 deg phase lead and is thus 180 deg out of phase with A_1. A_1 and B_1 cancel and no power enters the load. A_2 gains 90 deg and is thus in phase with B_2 and the total power enters the receiver.

A signal at frequency f_2 entering the same branching unit (Fig. 12(b)) is split by the hybrid but rejected by the filters and the total in-phase power leaves the unit via arm 2, the out-of-phase power being cancelled in arm 1.

If the two signals at frequencies f_1 and f_2 enter the branching unit simultaneously they reach their respective receivers without any interaction. If the two receivers are replaced by two transmitters the whole operation works in reverse.

The receiver Rx2 is protected from the signal at f_1 by the directivity of the hybrid which will be > 35 dB and the receiver Rx1 is protected from the signal at f_2 by the rejection of the filters at the frequency spacing $f_1 - f_2$.

6.2. *Complete Branching System*

It is apparent from the preceding arguments that by placing a series of these branching units in a suitable configuration a considerable number of transmitters and receivers can simultaneously utilize a common aerial.

As an example the case where any one aerial is utilized by two receivers and two transmitters is considered. The carrier frequencies and the frequency separation between adjacent equipments will be in accordance with the recommendations of C.C.I.R.[6] The relative frequency separation at each terminal and repeater station is as shown in Fig. 13.

The branching system is of the form shown in Fig. 14. For the purposes of this example the following parameters are used.

(a) Discrimination between adjacent
 transmitters > 40 dB
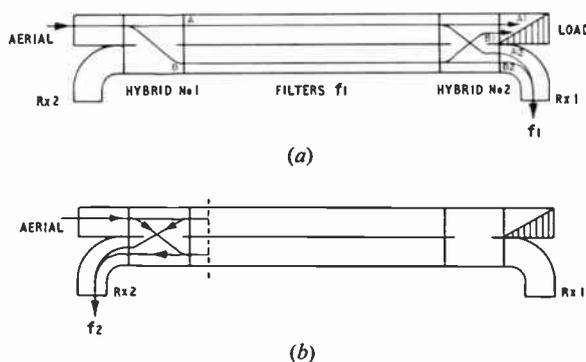

(a)

(b)

Fig. 12. Branching unit.

(b) Discrimination between adjacent
 receivers > 30 dB

(c) Transmitter breakthrough to any
 receiver < -80 dB

No difficulties should be encountered from unwanted breakthrough at local oscillator image frequencies as these have been taken into account in choosing the frequency plan.

6.3. *Design Considerations*

Because of built-in ferrite isolators each transmitter will have an inherent protection of 35 dB. The directivity of the hybrid junction will give them a protection from each other of a further 35 dB so that in spite of the close frequency spacing between transmitters it will not be necessary to use anything larger than 3-cavity filters in the transmitter branching units.

In the case of the receiver branching units, however, the total discriminations will be provided by the filters. It can be seen by referring to Fig. 2 that 5-cavity filters will be necessary in the receiver branching units.

Taking into account the directivity of the hybrid and referring to Fig. 2 it can be seen that the breakthrough of Tx2 at Rx1 will be considerably less than -80 dB.

6.4. *Prototype Branching System*

A prototype branching system was designed with $f_1 = 7442$ Mc/s, $f_2 = 7491$ Mc/s, $f_3 = 7603$ Mc/s and $f_4 = 7652$ Mc/s. Figure 14 shows the performance of the filters. The characteristics of the 3-dB hybrids were consistent with those of the original prototype. Taking into account a hybrid junction directivity of 35 dB minimum and referring to Figs. 14 and 15 it can be seen that the breakthrough of any transmitter at any receiver is better than the specified -80 dB and
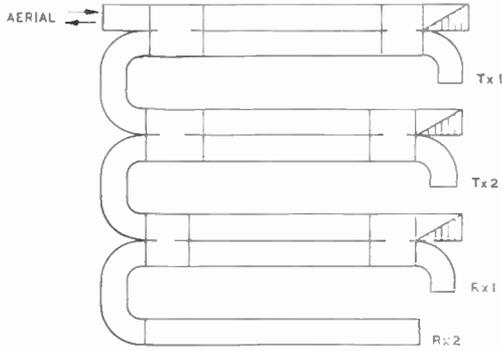

Fig. 13. Frequency plan.

Fig. 14. Complete branching system.

the discrimination between adjacent receivers is > 30 dB. Considering the additional protection of the ferrite isolators it is apparent that the discrimination between adjacent transmitters is greater than the specified 40 dB.

7. Conclusions

It has been thought in the past that a graph of $Q_L \Big/ \left(\dfrac{\lambda_g}{\lambda_0}\right)^2$ plotted as a function of θ was normalized since $Q_L \Big/ \left(\dfrac{\lambda_g}{\lambda_0}\right)^2 = f(B)$ and $\theta = f(B)$. Experimental results in the 4000 Mc/s frequency band lent credence to this assumption.

The susceptance of a brass post centrally located in waveguide is predominantly inductive. It has a small capacitive component which is negligible in the larger size waveguide of 4000 Mc/s. This component becomes an appreciable quantity at 7000 Mc/s. If θ is calculated from the relationship of Mumford[4] (eqn. 15) the resulting graph will be independent of frequency. If, however, it is calculated from the relationship derived from the equations of Marcuvitz which take into account the capacitive component the results will no longer be independent of frequency as can be seen from Fig. 5. It is, therefore, no longer permissible to treat the graph of $Q_L \Big/ \left(\dfrac{\lambda_g}{\lambda_0}\right)^2$ as a function of θ as a normalized curve and the filter design procedure outlined in Section 4 must be used to obtain accurate and consistent results.

The author has shown that utilizing the information outlined in this paper it is possible to design microwave filters, solely on a theoretical basis, with great accuracy. A certain amount of experimental cross checking is advisable, however, as the combination of a human mind and a slide rule is not an infallible calculating machine.

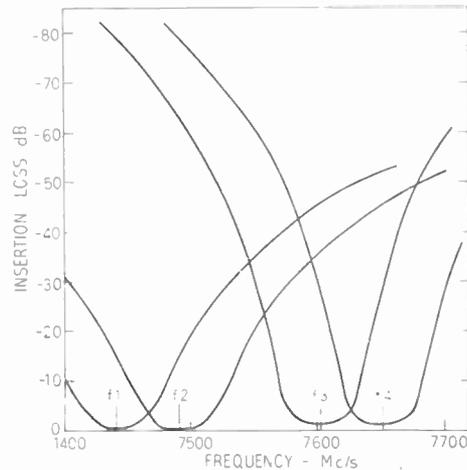In the case of the 3 dB short-slot coupler the design

Fig. 15. Branching system filter responses.

data do not take into consideration the v.s.w.r. of the component. A good match can be achieved by empirical methods and this should present no difficulties.

The type of branching system described in this paper is not the only available method of combining and separating a number of r.f. channels at microwave frequencies. It has a number of obvious advantages, however, in that its performance can be predicted accurately and r.f. channels can be added to or subtracted from an existing branching system without undue difficulty.

8. Acknowledgments

9. References

1. S. B. Cohn, "Direct-coupled resonator filters", *Proc. Inst. Radio Engrs*, 37, pp. 187–96, February 1957.

2. N. Marcuvitz, "Waveguide Handbook", pp. 257–65. 1st Edition (McGraw-Hill, New York, 1951).

3. M. H. N. Potok, "Design of inductive post-type microwave filters", *J. Brit.I.R.E.*, 18, pp. 263–72, May 1958.

4. W. W. Mumford, "Maximally flat filters in waveguide" *Bell Syst. Tech. J.*, 27, p. 684, 1946.

5. H. J. Riblett, "The short-slot hybrid junction", *Proc. Inst. Radio Engrs*, 32, pp. 180–4, February 1952.

6. C.C.I.R. "Recommendation No. 284", Vol. I. (International Telecommunication Union, Geneva, 1959.)

A High-power, Low-frequency Sonar for Sub-bottom Profiling

By

R. BOWERS, B.Sc.†

Summary: This is a continuous sub-bottom profiling system designed to give high resolution whilst retaining good penetration. By mounting the output transducer in the bottom of a fibreglass dinghy, towed well astern of the survey ship, the shortest possible output pulse has been achieved, and by using a line hydrophone towed between the ship and dinghy a very low background noise level has been obtained.

Using this system, surveys are carried out at $7\frac{1}{2}$ knots with a resolution of 6 ft and a penetration of up to 1000 ft.

1. Introduction

This system is a modern method of continuous sub-bottom profiling using a sonic reflection technique.[1-4] The "Boomer" is an electro-mechanical sound source producing a high-powered, low-frequency output pulse. This output source has now been mounted in the bottom of a fibreglass dinghy and towed well behind the survey ship. This removes multiple reflection effects which effectively lengthen the output pulse and reduce the resolution obtainable from the system. The receiving hydrophone is towed between the dinghy and the survey ship (see Fig. 1). This hydrophone is a

Fig. 1. Towing arrangement of Boomer and hydrophone.

tapered line array with a null on its axis so that it picks up no noise from the ship or dinghy. The signal from the hydrophone is amplified, filtered to remove unwanted noise, and recorded on a Mufax recorder (see Fig. 2). Using this system, surveys are carried out at $7\frac{1}{2}$ knots with a resolution of 6 ft and a penetration of up to 1000 ft.

2. The Output System

The Boomer output transducer consists of a flat copper coil, embedded in epoxy resin, with an aluminium plate held against it by a spring. A bank of capacitors is charged up and then discharged through the coil. The eddy currents produced in the aluminium plate cause it to be repelled from the coil, thus producing a pressure pulse in the water. In most applications the Boomer transducer has been mounted in a

"fish" which is towed, either alongside or behind the survey ship, at a depth of about 8 ft. This has an inherent disadvantage in that the output pulse contains the reflected pulse from the sea surface which effectively lengthens the output, thus reducing the resolution between strata obtainable with the device. Towing the fish alongside the survey ship has the added disadvantage that multiple reflections from the surface and ship's hull occur and lengthen the output pulse even more. It was decided at the National Institute of Oceanography to build a relatively high resolution system.

A 10-ft fibreglass dinghy was divided into three compartments, the centre one to house the Boomer output transducer, and the fore and aft compartments for buoyancy chambers. A 1000-joule Boomer‡ was obtained and the output transducer mounted in the dinghy. Power to the transducer is brought through a watertight cable gland in the sealed cover of the centre compartment. A circular hole for the aluminium plate to move through was cut in the bottom of the centre compartment, and the aluminium plate sealed to the
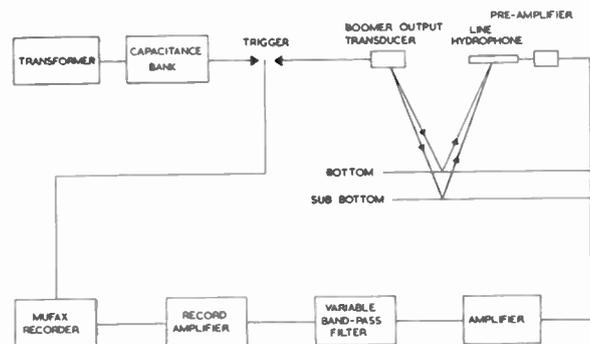

Fig. 2. Block schematic of the Boomer system.

† National Institute of Oceanography, Wormley, Godalming, Surrey.
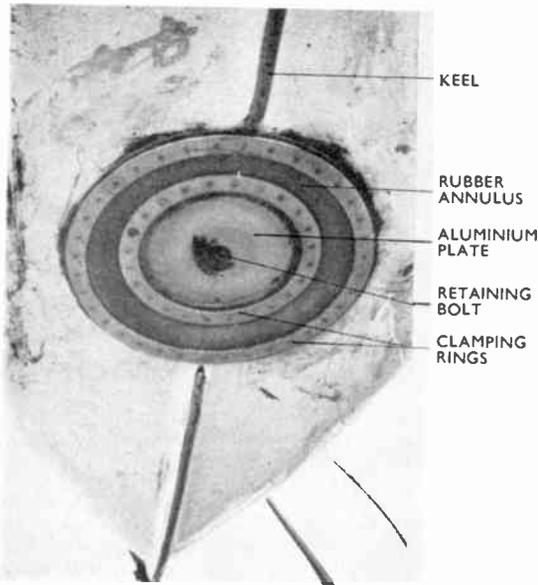
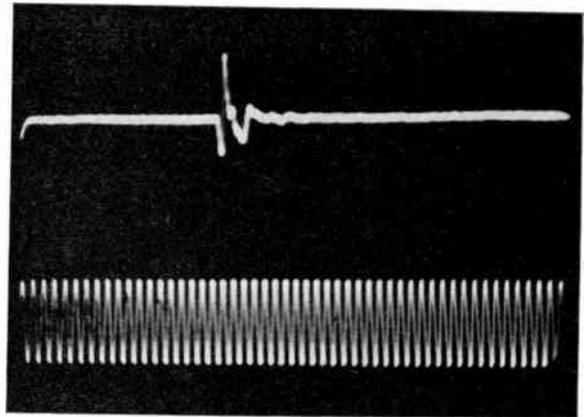Fig. 3. Bottom view of dinghy showing aluminium plate and rubber annulus.

Fig. 4. Output pulse from Boomer. Upper trace—output pulse with hydrophone 20 yd below the output transducer. Dinghy 5 yd from the stern of the towing ship. The hydrophone had a lower cut-off frequency of 100 c/s. Lower trace—1 kc/s sine wave from standard oscillator.

bottom of the dinghy by a thick rubber annulus (Fig. 3). The copper coil in its epoxy resin block was mounted above the plate and had a 150 kg concrete block on top of it to provide a reaction mass. The plate is held against the coil by a spring on a central retaining bolt, and also by hydrostatic pressure. Using this system, the aluminium plate is air-backed and this has two advantages. Firstly, there is no damage to the plate or coil due to cavitation. Secondly there is no reflected pulse from the water surface, and so the output pressure pulse length is merely determined by the electrical constants of the discharge circuit, assuming that the plate is large enough to provide sufficient loading. In this way the shortest practicable output pulse is obtained (see Fig. 4), and also a very reproducible one (see Fig. 5).

The dinghy is towed behind the survey ship on a 3 in. hemp rope with 100 yds of heavy electrical cable seized to it (the resistance of the electrical cable is 0·06 ohms). The dinghy normally tows 75 yards behind the ship and has been used successfully in 10 ft waves. A small drogue is normally attached to the stern of the dinghy to stop it broaching to. The buoyancy chambers have now been filled with polyurethane foam to make the dinghy unsinkable.

This output system has been run for long periods with good reliability and consistent results.

3. The Receiving System

The reflected signals from the sea bottom and sub-bottom are picked up by a hydrophone, amplified, filtered, half-wave rectified, and recorded on a Mufax facsimile recorder.

In sub-bottom profiling, the frequencies used in work on the continental shelf normally lie between 100 and 1000 c/s. Unfortunately, the survey ship usually transmits a lot of noise at these frequencies into the water and thus limits the usable gain of the receiver amplifier. For this reason it is desirable to tow the receiving hydrophone as far from the ship as is practicable to reduce the background noise level. This has the added advantage that it cuts out multiple reflections between the hydrophone, sea-surface, and ship which, as with the output transducer, reduces the discrimination obtainable. From the point of view of ship noise, it is obviously advantageous if the hydrophone used is a directional one with a sensitivity null which points at the ship. This may easily be achieved by using a line hydrophone towed behind the ship.

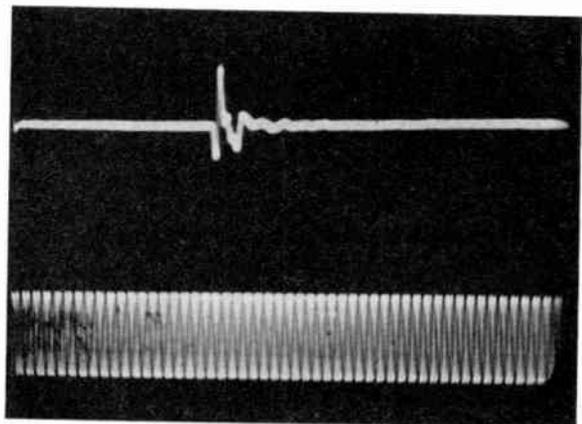The hydrophone used is made up of 10 barium titanate spheres connected in parallel, the array being

Fig. 5. Multiple output pulse. Recording conditions as for Fig. 4 but with 4 exposures superimposed.
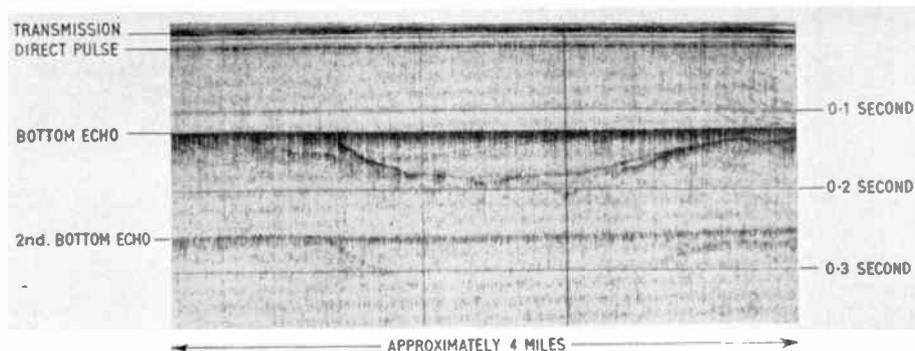
Fig. 6. A filled sub-bottom channel in St. George's Channel.

designed to have a sensitivity null on the axis and suppressed side-lobes. The spheres are 1¼ in o.d. with a ¼ in wall thickness. They have a resonant frequency of 82 kc/s but are very useful as receivers at low frequencies where the response is reasonably flat at −102 dB relative to 1 volt per dyne per cm². The spheres are connected into an array 12 ft long and inserted into a plastic hose pipe. Also in the hose pipe is a transistor pre-amplifier, designed to have a lower cut-off frequency of 100 c/s, and consisting of a cascade emitter follower input stage, amplifier, phase splitter, and push-pull emitter follower output. The pipe is filled with castor oil.

The hydrophone is towed on a 4-core armoured cable, the cores carrying the supplies to the pre-amplifier, and the push-pull output. The hydrophone itself is nearly neutrally buoyant and so by regulating the amount of towing cable out at any speed the depth of the hydrophone can be controlled. Attempts were made to regulate the depth of the hydrophone by

fixing a drogue on its rear end. This was abandoned for two reasons: firstly, it introduced vibration into the hydrophone and secondly, it tended to stretch the plastic hose pipe and as a result break electrical connections on the spheres.

This hydrophone is towed about 50 yds astern of the survey ship. This puts it between the ship and the dinghy and as it is in line with both it picks up very little noise from either. The present hydrophone is designed for 500 c/s and so begins to lose its directional properties at 100 c/s for which a longer array would be profitable. Using this hydrophone surveys can be made at twice the speed and eight times the receiver gain, compared with an omnidirectional hydrophone towed alongside the ship, for the same background noise level.

The push-pull output of the hydrophone is transformer-coupled into a transistor amplifier. The signal then passes through a variable band-pass filter. The Boomer output transducer in fact produces a broad
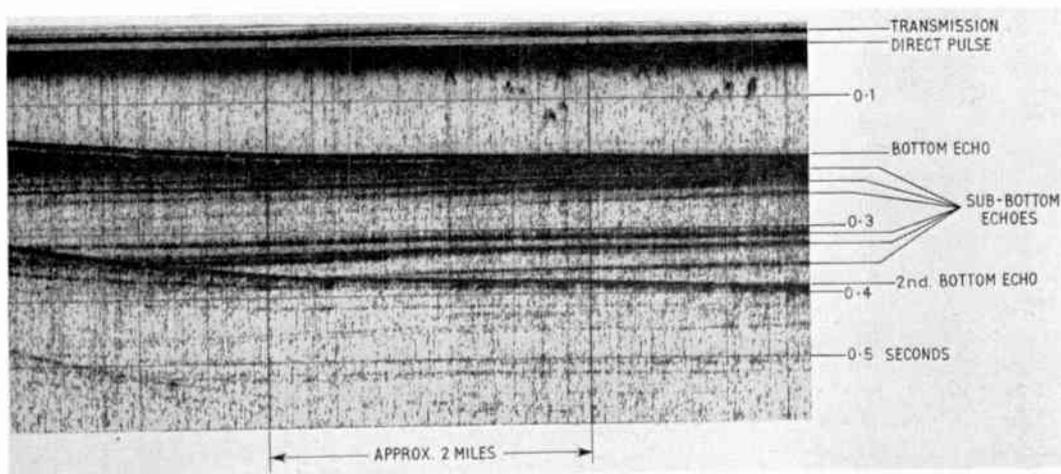

Fig. 7. Sub-bottoms on the edge of Great Sole Bank.

band spectrum of noise with a peak energy in the 200–400 c/s region (for a 100 joules storage). Thus the pass-band of the filter can be varied to give high resolution and low penetration at the high frequency end of the spectrum, or high penetration with lower resolution at the low frequency end. Also the filter can be used to remove any predominant background noise frequency. The filter is followed by the recording circuit which provides marking power for the facsimile recorder, the recording helix being connected to the transmission contacts. The gain normally used is about 400 000 but this is determined by the background sea noise.

Figures 6 and 7 illustrate the type of record obtainable with the equipment. Both were surveyed at 7½ knots, the filter pass-band for Fig. 6 being 300–500 c/s and for Fig. 7 100–300 c/s. As may be seen the higher pass-band gives better discrimination but reduces the penetration.

4. References

1. H. Hoskins and S. T. Knott, "Geophysical investigation of Cape Cod Bay, Mass., using the continuous seismic profiler", *J. Geol.*, 69, No. 3, pp. 330–340, 1961.

2. J. B. Hersey, A. H. Nalwalk and D. R. Fink, "Seismic reflection study of the geologic structure underlying Southern Narrogansett Bay, Rhode Island", Woods Hole Oceanographic Institution Report No. 61–19, 1961.

3. R. Bowers, "Modern methods of sub-bottom profiling using sonic reflection techniques", *Science Progress*, No. 1, pp. 80–84, 1962.

4. J. B. Hersey, E. E. Hays, D. D. Caulfield, H. E. Edgerton and S. T. Knott, "Adaptation of sonar methods for exploring the sediments and crust of the earth beneath the oceans". Paper read at the Symposium on "Sonar Systems" in Birmingham on 9th–11th July 1962, to be published in *J.Brit.I.R.E.*

Portable Ionosonde for H.F. Communication Tests

A new ionosonde for continuous rapid determination of the optimum wavelength for long range h.f. radio communication has recently been developed by EMI-Cossor Electronics Ltd., Halifax, Nova Scotia.

Due to the physical structure of the ionosphere, quality of reception of short wave radio transmissions varies considerably between one frequency and another. It is possible to forecast conditions to some extent but if the best possible wavelength is required it can only be ascertained, without the new equipment, by lengthy trial and error methods.

The new device can be carried by one man and is designed for use with existing transmitter/receivers. Frequency coverage is 1·8 to 28·8 Mc/s. Assuming it is required to communicate between points A and B, pulse transmissions are commenced at point A and the Ionosonde transmitter frequency is rapidly changed in a series of 128 logarithmic steps to cover the band from 1·8 to 28·8 Mc/s. At point B, the second Ionosonde has a receiver which similarly tunes through the same frequency steps in synchronization with the first Ionosonde. In this fashion the entire band is covered in just two seconds.

Pulses received at point B are visibly recorded on the face of a cathode-ray tube, with long persistence screen, built into the Ionosonde. Traces may be photographed by a Polaroid camera which produces developed prints in less than ten seconds after the frequency band has been covered.

The "ionogram" produced is in the form of a series of fine vertical lines, the "X" axis of the c.r.t. representing the transmission frequency. The pulse is indicated by one or more dots on each vertical sweep. Reception will be best at frequencies where just a single dot occurs—indicating that there is no multi-path propagation—and remains visible as the Ionosonde receiver gain is decreased.

In addition to its application in the field of h.f. communication, the Ionosonde can be used for the scientific study of conditions within the ionosphere.

An Experimental Incremental Computer

By

K. MILLINGTON,†

Presented at a meeting of the Computer Group in London on 25th October 1961.

Summary: This paper describes an experimental incremental computer using time-shared equipment. The basic operation provides approximate numerical integration by adding rectangular areas. There are 45 integrators in the computer, the integrands being represented serially by up to 22 bits at a digit rate of 500 k/second. The number of bits representing the values of increments in the computer is easily varied. A computer of more economical and flexible design is also described.

List of Symbols

The symbols used to represent quantities in the digital approximation to integration are:

y integrand

y_i value of the integrand at a time defined by i

Δy increment in y

y^* correct value of the integrand given by $(y + \Delta y)$

Δx increment in the variable of integration

z integral of y with respect to x

z_n value of the integral at a time n

Δz increment in z, sometimes called the integrator output

r^* remainder generated after forming Δz by a rounding-off process

r remainder used as a correction in forming Δz

w increment weighting factor

Δt increment in the independent variable

Other symbols are:

S   start instruction, which determines the effective length of the Y-register

C   complementing instruction, which operates on the integrator output

m number of bits used to represent incremental quantities

n number of bits used to represent an integrand

Definition of Time-Periods

Servicing period:

That period of time during which the arithmetic unit is associated with a particular integrator in generating an increment of the integral. It corresponds to the time during which y and r are available from store.

Selecting period:

That period during which the integrator has access

to the output store, via time-shared selecting equipment, in order to obtain incremental inputs to be used in its servicing period.

Step in the solution:

Corresponds to all integrators having been serviced in rotation, commencing with a nominated integrator.

1. Introduction

The computer described in this paper was constructed as part of a project whose purposes were to investigate the special techniques applicable to incremental computing and to gain operating experience. It has a capacity minimally adequate to serve these purposes, and also to assess the value of such a computer for general use. Little emphasis was placed upon speed of operation in the first instance, maximum economy of development effort being more important.

The design retains the simplicity of the earlier models, known as Digital Differential Analysers, first developed in America,[1] yet allows scope for further development. In particular, provision is made to represent incremental quantities by an arbitrary number of binary digits and not merely by two as in current practice. The main interest of the computer lies in this more general incremental representation and the appropriate term " incremental computer" is used.

Integrators only are provided in the computer, since these may be used for a wide variety of other purposes because they will accept an explicit variable of integration.[2] Certain facts relating to the principles of digital integrators are summarized in Section 2 and stated more fully in the Appendix. They are basically well known, but the opportunity is taken to generalize for the case of representation of increments by more than two binary digits.

The choice of storage system, which plays a large part in the organization of a computer, is discussed in Section 3. Section 4 deals with the functional design of the computer proper, and finally the methods of control, and input and output, are described.

† Ministry of Aviation, Royal Aircraft Establishment, Farnborough, Hants; now with the National Gas Turbine Establishment, Pyestock, Farnborough, Hants.

Experience in the use of the computer on realistic problems has indicated poor utilization of certain of the facilities provided. A more efficient design of computer, retaining the same basic techniques has been evolved as an improvement. The principles of this design, which has not been fully developed, are given in Section 7.

2. The Digital Integrator

The continuous process of integration must be replaced, in a digital system, by a summation in which the variables change by discrete amounts. An integrator has an input for increments of the integrand, Δy, and one for increments of the variable of integration Δx. The output, Δz, represents increments in the quantity z where

$$z_n \simeq \sum_{i=0}^{i=n} y_i \Delta x \qquad \ldots\ldots(1)$$

The expression for z approximates to the integral of y with respect to x, assuming that y_i does not change significantly over the interval represented by Δx, that is, if the increments in x are made very small.

The representations of all the incremental quantities have for convenience the same range of values, since the inputs to an integrator normally arise from the output of another integrator—or may feed back from the same integrator. Provision is usually made to sum several integrator outputs to form Δy whereas one output only forms the variable of integration (Δx). In order to keep the equipment used in an integrator to a minimum, relatively few digits are assigned to the representation of the incremental quantities. A rounding-off process is used in forming Δz, and to mitigate the effect of this on the accuracy of computation, the remainder, r, is preserved to make a contribution to the next value of Δz.

The equations which are instrumented are

$$y^* = y + \Delta y \qquad \ldots\ldots(2)$$

$$\Delta z + r^* = y^* \Delta x + r \qquad \ldots\ldots(3)$$

where the asterisk denotes the new values of y and r. The process of forming y^*, Δz and r^* is called "servicing" the integrator; this is shown diagrammatically in Fig. 1.

The incremental inputs are available simultaneously with y and r which are held in registers labelled Y and R respectively. The representation of the new value of the integrand is returned to the Y-register; the switch at the output of the ($y^* \Delta x + r$) adder passes the more significant digits in the representation of the sum as the integrator output, and returns the remainder to the R-register to be used in next servicing the integrator. A "step" in the solution of the problem is completed when all integrators have been serviced once.
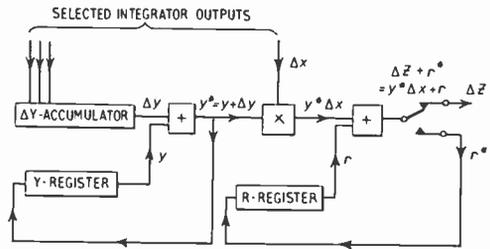

Fig. 1. Realization of a digital integrator.

The number of binary digits, m, used to represent the increments is usually made small to conserve equipment in the construction of a computer containing a number of integrators. A single-bit representation has been used,[1] but it is now general practice to use a redundant two-bit representation in which the possible values of an increment are zero, plus or minus one quantum. In this case the increments are designated "ternary". A general representation of increments, of which ternary is the minimal case, is derived in the Appendix. Provision for an arbitrary value of m is made in the computer to be described.

Increasing m from 2 clearly reduces the rounding-off error in servicing the integrator. It does not affect the accuracy of the integration process which assumes that y is constant for the step duration and which therefore generates an error due to truncation of the series which, ideally, expresses y in powers of x. In general, a reduction in one type of error alone does not radically improve integrator performance. The provision of an extensible representation for increments enables studies to be made of the increase in accuracy obtained however; and it enables advantage to be taken of any improvement in integration technique in addition to its value in applications where the rounding errors are in fact dominant.

A further benefit is the ability to represent rates of change less than the maximum more directly than by the time-average of a sequence of ternary-valued increments. This reduces the drift, or phasing, error which otherwise arises.

In general use, the increments in the computer are derived (directly or indirectly) from a single source which makes an increment of constant value available continuously. This increment is called Δt; an alternative name for the sequence of such increments is "machine rate". The most positive value within the capacity of the representation is usually assigned to Δt since this determines the range of values of the derived increments which will be generated. Other values of Δt may however be nominated by the operator as a means of studying the accuracy obtainable in a solution.

3. Design Considerations

The design of any digital apparatus is to a large extent determined by the type of storage system which it is intended to employ. The most flexible storage system at present available is the matrix of saturable magnetic cores, and a store of this type was considered in making a preliminary study of computer design. The requirements of economy, and the provision of a reasonably large number of integrators in the computer, led to a design in which common servicing equipment is allocated to each of the integrators as required, and to the use of serial digital representation. The computer has a fixed program in contrast to a general-purpose computer; the common equipment may therefore be allocated to each of the integrators in turn, i.e. in a predetermined consecutive manner. Long access time is not then a disadvantage for the bulk of the storage required, that is to say that the principle advantage of the matrix store is not needed in this type of incremental computer. This fact, coupled with improvements in wire-type acoustic delay lines led to the choice of a serial-consecutive computer using delay line storage.
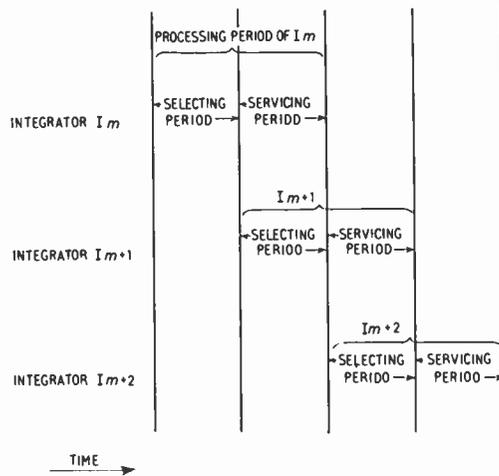

Fig. 2. Timing of selection and servicing periods of consecutive integrators.

The computer uses a common arithmetic unit to service all the integrators in rotation and common equipment to select quantities nominated as inputs to the separate integrators. The time for which the arithmetic unit is associated with an integrator is the servicing period of that integrator, and its selecting period is that during which the selecting equipment is used. The necessity for time-sharing of equipment between integrators applies equally in both servicing and selecting periods which are made of equal duration. The inputs to an integrator must be selected and manipulated into a suitable form prior to their use

in the servicing period however, so that an integrator servicing period follows its selecting period. Thus data relevant to an integrator are processed in two consecutive periods, but since the equipment used in each period is different, the processing time of consecutive integrators can be made to overlap as shown in Fig. 2.

The inputs to an integrator usually arise from its own, or other integrator, outputs and freedom in selection of these quantities is required. All outputs are therefore made available during each selecting period from a store which must have an access time no greater than the selecting period. If delay lines are used for this store (which is convenient for reasons of consistency), their circulation time must therefore be no greater than this period; and if only one such delay line were used, the number of integrators in the computer would have to be made too small for practical usefulness. The functional arrangement which has been chosen is a straightforward extension of the "precession-line" principle used in binary-increment computers; m delay lines are used, each one storing all the bits of the same weight from the integrator outputs. These outputs are therefore stored in an essentially parallel form, the y and r quantities on the other hand being stored in serial form. A serial-mode arithmetic unit is employed, so that conversion of Δy from parallel to serial form, and vice versa for Δz, is required. A minimum delay in the arithmetic unit is desirable. The design of the $y^* \Delta x$ multiplier (a major component of the arithmetic unit) then requires, as usual, that the multiplier quantity is present in parallel form for the duration of the multiplication. The obvious choice of multiplier quantity is then Δx since the design so far has been based on the assumption that it is represented by the lesser number of digits, and as stated above, it is available from the output store in a parallel representation.

The wire-type acoustic delay lines[3] used as stores have the merit of requiring very little ancillary equipment to drive the line and reconstitute its output. The digit-repetition frequency used in the computer is determined by the store and in the model described is 500 000 digits per second.

The employment of packaged logic elements enables logic design of the computer to proceed independently of engineering design, and in general implies simplicity in fault-finding and maintenance. The packages are constructed using readily-available point-contact diodes and alloyed transistors. The standard range of elements includes negating and diode-gating combinations, e.g. adders, subtractors, etc., together with an element of novel design called a "digit-period delay" element.[4] This generates a standard signal waveform in the digit period succeeding that in which the input is presented. The output has,

in addition to a margin of tolerance against attenuation, a margin of half of a digit-period tolerance against delay to be encountered in subsequent gating operations before arriving at the input of a further digit-period delay element. The element uses two transistors and a few sections of a mismatched delay network.

This element is used to afford restandardization of waveform in both timing and amplitude, as a single digit-period delay, and as a single-bit store in conjunction with a standard gating element.

4. Logic Design of a Delay-line Incremental Computer

4.1. Organization of the Computer

In the delay-line incremental computer, a fixed proportion of the capacity of a delay-line store is allocated to each integrator as its Y-register so that the representations of y for different integrators are available periodically in serial form. The corresponding representations of r are similarly available; in fact in the computer to be described, the y and r words are interleaved in a single store. All integrators are serviced in rotation by a common arithmetic unit, which is associated with each integrator in turn for the period during which its representations of y and r are available. The timing of these quantities is adjusted at the output of the store to facilitate the design of the arithmetic unit as shown in Fig. 3 and the representations of y^* and r^* are returned to the store by a similar means.
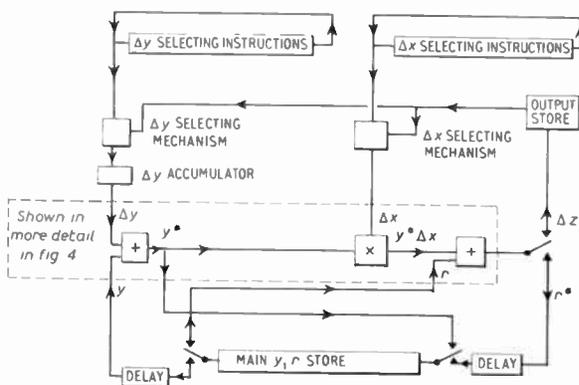

Fig. 3. Organization of the delay line incremental computer.

The most recent (Δz) outputs in respect of all the integrators in the computer are held in the output store and are made available for selection as inputs to any given integrator. The input-selection is time-shared amongst integrators on a similar basis to the arithmetic unit, for a similar period. Since the selection must have been made before computation of y^* and r^* commences, the selecting period for a given integrator occurs immediately before its servicing

period. The duration of the selecting period and the access time of the output store determine the number of integrators in the computer and the flexibility of interconnection between them. In the computer described, there are 45 integrators, each of which can have its own or any other integrator output selected as its variable of integration (Δx) input, and any number of outputs selected as contributing to its integrand (Δy) input. Selecting instructions are uniquely associated with each integrator and capacity in separate delay-line stores is provided for Δx and Δy instructions. These stores have the same circulation time as the main y, r, store so that the association between one instruction and its integrator is preserved. The integrator inputs are passed to the arithmetic unit in a suitable form for use in servicing.

4.2. Register Length

Nominated outputs of certain integrators contribute to the Δy input of a given integrator, and must be added together with the same weight to give Δy. This quantity is available in serial representation and its quantum must be given the same value as that of y. At the choice of the user, a reduction in the length of the Y-register may be made, which reduces the number of bits allocated to the representation of y thereby increasing the value of its quantum. Since the quantum of Δy, but not Δx, must be correspondingly increased, the binary scale factor of the Δy input is determined by the register length. An increased scale factor results in a faster rate of change in the value of y at the expense of an increase in the coarseness of its representation. The length of the R-register is, of course, determined by the representation of y^*.

The programmer scales each integrator by inserting a binary 1 into its Y-register in the digit-position having a weight next below that of the required quantum of y. This mark is called the "start" instruction, "S". On emerging from the computing store, S stimulates a circuit which allows the representation of Δy to be added to that of y, starting in the following digit period. The start instruction must not be itself regarded as conveying numerical information and is preserved in the Y-register, irrespective of arithmetical operations performed on y.

A fixed capacity of 23 digit-positions is allocated to each Y-register and 22 for the R-registers in this computer. The maximum effective representation of y is therefore 22 bits.

4.3. The Arithmetic Unit

The major components of the arithmetic unit are the ($y+\Delta y$) adder, the ($y^*\Delta x$) multiplier and the ($y^*\Delta x+r$) adder. In servicing an integrator, the latter two components are used for ($m+n-1$) digit-periods, where m is the number of bits used to represent Δx and n the bit-capacity of the Y-register. This

time, plus an allowance for cumulative delay within the arithmetic unit, determines the minimum duration of the servicing period. The representations of y and r are interleaved in the computing store of the computer being described, thus needing a total time of $(2n-1)$ digit-periods, out of the main store cycle time, to be allotted to one integrator. This is greater than the above-mentioned minimum duration of the servicing period. Some computing time is thus wasted, since no part of the arithmetic unit is fully employed during the servicing period, but there is the advantage that the number of digits used to represent the incremental quantities, in particular Δx can be increased without altering the servicing period, within the limit imposed by $m \leqslant n$. Advantage is also taken of the waste time to simplify the design of the arithmetic unit by rounding upwards its cumulative delays. The basic unit made up from standard logical packages is shown in Fig. 4, which shows the case of $m = 5$.

The servicing period of an integrator is now defined as that period during which the contents of its Y and R-registers become available from store. The timing of y is adjusted so that the arithmetic operations are performed in the latter part of the period, and extend into the subsequent servicing period, as shown in Fig. 5. This organization eases the design of the equipment which manipulates the Δx and Δy inputs into the forms in which they are used during servicing.

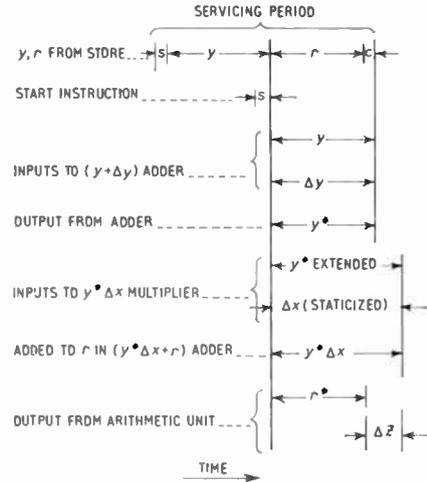Fig. 4. The basic arithmetic unit.

Fig. 5. Timing of the quantities represented in an integrator during servicing.

It is often required to complement the output of an integrator. For this purpose a complementing circuit is included in the Δz output channel and is brought into operation by a complementing instruction, C. The instruction is a single binary 1 placed in the R-register of the designated integrator; the register is extended by one digit-position at the more significant end to accommodate it. The instruction becomes available at the output of the arithmetic unit simultaneously with the least significant digit in the representation of Δz. It is not treated as numerical information but is stored while the digits of Δz are being generated. The complement of Δz is formed by the stored instruction passing without change the less significant digits in the representation of Δz, up to and including the first having a value of 1, and negating the remainder.

4.4. The Direct Adder

A frequent requirement in the use of the computer is an incremental representation of the sum of a number of contributory incremental sources for use as the Δx input to an integrator. The sum is sometimes generated by a further integrator connected as a "soft adder", that is, having its complemented output fed back to form one of its own Δy inputs; Δt is used as the Δx input. The sources to be summed are connected to the further Δy inputs. The integrator then behaves like a servo, tending to drive the contents of its Y-register to zero; the output is a smoothed version of the sum of the contributory inputs. The operation of the "hard adder" is similar, with the addition of a non-linearity in the feedback path. Adders of the servo type have the characteristic that the average output rate is equal to the average of the sum of the input rates. The output rate is limited since the representation of an output increment cannot exceed
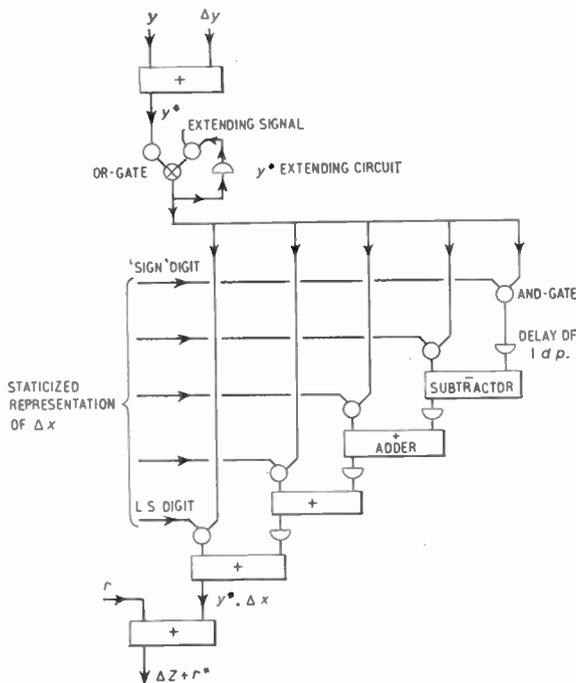
that of the corresponding Δx input, consequently an output lag is introduced by an input rate which transiently exceeds the maximum possible output rate. This lag reduces the accuracy obtainable in a solution, so a more direct type of adder is made available in the design of this computer.

The characteristic of an integrator nominated for use as a direct adder is that the output rate is proportional to the input rate sum without lag. The actual adding process is performed by the Δy accumulator whose output is scaled by the start instruction and added into the otherwise empty Y-register. The contents of this register are added to r under control of the Δx input to form an output increment, and the Y-register subsequently cleared to zero. The only source of error in this adder is the output rounding process; the error is minimized by use of the maximum scale factor which will not cause the Δy input to exceed the Y-register capacity. Thus, the lag is removed, but the ability to cope with transient overloads is sacrificed. The orthodox hard and soft adders can, of course, be used instead when this is preferable.
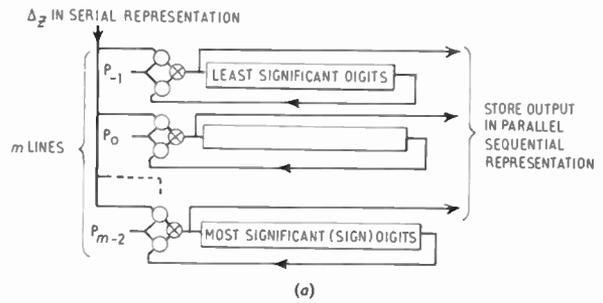
4.5. *The Output Store*

The method used to store current integrator outputs is an extension of that used in previous consecutive incremental computers in which Δz is represented by one bit only. The precession-line store there used is replicated m times in this computer, as shown in Fig. 6(*a*), where m is the number of bits used in representing Δz.

The sequence in which integrator outputs become available during the input-selection period is of no consequence providing none are missed. Delay lines may therefore be used for the output store. The number of integrators in the computer is limited to the number of outputs which are available during a selecting-period, if no restrictions are to be imposed on input selection. The minimum time which may be allowed for selection of an output from the store is one digit-period. The number of integrators is then made equal to the number of digit-periods in a selecting, or servicing period.

An integrator output is formed as a number in serial representation. It must be stored in a parallel manner if all outputs are to be available from the store at digit-period intervals. The digits of the numbers representing Δz are separated and routed to the store input on m wires whilst retaining their serial relative timing. This form of representation is called "parallel-sequential". A single delay-line store holds all the digits of the same significance, and m such stores constitute the output store.

The output of an integrator replaces previously-held information in the store. The circulation-time of the store must differ from a servicing period in

Fig. 6. (*a*) Output store using m precession lines.

(*b*) Output pattern from precession line storing least significant digits of Δz quantities in a 4-integrator computer.

order that an integrator output does not replace that of the previously-serviced integrator, and is in fact made one digit-period less. Outputs from consecutive integrators are then packed into the store sequentially as in Fig. 6(*b*). The digits of the selected inputs are used sequentially, so the selecting period is determined by the availability of the least significant digits of integrator outputs from the store. In particular, the most recent output of the previously-serviced integrator is available at the input to the store in the last digit-period of its own servicing period. Thus the selecting period of an integrator corresponds to the servicing period of the previous integrator, and the selecting point to the store input.

The pattern of outputs from the store advances or precesses, by one digit-period in successive selecting periods by virtue of the relationship between its circulation-time and the servicing period. The information destroyed by storing a fresh integrator output is thus the last output held in respect of the integrator next to be serviced. This information was the first available for selection in the period in which it is destroyed, and will be replaced by a fresh output at the end of the next selecting period.

4.6. *Input Selection*

The output of an integrator is selected from the output store by specifying the time at which it becomes available in the selecting period. A sufficient specification is the digit-period in which the least significant

digit of the nominated output is available since the higher-order digits follow sequentially at digit-period intervals. A selecting instruction is a binary 1 having the specified timing, which is peculiar to the integrator having its inputs selected, and would be in a different digit-period to select the same quantity in a different selection period. Selecting instructions are in any case associated with each integrator so that this presents no functional difficulty. The provision of storage capacity for selecting instructions in this form, particularly for Δx instructions, is admittedly redundant in the information-theory sense, but more sophisticated systems would be more expensive.

The instruction itself selects the least significant digit of the required input, and delayed versions select the remaining digits from the output store as in Fig. 7. Only one number is selected as the variable of integration of an integrator. This is held in the Δx temporary store pending servicing of the integrator. It is economical to use a parallel store here since Δx is represented by relatively few digits. The transfer of Δx to the staticizer associated with the $y^* \Delta x$ multiplier is initiated by the start digit of the integrator to be serviced.
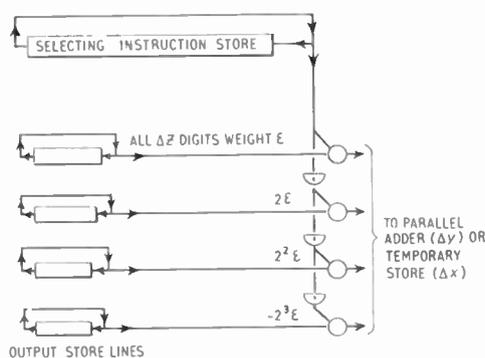

Fig. 7. Method of selecting the digits of the nominated ∿input ($m = 4$).

The number representing Δy is the sum of several incremental inputs. These inputs are in parallel-sequential representation and can follow each other at one-digit-period intervals. The selected increments are summed in the Δy adder. This is essentially a parallel-adder having a settling time of one digit-period per stage. The number of stages is determined by the maximum number, and range of values, of increments selected to form Δy. The least significant digit in the representation of Δy is generated by the adder in the digit-period following the presentation of the least significant digit of the last increment. The remaining digits are similarly available in parallel-sequential representation. The number formed is transferred to the Δy temporary store at the end of the selecting period. A serial representation of Δy is read from this store by a shifting-register technique initiated by the start digit.

The provision of an input representing time to an integrator is a common requirement in the computer. This is provided by an increment of constant value generated at each step in the solution, since a step occupies a fixed period, or increment of time. These increments are called increments in the independent variable, designated t. It is advantageous to use the existing selecting equipment to specify t. The increment is therefore held in the output store; the necessary capacity is provided by suppressing one integrator output. The value of the increment is chosen as the most positive which can be represented, and allows the output of an integrator, having Δt as its independent variable input, to take on the full range of values.

5. Control

5.1. Modes of Operation

A delay line store holds the representations of the initial values of the y and r quantities in respect of every integrator. A repetitive computation of a predetermined number of steps is carried out on this data. This allows presentation of the solution using c.r.t. traces as the display medium when the problem time is short and is particularly useful in problems of an exploratory nature.

As an alternative to computing, the computer may be restored to an idling mode, in which case all data at that stage in the solution will be preserved indefinitely. Either mode can exist for an integral number of main store circulations (4 ms periods).

No provision is made for starting a computation with initial data in the integrator output store, so that a stimulus to the system is required. This is provided by the externally derived Δt signal. The integrator whose output is superseded by Δt is therefore arranged to be the first serviced in the step. The number of bits used to represent Δt is used as a convenient control of the number of bits representing increments in the computer.

The transition from the computing to the idling mode of operation is initiated by a "stop" instruction, and that from the idling to the computing mode by a "compute" instruction. The modes of operation are complementary in that the same control circuit is set or reset by the compute and stop instructions respectively. The instructions become effective at the end of the step in which they originate. A "reset" instruction causes the transfer of the initial conditions to the computing stores, after which the computer returns to its previous mode of operation. The three control instructions—compute, stop and reset—can be provided by a source external to the computer; stop and reset instructions can also be internally

generated. An external indication of the mode in which the computer is operating is provided.

An additional facility, that of "single-step" operation, is incorporated in the control of the computer. It is used when the computer is otherwise idling and advances the progress of the computation by a single step in response to each simulation of the external control.

5.2. *Idling Mode*

The stop instruction requires that computation ceases at the end of the current step in the solution and that data contained in all stores at that time are preserved. Computation is stopped by inhibiting the Δy input to the $y + \Delta y$ adder and the $y^* \Delta x$ input to the $y^* \Delta x + r$ adder. Data are preserved automatically in all but the output store by regeneration; an extra bit capacity must be added to each delay line in the output store in order to preserve its contents. It is logically attractive to allow the periodic interruption of the storage loops in the output store to continue whilst the computer is idling. The information otherwise lost by this process is retrieved and held in the additional capacity provided. It is then used as the input to the store when the circulation is next interrupted; simultaneously the additional storage accepts fresh information. The process is regenerative and corresponds to the use of the output store in the computing mode since the output in respect of an integrator replaces that of the integrator next to be serviced. All integrator outputs are zero when the computer is idling and do not affect the data preserved in the output store.

A stop instruction is generated internally by the overflow of a Y-register, caused by adding an increment to y such that the magnitude of the resultant number cannot be expressed by the number of bits assigned to it. This is, in general, an indication of faulty programming, but can be used deliberately to stop the computer in order to assess the progress of a computation. An integrator used for this purpose counts machine rate in its Y-register; the number of steps in the computation before stopping is determined by the position of the start instruction and initial value held in the register. Each integrator has an overflow indicator.

The setting-up and modification of the contents of either input-selection store or initial condition store are carried out in the idling mode, to preclude the possibility of computation on incomplete data.

5.3. *Reset*

A reset instruction can be generated internally from the overflow of a Y-register which is prevented from causing a stop instruction. The integrator whose output is superseded by Δt is retained for this purpose.

Its integrand input and the number of steps in the solution are determined by the number of digits in the representation of an increment in machine time, by the initial value of the register contents and by the position of its start instruction. The maximum number of steps which may be determined by this means is approximately 30 000 using a 23-bit capacity register and a 7-bit representation of an increment. This corresponds to a solution time of approximately 2 hours.

The reset control signal exists for the duration of one step. Under this control, computation ceases, the output store clears itself, and the contents of the computing registers are replaced by information from the initial values store. The point of entry is at the output of the arithmetic unit so that the new values in the register do not become available until the step following the reset step.

The computer returns to its previous mode of operation following a reset step and reverts to the idling mode if a stop instruction was generated during the computing step prior to the reset step.

6. Input and Output

The primary method of introducing instructions and data, i.e. both set-up and initial conditions, into the computer stores uses punched paper tape. Data are transferred in separately-addressed 45-bit blocks via a buffer store. Each block specifies either the contents of the Y and R-registers of an integrator or its input-selecting instructions. Data are superseded by subsequent data if these have the same destination address, thus allowing for afterthoughts. A block of data is read from the tape and transferred to the computer in approximately 80 milliseconds; the total time required to set a full-scale problem on the computer is typically 15 seconds.

The basic input data are binary coded but the buffer mechanism is easily adapted to accept binary-coded-decimal input, and to cope with certain variations, such as variable-length structure, of the block.

A supplementary input mechanism, which uses manually-operated switches, is provided for convenience in making minor program modifications.

The solution is in general converted to an analogue quantity and displayed by a long-persistence c.r.t. or a plotting table dependent on the solution time. A parallel version of the contents of a register representing the solution is produced by a chain of restandardizing elements and standard gates. A parallel-binary to voltage-analogue converter, operating on the non-return-to zero representation which is used, produces an output in a form convenient for display. The solution has a constant value for the major duration of a step, i.e. 4 ms, and is available for display for this period. If a higher accuracy is required, binary

numbers can be obtained directly from the main store contents display.

Incremental inputs can be introduced into the arithmetic unit of the computer from an external source during the first part of any servicing period. Selected integrator outputs are similarly available for external use. Thus it is practicable and quite economical to operate two or more similar computers in parallel. The timing and control equipment is common under these circumstances but additional capacity for input-selection instructions must be provided. Incremental outputs can be obtained on a time-scale suitable for tabulators and incremental plotting tables by using smoothing techniques.

7. An Improved Computer Design

Since only integrator units are provided in the computer which has been described in the previous section, it is necessary to use these for all other operations, besides integration, which are required. There is no great difficulty in doing this, but the computing equipment is not used to its full capacity. This is particularly noticeable in the case of multiplication by a constant, an operation of frequent occurrence, which necessitates the use of one integrator for each constant multiplier. As many integrators are used for this purpose in practice as for all other operations, including integration.

This consideration stimulated the design of an improved computer which does not use a fixed number of self-contained similar units, resulting in increased utilization of equipment without sacrifice of accuracy or convenience in use.

The advantages achieved may be summarized as:

(i) Only one rounding error is introduced for a weighted sum, instead of one rounding error for each term in the sum. No rounding error is introduced if the sum is to be used directly as the Δy input to an integrator.

(ii) The expensive Δy accumulator, which is considerably under-employed, is deleted and replaced by a simpler equipment which is used much more intensively.

(iii) The number of rounding operations is reduced, compared with a computer having a similar main store but providing only conventional integrator units. Thus the improved computer can have a higher speed of operation for the same computing capacity, although this is off-set by the weighting operation which must be performed on a single integrand input to an integrator when binary weighting, as effected by a start instruction, would otherwise suffice.

The improved computer, which will now be described, has separate storage systems for whole quantities and for increments. Whole quantities are available in fixed sequence from a store of long access time in consecutive word-periods. One increment only, Δx, is selected from the faster-access increment store at each word-period; the following description relates to ternary increments although the representation may be extended as required. The increment is scaled by its use as the multiplier input to the arithmetic unit; the corresponding multiplicand input is the fixed-value whole quantity, w, representing its scaling, or weighting factor. The product $w\Delta x$ then represents the weighted quantity which in general is one contribution to a weighted sum. A store of capacity one word, and an associated adder together form an accumulator in which the running sum $\Sigma w\Delta x$, of terms generated in consecutive word-periods is held. The weighted sum may be converted directly to an output increment for subsequent use as the variable of integration (Δx) input to an integrator, or as a Δy input to more than one integrator. For conversion to an increment, the accumulator contents are added to the representation of r from the main store (no y is involved), and the rounded output is passed to the increment store. It is then available for selection and use as required. The term "summing unit" describes the use of the equipment in this way. This technique avoids the necessity to use integrator units as constant multipliers and servo adders, and automatically generates the weighted sum of several increments in the standard incremental representation.

When it is alternatively required to use the weighted sum as the Δy input to one integrator only, there is no need to round the accumulator contents before adding them to y. The representation of y is made available in the word-period following that in which the final term contributing to the weighted sum is produced, and the accumulator contents added directly to form y^*. An increment is selected as the Δx input in this word-period, and the integrator output is rounded in the subsequent word-period. The quantities w, y^* and r^* are returned to the main store as applicable.

The design takes advantage of the fixed nature of the computer programme to organize the required processes such that some partial results may be stored in the accumulator, rather than rounded and stored as increments. The minimum equipment, commensurate with the part-processes to be instrumented, is provided, e.g. only one increment is used in any period; the full process is completed in the necessary number of periods by consecutive operation. This organization allows the programmer more freedom in nomination of the type and size of computing units than in earlier computers, and results in a more efficient use of the equipment provided. A diagram of the computer is shown in Fig. 8. The multiplier reduces to a gating and complementing circuit for ternary increments.
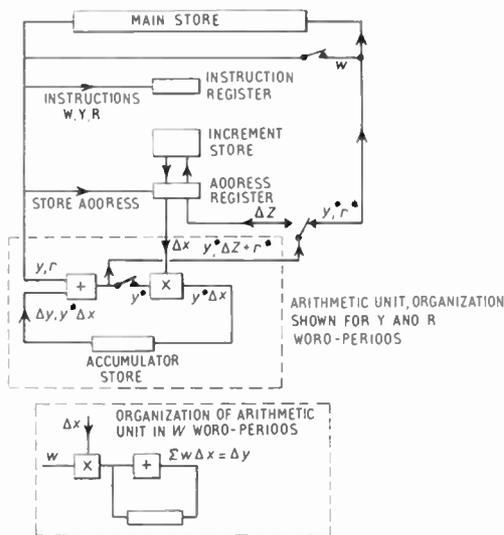
Fig. 8. Organization of improved computer.

The switching arrangement is controlled by program instructions.

Some points of difference between this computer and that previously described are:

(i) A similar capacity in the main store is allotted to each of the whole quantities, irrespective of type, in order to simplify engineering design. The representation of a weighting factor is therefore the same as that of an integrand quantity, and a weighted increment has the same range of values as an integrand. The effective representation of an integrand is thus adequately determined by the weighting factors associated with its input and there is no need to employ a start instruction, together with the necessary temporary store and associated circuits, for this purpose. The representation of the remainder, compared with the integrand, does not use the most significant digit-position. This position could be used to hold an output complementing instruction but it is uneconomical to do so since it is then necessary to provide equipment to implement the instruction. The effect of complementing can usually be achieved by the subsequent use of weighting factors which have both positive and negative ranges.

(ii) Fewer increments need be stored in the increment store for the same computing capacity as in the previous design. The restriction that the number of computing units in the computer should be the same as the number of digit-periods in a word therefore does not arise directly.

The last point directs attention to the increment store and method of increment selection. It is possible to use a system of precession-line store and stored selection instructions similar to that previously used. The smaller number of increments to be stored however, and the selection of only one increment in each period, characteristic of this design, allow more scope in the choice of storage system. The system shown in Fig. 8 is considered to be a random-access store for the purpose of this description, but cheaper arrangements are possible. The address of the increment to be selected is directly specified by a few bits; these are conveniently held in the main store adjacent to each whole quantity register. The increment is then selected at the appropriate time to be processed together with the corresponding whole quantity. The address stored adjacent to an R-register is used to specify the location in the increment store for the output increment of the unit.

The computer has three alternative modes of operation, corresponding to the designation of a word period as W, Y, or R. The instruction which specifies this is binary-coded, requiring two bits, for which capacity in the main store is again made available, as for the increment addresses.

Figure 8 and Table 1 show the design of the computer and its use to provide summing and integrating units.

Table 1
Processing Sequence in the Improved Computer

	Summing Unit			Integrator Unit			
Word Type	W	W	R	W	W	Y	R
Main Store Output	w_1	w_2	r	w_1	w_2	y	r
Multiplier Md. Input	w_1	w_2	—	w_1	w_2	y^*	—
Multiplier Mr. Input	Δx_1	Δx_2	—	Δx_1	Δx_2	Δx_3	—
Adder Inputs	$w_1 \Delta x_1$	$w_2 \Delta x_2$	r	$w_1 \Delta x_1$	$w_2 \Delta x_2$	y	r
	—	$w_1 \Delta x_1$	$\Sigma w \Delta x$	—	$w_1 \Delta x_1$	$\Sigma w \Delta x$	$y^* \Delta x$
Adder Output	$w_1 \Delta x_1$	$\Sigma w \Delta x$	$\Delta Z + r^*$	$w_1 \Delta x_1$	$\Sigma w \Delta x$	y^*	$\Delta Z + r^*$
Main Store Input	w_1	w_2	r^*	w_1	w_2	y^*	r^*
Increment Store Input	—	—	ΔZ	—	—	—	ΔZ

8. Conclusions

The computer described in the earlier sections of this paper was constructed to supplement theoretical studies of incremental computing techniques. The actual number of digits representing increments can be varied simply by replicating existing equipment, particularly in the multiplier, increment store and Δy increment accumulator. The cost per additional digit in the increments is of the order of 5% of the overall cost of the computer excluding peripheral (i.e. input and output) equipment. Extension of the incremental representation is a necessary first step in radically improving the performance of the computer. Rounding and phasing errors only are reduced by this means so that the basic accuracy of the computer is limited by truncation in the integration process. Rectangular integration, characteristic of consecutive incremental computers which use unsophisticated integration techniques, is used in this computer since it avoids the need to differentiate between integrator inputs generated in the current step and those generated in the previous step, in servicing the integrator. Trapezoidal integration (linear extrapolation) is a possible refinement but requires that the input-selecting equipment has access to all the increments generated in the previous step, and thus duplicated increment stores must be provided. Any further refinement of the integration process, such as the use of backward difference series, will inevitably require a more adequate representation of increments than is afforded by ternary representation. Although no suitable integration formula has yet been found, the design of this computer has at least provided valuable experience in techniques applicable to the use of a general representation of increments.

The improved consecutive computer described in Section 7 is a more economical design; the basic cost is estimated as being half that of a comparable computer of the previous design. In comparison, the programming techniques applicable to the improved design have not been fully explored, but have the advantage of some flexibility in the program without correspondingly increased complexity. The design also eliminates certain error-producing mechanisms, notably those inherent in previous scaling and summing devices.

Accuracy may of course be improved by extending the time scale of the solution, subject to an adequate representation of whole quantities being available. The reverse is also true, hence computer performance is improved by an increase in digit repetition-frequency which reduces errors from all sources whilst producing a solution to the original time scale. It is economical to pursue the construction of a computer of the improved design, but using ten times the digit repetition rate (that is 5 000 000 per second) of the previous

computer since computing elements and delay-line stores are currently available at less than ten times the cost of the slower elements.

9. Acknowledgments

10. References

1. "Computing machines", *Mechanical Engineering*, 73, p. 325, April 1951.
2. G. C. Tootill, "The incremental digital computer (digital differential analysers): First principles of operation and use", *Process Control and Automation*, 5, No. 10, p. 350, September 1958.
3. G. G. Scarrott and R. Naylor, "Wire-type acoustic delay lines for digital storage", *Proc. Instn Elect. Engrs*, 105, B, Supplement No. 3, p. 497, 1958. (I.E.E. Paper 2027M, March 1956.)
4. K. Millington, "A Restandardizing Element for General Use in High-speed Digital Apparatus". Unpublished Ministry of Supply Report, January 1959.

11. Appendix

Representation of Quantities in the Integrator

The equation of Section 2 describing approximate digital integration, and the equations which are instrumented by a rectangular integrating process are re-stated here:

$$z_n \simeq \sum_{i=0}^{i=n} y_i \Delta x \qquad \ldots\ldots(1)$$

$$y^* = y + \Delta y \qquad \ldots\ldots(2)$$

$$\Delta z + r^* = y^* \Delta x + r \qquad \ldots\ldots(3)$$

Equation (1) implies that $\Delta z \simeq y \Delta x$, i.e. that the quantities r and r^* in the more accurate equation (3) are small. Since, Δz and Δx have the same range of values, it follows that the maximum value of $|y|$ (and of $|y^*|$) must be 1. A number n of binary digits (n bits) is used to represent y in the "noughts-complement" system which caters for positive and negative values. The weights of the digit places 0 to $(-n+1)$ are therefore $2^0, 2^{-1}, 2^{-2}, \ldots, 2^{-n+1}$. The weight of the most significant (2^0) digit is negative and that of each of the less significant (or lower) digits positive. Thus negative numbers are characterized by a one, and positive numbers by a zero in the most significant digit position. It follows that

$$-1 \leqslant y^* \leqslant 1 - 2^{-n+1} \qquad \ldots\ldots(4)$$

i.e.

$$-1 \leqslant y^* \leqslant 1 - \varepsilon$$

where ε is the quantum of the representation, i.e. the smallest non-zero change in y^* which can be represented.

From equation (2), Δy must have the same quantum as y and y^* but is in general represented by fewer bits

British Participation in the International Years of the Quiet Sun

The United Kingdom is to make a significant scientific contribution to the International Years of the Quiet Sun, a period of two years from 1st January 1964 to 31st December 1965, during which the minimum point in the sun's activity will fall. The activity of the sun, as judged by the behaviour of solar prominences, sunspots etc., exhibits an eleven year cycle and the last period of least solar activity occurred in 1954. In order to investigate the behaviour of the environment of the earth during the following sunspot maximum period, the now-famous "International Geophysical Year", (IGY) was proposed and carried out in 1957–58. From this co-operative effort by over sixty nations, emerged a great deal of valuable scientific data which has been collected and catalogued at World Data Centres and freely interchanged between scientists.

It had been realized that the value of the scientific data obtained during the IGY would be considerably enhanced were similar data to be obtained during the period when the sun's activity was next expected to be at a minimum. Accordingly, it was proposed that a special scientific effort be made in 1964 and 1965, using both techniques similar to those employed during the IGY and more refined techniques since developed.

Some of the radio investigations during the IGY were described in a paper by Professor W. J. G. Beynon, C.B.E., in a paper in the *Brit. I.R.E. Journal* for July 1958, entitled "Radio studies during the International Geophysical Year 1957–8". Professor Beynon was IGY Reporter for the Ionosphere and he is now chairman of the Royal Society's British National Committee for Co-operation in Geophysics, in addition to continuing his special interests as British National Correspondent for the Ionosphere. The National Committee is responsible for the preparation and co-ordination of the United Kingdom's IQSY programme.

The United Kingdom programme, like those of many others of the 58 nations participating in the IQSY, comprises special projects planned specifically for the IQSY, programmes repeating IGY observations, experiments of a singular nature such as those that are satellite-borne, and routine synoptic observations which are made regularly at permanently occupied stations by observers of meteorological parameters and of auroral displays.

Radio engineers will be particularly interested in the ionospheric investigations and a comprehensive programme has been planned for IQSY using the synoptic network of ground stations between longitudes 0 deg and 110 deg E, and experiments borne in vertical-sounding rockets and earth satellites.

Vertical incidence soundings. The network of stations operating during the IQSY will be Aberystwyth, Slough and Sidmouth in the U.K., Singapore in equatorial latitudes, and Port Stanley, Argentine Islands and Halley Bay in high southern latitudes. At most of these stations, soundings will continue using similar ionosondes to those used during the IGY though it is hoped to install improved ionosondes at some stations. At Halley Bay, tests will be conducted to investigate the obliquity of echoes in the sounding of the ionosphere.

Absorption. The study of absorption by the pulse-reflexion method will be made at Aberystwyth, Singapore and Halley Bay. At Halley Bay and at Edinburgh, the absorption will be studied by measuring the cosmic radio noise with, respectively, a variable frequency (10–50 Mc/s) and a fixed frequency (20 Mc/s) riometer.

Drifts. Regular measurements of ionospheric drifts by the three-receiver, short base, fading method will be made at Aberystwyth, Singapore and Halley Bay giving data complementary to those obtained during the IGY. Radio-echo measurements of the magnitude distributions and incident fluxes of meteors by the dual wavelength method will be made at Sheffield.

Special experiments at ground stations. At Sidmouth, particular attention will be devoted to the study of the D and E regions by scatter soundings for the lower ionosphere. Incoherent scatter observations will be made at Malvern. To obtain data on ionospheric disturbances complementary to those obtained during the IGY back scatter measurements will be made on 17 Mc/s at Sheffield. It is proposed to establish a forward scatter link between St. Lawrence (I.o.W.) and Gozo, near Malta, and it is hoped to install a receiver at Halley Bay as part of a one-way forward scatter link with the U.S. South Pole Station. Radio-echo observations of aurorae will also be undertaken at Halley Bay.

Electron density and top-side soundings. The electron density of the ionosphere will be studied by recording whistlers at Argentine Islands. By an analysis of radar echoes reflected from the lunar surface (on two frequencies) it is intended to study at Jodrell Bank the total electron content and gross shape of the ionosphere, the diurnal, seasonal and storm-time magnetic variations of the content and shape and the dependence of these variations on solar activity. By co-operating with other observers, to obtain a long base line, it is intended to study the variation of electron content with latitude and longitude and the structure of the large irregularities. Polarization fluctuations caused by irregularities of ionospheric origin will also be investigated using this moon-radar technique with the 250 ft radio telescope.

The ground stations at Aberystwyth, Slough, Sidmouth, Singapore and Port Stanley will be equipped to receive signals propagated from above the ionosphere by transmitters in earth satellites.

Rocket and satellite experiments. Plasma probes will be launched in either rockets (from Woomera) or satellites to obtain information on the concentration, temperature and mass of ions throughout the ionosphere. The data obtained will be used to study the correlation of ionospheric and solar behaviour, sporadic E ionization and its relation to wind structure, and the role of negative ions in the D region. The propagation of radio waves by rockets making vertical traverses of the ionosphere will be studied to give information on the electron density of the ionosphere.

It is hoped to study the electron profile through the D, E and F layers using rocket-borne high sensitivity r.f. electron density probes. It is possible that a stand-by unit of the mass spectrometer probe flown in the *Ariel I* satellite will be incorporated in a U.S. top-side sounding satellite to be flown during the IQSY.

Radio Engineering Overseas . . .

The following abstracts are taken from Commonwealth, European and Asian journals received by the Institution's Library. Abstracts of papers published in American journals are not included because they are available in many other publications. Members who wish to consult any of the papers quoted should apply to the Librarian, giving full bibliographical details, i.e. title, author, journal and date, of the paper required. All papers are in the language of the country of origin of the journal unless otherwise stated. Translations cannot be supplied. Information on translating services will be found in the Institution publication "Library Services and Technical Information".

TUNNEL DIODE FREQUENCY MULTIPLIERS

The "pulling effect" which takes place in tunnel diode oscillators can be used for frequency multiplication. An oscillator can operate as a source for a harmonic of its oscillating frequency and synchronize a second oscillator tuned to this higher frequency. A graphical method is described in a German journal which can be used for a quantitative determination of the behaviour of a pulled tunnel diode oscillator within the pulling range. Then a cascade circuit of tunnel diode oscillators for frequency multiplication is discussed. It has been found that the number of stages which can be connected in series without an intermediate decoupling section is limited.

"Frequency multiplication by pulling tunnel diode oscillators to a harmonic of the drive frequency", H. Graf. *Nachrichtentechnische Zeitschrift*, 16, pp. 188–95, April 1963.

RADAR METEOR-HEAD ECHOES

Measurements have recently been published on some 500 radar meteor-head echoes observed at Ottawa by the National Research Council of Canada during the 1961 Perseid meteor shower. Mean absolute powers of head echoes and of the associated enduring echoes are given as a function of the angular position of the meteor along its trajectory, and the detailed amplitude variation of three head echoes is discussed in relation to various scattering mechanisms. It is shown that a solar-controlled parameter of the atmosphere has a strong influence on head echoes.

"Experimental study of the amplitude of radar meteor-head echoes", B. A. McIntosh. *Canadian Journal of Physics*, 41, pp. 355–71, 1963.

MISSILE TELEMETRY AERIAL

A description has recently been published of a French installation for the reception of telemetry signals transmitted from a missile. The aerial assembly, orientated in azimuth and angle, incorporates a reflector with a diameter of 20 metres and provides a beam sweep movement of conical form. The gain is 28 dB in the band 214 to 254 Mc/s. Focusing is achieved by an array of 4 dipoles spinning at 600 turns/minute and allowing the simultaneous reception of the right and left circular components of the incident wave. The aerial can track with a precision of 0·25 deg for an input signal level of 1 microvolt.

"The 28 dB self directing antenna of S.E.C.T.", J. Combelles. *L'Onde Electrique*, 43, pp. 265–72, March 1963.

STEREOPHONIC BROADCASTING

In the Zenith-General Electric system, called the "pilot-tone stereophonic system", a small proportion of the available modulation capacity is taken by a pilot signal used in the demodulation process at the receiver. The remainder is divided between the sum of the left- and right-hand stereophonic signals, transmitted in the same way as a monophonic programme, and the difference between these signals which is transmitted by modulation of a sub-carrier. An investigation has been carried out by the B.B.C. Research Department to determine how far the level of the sum signal is lowered by the presence of the difference signal. Measurements made with an audio-frequency circuit designed to simulate the combination of the sum and difference signals in the transmitter yield a figure which, for the commonest types of programme, varies from 2 to 4 decibels; in calculating the signal received by the monophonic listener, this figure must be added to the losses from other causes.

"Determination of the effective modulation depth of monophonic programme transmitted on the pilot-tone stereophonic system", D. E. L. Shorter. *E.B.U. Review*, No. 77A, pp. 2–7, February 1963.

TELEVISION REMOTE CONTROL SYSTEMS

A recent Australian paper discusses remote controls for television receivers. The principles of operation are classified according to the control media between the viewer and the receiver, namely direct electrical communication by a cable, a light beam, ultrasonic waves, and radio frequency waves.

After a comparison of the relative complexity and susceptibility to interference of these systems, a cable type remote control for Australian use is described in detail. Attention is given to the choice of control functions, the problems encountered in providing these functions, and to the means of overcoming the problems.

The latter part of the paper gives a mechanical description of a power tuner unit currently produced for Australian use. Mention is made of the design problems encountered, with particular attention to noise, gear whine, method of power transmission, channel selection, muting, and power switch of operation. The influence of tuner indexing and mounting on general noise level and gear whine is also considered.

"Television remote control systems", J. T. Pope and M. Tinka. *Proceedings of the Institution of Radio Engineers, Australia*, 24, pp. 295–304, March 1963.

VIDICON PERFORMANCE

The performance of the vidicon under various conditions has been studied at the Chalmers University of Technology, Sweden, in order to estimate the usefulness of this camera tube in scientific applications. Investigations were carried out on the ability of the vidicon to work in different illumination and contrast regions and to reproduce objects in motion. Special attention was devoted to the properties of the vidicon at very low target illumination and to the possibility of transmitting pictures with an extremely high number of picture elements.

Starting from the fundamental properties of the photo-conductive layer, the variation of signal was examined as a function of charging time and of various scanning conditions, mainly different raster sizes and scanning times. At low light levels the number of picture elements attainable in the presence of noise was studied as these factors were varied. In connection with the problem of optimizing vidicon sensitivity at low light levels the sensitivity of a complete television system using a vidicon was investigated.

For camera tubes of vidicon type the maximum obtainable number of picture elements is essentially determined by the dimensions of scanning electron beam. Measurements of the electron beam dimensions were therefore carried out at different operating points of the vidicon. The aperture response of the vidicon was derived for various assumptions, and the resolution and the contrast transmission measured as raster size, focusing field and other scanning parameters were varied. The attainment of high resolution in a complete television system using the vidicon is also discussed in the Report.

The relatively limited capability of the vidicon to reproduce objects with rapidly changing image content is not such a limitation in scientific applications as it is for studio use. For this reason the static properties of the vidicon were the principal objects of investigation in this study. Some information on the transient response of vidicons and vidicon television systems was however obtained by means of a moving test wedge.

"Optimized performance of the vidicon", Ove Strindehag. *Transactions of Chalmers University of Technology*, Gothenburg, No. 265, (*Avd. Elektroteknik* 73), 1963.

COMPARISON OF N.T.S.C. AND SECAM COLOUR TELEVISION

Tests relating to colour television propagation and reception and carried out in the region of Berne and Thun during the early summer of 1962, are the subject of a report by a Swiss engineer. During these tests a SECAM--f.m. system with video and carrier-frequency pre-emphasis was compared with a modified N.T.S.C. system. The investigation covered the susceptibility to interference from noise, man-made noise and multi-path reception as well as compatibility. It was found that the new SECAM system has, as far as propagation and reception are concerned, a slight advantage over the modified N.T.S.C. system because of its somewhat more favourable properties under conditions of multi-path reception.

"Comparison observations of reception conditions with N.T.S.C. and SECAM colour television systems", K. Bernath. *Nachrichtentechnische Zeitschrift*, 16, pp. 181–8, April 1963.

DETECTION IN WHITE NOISE

Shannon's well-known formula gives the maximum value of the information quantity per unit time which can be transmitted without error through a channel subjected to white noise. Trying to apply it to practical problems raises two points: (1) the formula involves bandwidth, a more or less arbitrary quantity, since any real signal occupies the whole of the frequency axis, from zero to infinity; (2) the formula relies on the hypothesis of a detector operating for an infinitely long time and capable of selecting a message among an infinite number of them. A practical detector can effect no such selection, but only a simpler one among a finite and generally small number of messages. It results from this that detection is always associated with some error rate.

The purpose of a paper in *Cables & Transmission* is to study the operation of the detector, starting from such fundamental quantities as power available for message transmission (or number of messages per second and power allotted to each message), noise power per unit frequency band, and resolving power of the detector, the latter being defined as the number of messages between which a choice is possible. Assuming these three quantities to be known, the question of the optimum transmission speed for maximum information is studied, together with that of the limiting value of the information which can be transmitted through a given channel when the resolving power of the detector increases indefinitely.

"Optimal detection of a coded message in white noise". H. Debart. *Cables & Transmission*, 17, No. 2, pp. 98–105, April 1963.

THIN FILM STRIP LINE

With a view to the development of stores with short access times for computers, a recent German paper calculates the attenuation and distortion of pulses on a thin-film magnetic strip line with thin intermediate layers. One of these is a conductor of high permeability (magnetic layer). The strip line is assumed to be of infinite width and terminated without reflection. After a calculation of the propagation constant of the fundamental wave an approximation method of general validity is used for determining the receiving function. This method is based on a separation of the propagation constant into two terms and a corresponding solution in two steps of the Fourier integral. It is found that strip lines with a conductor spacing of less than 10^{-3} cm and a conductor thickness of less than 10^{-3} cm can hardly qualify for stores because of their high attenuation, and distortion. On a copper line with a spacing $D = 2 \cdot 1 \times 10^{-4}$ cm, a conductor thickness of 10^{-4} cm, a thickness of the nickel-iron layer of 10^{-5} cm, for instance, the pulse attenuation is about lN with a line length of $l = 20$ cm. On a copper line with a spacing $D = 1 \cdot 2 \times 10^{-2}$ cm, a conductor thickness of 3×10^{-3} cm, and a thickness of the nickel iron layer of 10^{-5} cm, however, the attenuation and distortion of the pulse can be neglected even with line lengths of 50 cm.

"Attenuation and distortion of pulses on a thin film magnetic strip line", G. Piefke. *Archiv Der Elektrischen Übertragung*, 17, pp. 153–62, April 1963.